Hydration of polysaccharides by the use of hyaluronan as a model system

Dissertation

Zur Erlangung des akademischen Grades eines

Doktors der Naturwissenschaften

Fachbereich 7: Natur- und Umweltwissenschaften

Universität Koblenz-Landau

vorgelegt von

Dipl.-Ing.

Alena Průšová

1. Gutachter: PD. Dr. Jiri Kučerík (Universität Koblenz-Landau, Germany)
2. Gutachterin: Prof. Dr. Gabriele Schaumann (Universität Koblenz-Landau, Germany)

Landau, Februar 2013

To my father Jaromír Průša

Declaration

I herewith declare that I autonomously carried out the PhD thesis entitled "Hydration of polysaccharides by the use of hyaluronan as a model system". All used assistances are declared and parts of involved contributors and other authors are clearly indicated. This or another thesis has never been submitted elsewhere for an exam, as thesis or for evaluation in a similar context; neither to any department of this university nor to any other scientific institution.

Place, date signature

The following parts of this thesis are published or submitted for publication:

Appendix 1 is published: Průšová, A., Šmejkalová, D., Chytil, M., Velebný, M., Kučerík, J. (2010). An alternative DSC approach to study hydration of hyaluronan. Carbohydrate Polymers 82: 498–503. My own contribution to this work consists of ~75% which includes sample preparation, conducting of all measurements, data elaboration and writing of the manuscript.

Appendix 2 is published: Kučerík, J., Průšová, A., Rotaru, A., Flimel, K., Janeček, J., Conte, P. (2011). DSC study on hyaluronan hydration and dehydration. Thermochimica acta 523: 245–249. My own contribution to this work consists of ~ 50% which includes sample preparation, conducting of all measurements, data elaboration and participation on writing of the manuscript.

Appendix 3 is published: Šmejkalová, D., Hermannová, M., Šulánková, R., Průšová, A., Kučerík, J., Velebný, M. (2012) Structural and conformation differences of acylated hyaluronan modified in protic and aprotic solvent system. Carbohydrate Polymers 87: 1460–1466. My own contribution to this work consists of ~ 40% which includes preparation of samples for DSC, conducting of all DSC measurements and related data elaboration and participation on writing of the manuscript.

Appendix 4 is published: Kučerík, J., Bursáková, P., Průšová, A., Grebíková, L., Schaumann, G. E. (2012) Hydration of humic and fulvic acids studied by DSC. Journal of thermal analysis and calorimetry 110: 451–459. My own contribution to this work consists of ~ 30%, which includes conducting of some DSC measurements and some data elaboration and participation on writing of the manuscript. This work is a part of PhD thesis of Dr. Bursáková as well, in present thesis

represents only a minor part and it is included in order to clarify better the approaches applied in other appendixes.

Appendix 5 is published: Průšová, A., Conte, P., Kučerík, J., Alonzo, G. (2010) Dynamics of hyaluronan aqueous solutions as assessed by fast field cycling NMR relaxometry. Analytical and Bioanalytical Chemistry 397: 3023–3028. My own contribution to this work consists of ~ 75% which includes sample preparation, conducting of all measurements, data elaboration and participation on writing of the manuscript.

Appendix 6 is submitted to the journal "Carbohydrate Polymers" as: Průšová, A., Vergeldt, J. F., Kučerík, J. Influence of water content and drying on the physical structure of native hyaluronan. My own contribution to this work consists of ~ 80% which includes sample preparation, conducting of all DSC, SEM and NMR measurements, all data elaboration and writing of the manuscript.

Part of the published work has been conducted at Brno University of Technology, Czech Republic, thus my affiliation on these scientific papers is to Brno University of Technology.

Additionally, this thesis benefited from the supervision by Assoc. Prof. Dr. Jiří Kučerík as well as by supervision by Prof. Dr. Gabrielle E. Schaumann who helped me by suggestions, advices and ideas which cannot be enumerated. Measurements on FFC NMR were conducted under supervision of prof. Pellegrino Conte.

Acknowledgements

First of all I wish to thank to my supervisor Assoc. Prof. Dr. Jiří Kučerík for his enormous help and support. Without his guidance, encouragement, enthusiasm, and unselfish help I would not had been able to finish my doctoral work. I wish to thank to Prof. Dr. Gabriele E. Schaumann for her warm attitude and help. I wish to thank to Assoc. Prof. Dr. Pellegrino Conte for his help, support, and for showing me the beauty of NMR. I wish to thank to Dr. Anne E. Berns and to Dr. Dörte Diehl for their help. I wish to thank also to Assoc. prof. Vladimír Velebný for providing of hyaluronan samples. Last but not least I wish to thank to some former colleagues from Brno University of Technology in the Czech Republic.

TABLE OF CONTENTS

1 GENERAL INTRODUCTION 1

1.1 Polysaccharides 1

1.2 Classification of polysaccharides 1

1.2.1 Proteoglycans 1

1.2.2 Glycoproteins 3

1.2.3 Glycolipids 4

1.3 Polysaccharides structure 4

1.4 Important polysaccharides 5

1.4.1 Cellulose 5

1.4.2 Hemicellulose 6

1.4.3 Pectins 7

1.4.4 Starch 8

1.4.5 Glycogen 10

1.4.6 Dextran 10

1.4.7 Chitin 10

1.4.8 Hyaluronan 11

1.4.9 Heparin and Heparan sulfate 13

1.5 Intermolecular and intramolecular weak interactions in polysaccharides 15

1.5.1 Electrostatic weak interactions 16

1.5.2 Van der Walls forces 16

1.5.3 Dispersion (London) forces 17

1.5.4 Hydrogen bond 18

1.5.5 Hydrophobic interaction 20

2 STATE OF THE ART 22

2.1 Hydration of polysaccharides 22

2.1.1 Thermal analysis 22

2.1.2 Nuclear magnetic resonance techniques 26

3 MAIN RESEARCH QUESTIONS 30

4 OVERVIEW OF RESULTS AND DISSCUSION 31

5 REFERENCES 38

6 LIST OF ABBREVIATION 49

APPENDIX 1 50

APPENDIX 2 57

APPENDIX 3 63

APPENDIX 4 71

APPENDIX 5 81

APPENDIX 6 88

7 PUBLICATIONS 108

8 CURRICULUM VITAE 110

SUMMARY

The polysaccharide hydration phenomenon is nowadays the subject of intense research. The interaction of native and modified polysaccharides and polysaccharides-based bioconjugates with water has an important influence on their functional behaviour. Notwithstanding that the hydration phenomenon has been studied for decades, there is still a lack of awareness about the influence of hydration water on the polysaccharide´s structure and consequences for industrial or medicinal applications.

The hydration of polysaccharides is often described by the existence of water layers differing in their physical properties depending on the distance from the polysaccharide. Using the differential scanning calorimetry (DSC) such water layers were categorized according their properties upon cooling in hyaluronan (HYA, sodium salt of β-1,4-linked units of β-1,3-linked D-glucuronic acid and N-acetyl-D-glucosamine), a model polysaccharide in the present work. The amount of non-freezing water, i.e. water in close proximity of HYA chain which does not freeze et all, was determined around $0.74 g_{H2O}/g_{HYA}$ for HYA with molecular weight from 100 to 740kDa and $0.84 g_{H2O}/g_{HYA}$ for molecular weight of 1390kDa. The amount of freezing-bound water, the water pool which is affected by presence of HYA but freezes, was determined in the range from 0.74 to $2 g_{H2O}/g_{HYA}$. Above this value only non-freezing and bulk water are present since melting enthalpy measured above this concentration reached the same value as for pure water. Since this approach suffers from several experimental problems, a new approach, based on the evaporation enthalpy determination, was suggested. The analysis of the evaporation enthalpies revealed an additional process associated with apparent energy release taking part below the water content of $0.34 g_{H2O}/g_{HYA}$. Existence of this phenomenon was observed also for protonated form of HYA. The existence of energy compensating process was confirmed with the Kissinger-Akahira-Sunose method which allowed determination of actual water evaporation/desorption enthalpies in all stages of the evaporation process. In fact, the apparent evaporation enthalpy value increased until water content of $0.34 g_{H2O}/g_{HYA}$, and then dropped down to lower values which were, still higher than the value of the pure water evaporation enthalpy. By the use of time domain nuclear magnetic resonance (TD-NMR) technique it was revealed that this phenomenon is the plasticisation of HYA. Further, it was revealed that the non-freezing water determined by the use of DSC consists of two water fractions, i.e. 15% of water structurally integrated, interacting directly with polar sites, and 85% of water structurally restricted, embedded in-between the HYA chains. The

occurrence of plasticisation concentration close to equilibrium moisture content provided the possibility to influence the HYA physical structure during the drying. In this way three samples of native HYA, dried under various conditions were prepared and their physical properties were analyzed. The samples differed in kinetics of rehydration, plasticisation concentration, glass transitions, and morphology. The properties of water pool were studied in solutions of 10–25mg HYA/mL as well. The fast filed cycling (FFC) NMR relaxometry showed the existence of three water fractions which correlation times spanned from 10^{-6} to 10^{-10} seconds, progressively decreasing in dependency on its distance from HYA chain. The formation of a weak and transient intramolecular water bridge between HYA chains was observed.

It was shown that, unlike the inorganic electrolytes, polyelectrolytes hydration is a dynamic process which reflects not only the technique used for the analysis, experimental conditions but also the conformation of the polysaccharide and its “thermal” and “hydration” history. It was demonstrated that some native polysaccharide structures can be easily modified by manipulation of preparation conditions, giving fractions with specific physicochemical properties without necessity of any chemical modification.

ZUSAMMENFASSUNG

Die Wasseraufnahme von Polysacchariden wird derzeit intensiv erforscht. Wechselwirkungen zwischen Wasser und herkömmlichen oder modifizierten Polysacchariden und Polysaccharid-basierten Biokonjugaten bestimmen maßgeblich deren Funktionalität. Trotz intensiver Forschung gibt es weiterhin eine Reihe offener Fragen darüber, wie Wasser die Struktur der Polysaccharide beeinflusst und welche Konsequenzen das für ihre industrielle und medizinische Anwendung hat.

Die Wechselwirkungen zwischen Wasser und Polysacchariden werden oft durch übereinanderliegende „Schichten“ von Wasser verbildlicht, dessen physikalische Eigenschaften sich in Abhängigkeit vom Abstand zur Polysaccharid-Moleküloberfläche verändern. In der vorliegenden Arbeit wurden solche „Wasserschichten“ in dem Modell–Polysaccharid Hyaluronan (HYA), einem Natriumsalzsalz bestehend aus β-1,4-Verknüpfungen der β-1,3-verknüpften D-Glucuronsäure und des N-Acetyl-D-Glucosamins, untersucht. Mithilfe der Dynamischen Differenzkalorimetrie (engl.: Differential Scanning Calorimetry, DSC) können diese Wasserschichten hinsichtlich ihres Gefrierverhaltens unterschieden werden. Bei HYA-Molekülgewichten von 100 bis 740kDa betrug die Menge “nicht gefrierbaren” Wassers, d.h. von Wasser in unmittelbarer Nähe der HYA Molekülketten, $0.74 g_{H2O}/g_{HYA}$ und bei einem Molekülgewicht von 139kDa betrug sie $0.84 g_{H2O}/g_{HYA}$. Die Menge von “gefrierbar gebundenem” Wasser, also des Anteiles, der zwar noch vom HYA Molekül beeinflusst wird, aber trotzdem gefrierbar ist, betrug zwischen 0.74 und $2 g_{H2O}/g_{HYA}$. Oberhalb dieses Wassergehaltes liegt nur „nicht gefrierbares“ und „freies“ Wasser vor, da die Schmelzenthalpie bei höheren Wassergehalten der von reinem Wasser entspricht. Die Charakterisierung der Wasserbindung durch die Bestimmung von Schmelzenthalpien unterliegt experimentellen Einschränkungen. Daher wurde ein neuer Ansatz basierend auf der Bestimmung von Verdampfungsenthalpien vorgeschlagen. Verdampfungsenthalpien von HYA unterhalb eines Wassergehaltes von $0.34 g_{H2O}/g_{HYA}$ wiesen auf einen zusätzlichen möglicherweise exothermen Prozess hin, der auch in der protonierten Form des HYA beobachtet werden konnte. Dieser Prozess wurde durch die Kissinger-Akahira-Sunose Methode bestätigt, die Bestimmung der tatsächlichen Verdampfungs- und Desorptionsenthalpien des Wassers in allen Stadien des Verdampfungsprozesses erlaubt. Tatsächlich nahm die scheinbare Verdampfungsenthalpie bis zu einem Wassergehalt von $0.34 g_{H2O}/g_{HYA}$ zu und sank dann wieder zu niedrigeren Werten ab, die allerdings immer noch deutlich über der Verdampfungsenthalpie von reinem Wasser lagen. Mithilfe von zeitlich aufgelöster Kernspinresonanz Technik (engl.:

Time Domain Nuclear Magnetic Resonance, TD-NMR) wurde gezeigt, dass es sich bei besagtem Prozess um die Plastifizierung von HYA handelt. Außerdem konnte das mithilfe der DSC bestimmte „nicht gefrierbare“ Wasser in zwei weitere Fraktionen unterteilt werden. Ein Anteil von 15% dieses Wassers tritt direkt in Wechselwirkung mit den polaren funktionellen Gruppen und wird als „strukturell integriertes“ Wasser bezeichnet und ein Anteil von 85% ist zwischen HYA Molekülketten eingebettet und wird als „strukturell eingeschränktes“ Wasser bezeichnet. Da der Erweichungspunkt in der Nähe des Gleichgewichtswassergehalts liegt, bietet die er die Möglichkeit, die physikalische Struktur von HYA durch Trocknung zu beeinflussen. Dafür wurden drei Proben des ursprünglichen HYA unter unterschiedlichen Bedingungen getrocknet und ihre physikalischen Eigenschaften untersucht. Die Proben unterschieden sich in der Kinetik der erneuten Wasseraufnahme, im Glasübergangsverhalten und in ihrer Morphologie. Die Eigenschaften der Wasserfraktionen wurden in Lösungen mit 10–25 mg HYA/mL bestimmt. Feldzyklus-NMR (eng.: Fast-field-cycling FFC-NMR) Messungen zeigten drei Wasserfraktionen die mit dem Abstand zur HYA Moleküloberfläche abnehmende Korrelationszeiten zwischen 10^{-6} bis 10^{-10} s aufwiesen. Außerdem wurde die Bildung schwacher relativ kurzlebiger Wasserbrücken zwischen den HYA Molekülketten beobachtet.

Anders als für anorganische Elektrolyte, ist die Wasseraufnahme durch organische Polyelektrolyte ein dynamischer Prozess, der nicht nur die Analysetechnik und die experimentellen Bedingungen sondern auch die Konformation der Polyelektrolyte und deren thermische und Wassergehalts-Vorgeschichte widerspiegelt. Dadurch können einige Polysaccharidstrukturen nur durch Veränderung der Probenvorbereitung und ohne chemische Modifikationen verändert und Produkte mit spezifischen physiko-chemischen Eigenschaften gewonnen werden.

1 GENERAL INTRODUCTION

1.1 Polysaccharides

Polysaccharides belong among the most important biopolymers present in living systems. Therefore, the knowledge of their interaction with water and other (bio)molecules is of a great importance. Despite water's relatively simple molecular structure, liquid water exhibits unusual thermodynamic behavior and some anomalous properties that differentiate it from other liquids. For that reason the nature of liquid water, the water molecules organization and interactions have attracted the interest of chemists for many years. It is well known that due to mutual affinity of water molecules, they form specific structures which composition and physical properties are affected by the presence of macromolecules e.g. polysaccharides which are hydrated (Dei and Grassi, 2006). Hydration is also a crucial factor influencing the secondary structure and consequently the mutual interactions of polysaccharides. In this way, the function of molecules present in the living systems is controlled and regulated. Thus, the detailed knowledge on hydration of polysaccharides might be helpful in their technological and pharmaceutical applications such as hydrogels, drug delivery systems, and the tissue scaffolds research and design. Polysaccharides have been proposed as the first biopolymers to have formed on the Earth (Tolstoguzov, 2004). The majority of carbohydrates found in nature occur as polysaccharides. Polysaccharides are large, high-molecular weight molecules containing more than 100 monosaccharide units, some have thousands of units. These macromolecules consist of monosaccharide units linked together by the glycosidic bonds. Polysaccharides act mainly as the food storage or structural materials. Polysaccharides differ from each other in the character of their repeating monosaccharide units, in the length of their chains, in the types of glycosidic bonds linking the units, and in the degree of branching. Besides the structural and storage homopolysaccharides discussed below, in living systems there also exist the informational carbohydrates. Those are covalently joined to a protein or a lipid to form a glycoconjugates which are the biologically active supramolecules.

1.2 Classification of polysaccharides

1.2.1 Proteoglycans

Proteoglycans are macromolecules of the cell surface or the extracellular matrix in which one or more glycosaminoglycan chains are joined covalently to a core protein. The glycosaminoglycan

moiety commonly forms the greater fraction (by mass) of the proteoglycan molecule, dominates the structure, and often it is the main site of biological activity. The biological activity of proteoglycans is caused by the presence of the multiple binding sites. Further reason is the huge amount opportunities for hydrogen bonding and electrostatic interactions with other proteins of the cell surface or the extracellular matrix. Proteoglycans are major components of connective tissue such as cartilage, in which they non-covalently interact with other proteoglycans, proteins, and glycosaminoglycans (Iozzo and Murdoch, 1996; Nelson and Cox, 2004).

Some proteoglycans can form proteoglycan aggregates, for example enormous supramolecular assemblies of many core proteins are bound to a single molecule of polysaccharide called hyaluronan. Aggrecan, the core protein with molecular weight ca 250kDa, has multiple chains of chondroitin sulfate and keratan sulfate joined to serine residues through trisaccharide linkers, therefore an aggrecan monomer has molecular mass ca 2MDa. When a hundred or more of these aggrecan monomers core proteins bind a single, extended molecule of hyaluronan (Figure 1), the resulting proteoglycan aggregate has molecular mass > 200MDa and its associated water of hydration occupy a volume almost equal to that of a bacterial cell.

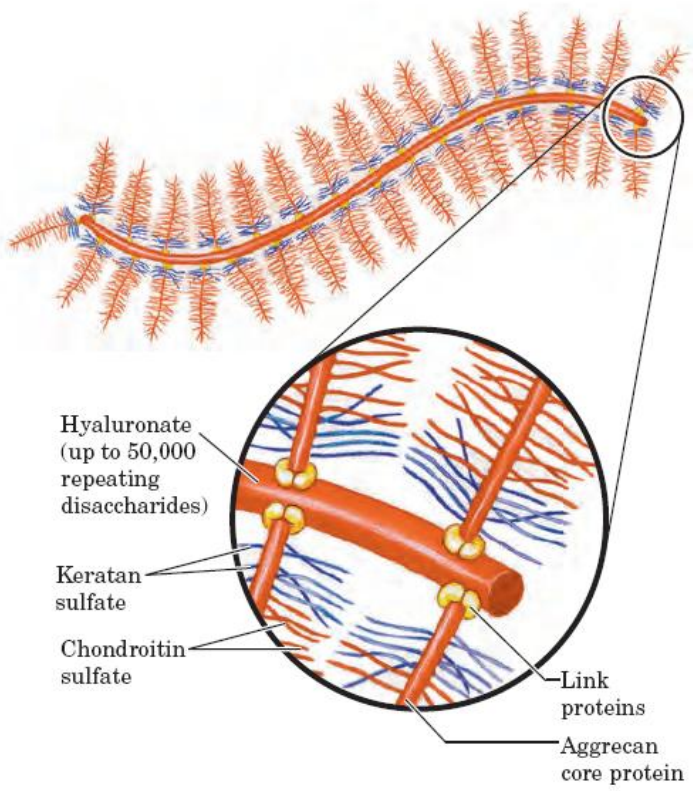

Figure 1: Proteoglycan aggregate of the extracellular matrix (Campbell, 2006).

Table 1: Main repeating structures in the glycosaminoglycans (Mulloy and Forster, 2000).

Glycosaminoglycan	Structure of main repeating dicaccharide
Hylauronan	-4)-β-D-GlcA-(1→3)-β-D-GlcNAc-(1-
Chondroitin-4-sulfate	-4)-β-D-GlcA-(1→3)-β-D-GalNAc4(OSO_3^-)-(1-
Chondroitin-6-sulfate	-4)-β-D-GlcA-(1→3)-β-D-GalNAc6(OSO_3^-)-(1-
Dermatan sulfate	-4)-α-L-IdoA-(1→3)-β-D-GalNAc4(OSO_3^-)-(1-
Heparin	-4)-α-L-IdoA2(OSO_3^-)-(1→4)-α-D-GlcNSO_3^-,6(OSO_3^-)-(1-
Heparin sulfate	-4)-β-D-GlcA-(1→4)-α-D-GlcNAc-(1-
Keratan sulfate	-3)-β-D-Gal-(1→4)-β-D-GlcNAc6(OSO_3^-)-(1-

Glycosaminoglycans (mucopolysaccharides) are linear polysaccharides with alternating uronic acid and hexosamine residues, in which a limited set of monosaccharide units gives rise to a number of complex sequences by variable substitution with *O*-sulfate, *N*-sulfate, and *N*-acetyl groups. Glycosaminoglycans usually exist as the *O*-linked side-chains of proteoglycans and tend to be negatively charged, because of the prevalence of acidic groups. The most common glycosaminoglycans are reported in the Table 1 (Mulloy and Forster, 2000).

1.2.2 Glycoproteins

These macromolecules are complexes where carbohydrates are attached covalently to asparagine or serine/threonine residues of peptides. In these carbohydrate-protein conjugates the carbohydrate moieties are smaller and more structurally diverse than the glycosaminoglycans of proteoglycans. One or several of these oligosaccharides, of varying complexity, are joined covalently to a protein. Glycoproteins are found on the outer face of the plasma membrane, in the extracellular matrix, and in the blood. One of the best-characterized membrane glycoproteins is glycophorin A of the erythrocyte membrane which contains 60% of carbohydrates by mass, in the form of 16 oligosaccharide chains covalently attached to amino acid residues located near the amino terminus of the polypeptide chain. Inside cells they are found in specific organelles such as Golgi complexes, secretory granules, and lysosomes. Oligosaccharide portions of glycoproteins are rich in information, forming highly specific sites for recognition. With this respect, to the group of glycoproteins belong the imunoglobulins (Nelson and Cox, 2004).

1.2.3 Glycolipids

To this group of glycoconjugates belong membrane lipids in which the hydrophilic head groups are oligosaccharides, which, as in glycoproteins, act as specific sites for recognition by carbohydrate-binding proteins. The oligosaccharide moieties of the glycolipids are generally found on the outer face of the plasma membrane (Campbell, 2006).

1.3 Polysaccharides structure

There are many aspects how to differentiate the polysaccharides´ structures. First of all the character of the glycosidic bound can be either α or β configuration. The type of the glycosidic bond depends on the hemiacetal conformation. Further if the repeating unit is in the α conformation consequently the glycosidic bond is in α configuration and similarly as for β repeating unit conformation. Polysaccharides can be divided into homopolysaccharides and heteropolysaccharides. The former contains only a single type of a monomer; the latter contains two or more different kinds of a monomer. Some homopolysaccharides serve as storage forms of monosaccharides that are used as a source of energy; homopolysaccharides of this type are glycogen, inulin, and starch. Other homopolysaccharides (cellulose and chitin, for example) serve as structural elements in plant cell walls and animal exoskeletons. Heteropolysaccharides provide extracellular support for various organisms. For example, the rigid layer of the bacterial cell envelope is partly composed from a heteropolysaccharide consisting of two alternating monosaccharide units. In animal tissues, the extracellular space is occupied by several types of heteropolysaccharides, which form a matrix that holds individual cells together and provides protection, shape, and support to cells, tissues, and organs. Moreover, the polysaccharide structures are either linear (cellulose, amylose), or branched (amylopectine, dextrans). Apparently, it is also possible to consider the classical protein research inspired diversification into primary, secondary and tertiary level. The primary level can be consider as a chemical structure that reflects the pattern of covalent bonding in polysaccharide molecules, in another words it is the sequence of the repeating monosaccharide units. The secondary level can be considered the spatial conformations of individual molecules. It defines the relative organization of the repeat units of an individual molecule in space. The tertiary level reflects the spatial arrangement of the molecules segments relative to each other in the native conformation.

1.4 Important polysaccharides

Polysaccharides have wide range of roles, their function in living organisms is either storage- or structure-related, the most important storage polysaccharides in plant cells are starch and inulin; glycogen in the animal cells. Further the most important structural polysaccharides in plant are cellulose, hemicellulose, pectins and chitin; in the vertebrates' cells which are proteoglycans where form the extracellular matrix, even the cartilages (i.e. special type of the connective tissue). Polysaccharides are also information carriers: they serve as destination labels for some proteins and as mediators of specific cell-cell interactions and interactions between cells and the extracellular matrix. Specific carbohydrate-containing molecules act in cell-cell recognition and adhesion, cell migration during development, blood clotting, the immune response, and wound healing.

1.4.1 Cellulose

The cellulose molecule is a linear, unbranched homopolysaccharide, consisting of 10,000 to 15,000 D-glucose units; cellulose exhibits a great chemical variability and potential in applications; the glucose residues have the β-configuration and are linked by ($\beta 1 \rightarrow 4$) glycosidic bonds (Figure 2) (Zugenmaier, 2008). Cellulose accounts for half the carbon in the biosphere and is the most abundant carbohydrate polymer and the most abundant polysaccharide on Earth (Stern and Jedrzejas, 2008). It is a water-insoluble fibrous, semicrystalline biopolymer with microfibrillar morphology (Hatakeyama, 2004); it is found in the cell walls of plants, particularly in stalks, stems, trunks. It constitutes much of the wood mass, cotton is almost pure cellulose. Cellulose provides shape and structure, additionally; it must have enormous weight-bearing properties, with the ability to withstand osmotic pressures as high as 2MPa between extracellular and intracellular spaces.

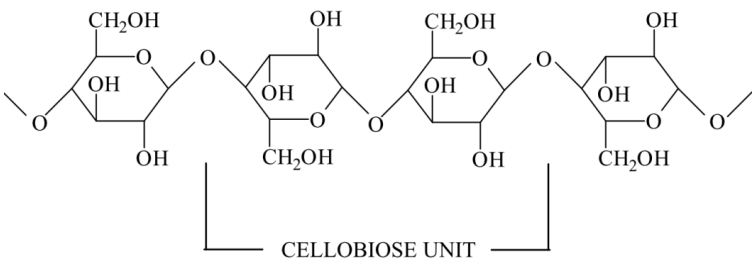

Figure 2: β–1$\rightarrow$4 linked D-glucose units (Ibrahim, 1998).

The parallel chains of cellulose, lying in alternating perpendicular patterns (Voet, 2004), are stabilized by the intermolecular hydrogen bonds between glucose units of the neighbouring chains. Cellulose is present in the small, crystalline microfibrils that are arranged in the multilayer structures. Although the cellulose molecules associate into crystals - the crystalline regions where the water is excluded almost completely (Zhao et al., 2005) - a certain fraction of cellulose is considered amorphous (Lewin, 2007). In the plant cell wall, the cellulose fibers are cross-linked by a number of polysaccharides containing glucose and other saccharides (Stern and Jedrzejas, 2008).

Cellulose has four polymorphs: cellulose I, II, III, and IV. Cellulose I is the crystal form of the native cellulose and has high degree of polymerization. Cellulose II is generally formed in the regenerated cellulose or the mercerized cellulose. Cellulose III is prepared by the chemical treatment. Cellulose IV_I is prepared only from cellulose III_I. Cellulose IV_{II} is obtained from both, cellulose II and III_{II} by the thermal treatment (Isogai et al., 1989). Recent crystallographic studies of cellulose suggest that cellulose I consists of two kinds of crystals, I_α (triclinic) and I_β (monoclinic); α-cellulose is more abundant in nature than β-cellulose (Hatakeyama, 2004; Zhao et al., 2005; Leppanen et al., 2009).

Cellulose is the major constituent of paper, paperboard, and card stock and of textiles made from cotton, linen, and other plant fibers (Wakelyn, 2007). Because of its linear (1→4)-β-glucan structure with three reactive hydroxyl groups per anhydroglucopyranose unit, cellulose has broad potential in the design of advanced polymeric materials (Ifuku and Kadla, 2008). The purified cellulose (about one third of the world`s production) is used as a base material for water-soluble derivatives. Such cellulose derivatives can be designed with a wide range of properties depending on functional groups involved in the derivation reaction (Clasen and Kulicke, 2001). Ester and ether cellulose derivates are recently the most important commercial materials. Cellulose nitrate and cellulose acetate are important derivatives for solid-state applications. In principle cellulosic polymers are renewable resources (Clasen and Kulicke, 2001).

1.4.2 Hemicellulose

It is an extensive group of heteropolymers (matrix polysaccharides), which are embedded in the cell walls of plants, sometimes in chains that form a ground matrix. They bind with pectin to cellulose to form a network of cross-linked fibers. Hemicelluloses have a random, amorphous structure which contains many different sugar monomers. They can be divided into four general classes: xylans, mannans, β-glucans with mixed linkages and xyloglucans (Sun et al., 1998). Xylan

is a generic term used to describe a wide variety of highly complex polysaccharides that are found in the plant cell walls and some algae. Xylans are heteropolymers possessing a β–(1→4)-D-xylopyranoses backbone, which is branched by the short carbohydrate chains. They comprised D-glucuronic acid or its 4-*O*-methyl ether, L-arabinose and/or various oligosaccharide, composed of D-xyloses, L-arabinoses, D- or L-galactose and D-glucose. The xylan-type polysaccharides can be divided into homoxylans and heterosylans, which include glucuronasylans, (arabino)glucuronasylans, (glucurono)arabioxylans, arabionoxylans, and complex heteroxylans (Heinze, 2005). Mannans are generally found in plants, bacteria and yeast. Mannans can be divided into galactomannans and glucomannans. Whereas the backbone of the galactomannans is made up exclusively of β–(1→4) linked D-mannopyranose residues in linear chains, the glucomannans has both β–(1→4)-linked D-mannopyranose and β–(1→4)-linked D-glucopyranose residues in the main chain. As single side chains, D-galactopyranose residues tend to be 6-linked to the mannan backbone of both mannan-type polymers in different proportions. The resulting polymers are named galactomannans and galactoglucomannans (Heinze, 2005). β-glucans occur most commonly in plants, in the bran of cereal grains, the cell wall of bakers' yeast, certain fungi, mushrooms and bacteria. β-glucans with mixed linkages are composed of β–D(1→3) and β–D(1→4)-linked glucosyl residues. Typically there are regions of 2–5 β–D(1→4)-linked residues separated by β–D(1→3)-linkages. The β–D(1→4)-linked residues form rigid regions of the structure while the β–D(1→3)-links are flexible (Sun et al., 1998). Xyloglucan is the most abundant hemicellulose in the primary cell wall of many dicotyledonous plants, and occurs in the primary cell walls of all vascular plants (Fry, 1989). Xyloglucan binds to the surface of cellulose microfibrils and may link them together. Xyloglucan has a backbone of β–(1→4)-linked glucose residues most of which are substituted with 1–6 linked xylose sidechains. The specific structure of xyloglucan varies among plant families (Heinze, 2005).

1.4.3 Pectins

Pectins are heterogeneous group of plant polysaccharides with a complex structure depending on their source. Pectins are found in fruit and vegetables, and mainly prepared from “waste” citrus peel and apple pomace. It makes up between about 2% and 35% of plant cell walls (Ovodov, 2009). Among all of plant cell polymers, pectins have the greatest number of functions. They make up part of the cell wall, but they also make up a layer between adjacent cell walls, that is, the middle lamella that binds cells together. Pectins also form complexes with many globular proteins

(Tolstoguzov, 2004). Generally, pectins do not possess exact structures. The majority of the structure consists of homopolymers of partially methylated poly-R-1,4-D-galacturonic acid residues, but there are substantial non-gelling areas of alternating R-1,2- L rhamnosyl-R-1,4-D-galacturonosyl sections containing branch points with mostly neutral side chains containing from 1 to 20 residues of mainly L-arabinose and D-galactose (Perez et al., 2000). Pectins are mainly used as gelling agents, but can also act as thickener, water binder and stabilizer. Low methoxyl pectins (< 50% esterified) form thermoreversible gels in the presence of calcium ions and at low pH, whereas high methoxyl pectins rapidly form thermally irreversible gels in the presence of sucrose and at low pH. Highly (2-O- and/or 3-O-galacturonic acid backbone) acetylated pectin from sugar beet is reported to gel poorly but have considerable emulsification ability due to its more hydrophobic nature (Dickinson, 2003).

1.4.4 Starch

Starch is the major carbohydrate reserve in plant tubers and seed endosperm where it is found as granules (Buleon et al., 1998). Starch consists of two types of glucose polymer, amylose (normally 20–30%) and amylopectin (normally 70–80%) (Figure 3 and Figure 4). Macromolecule of amylose consists of long, unbranched chains of D-glucose residues connected by (α1→4) linkages. Such chains vary in molecular weight from a few thousand to more than a million Da. Amylopectin has a high molecular weight, up to 100MDa, and unlike amylose, it is highly branched. The glycosidic linkages joining glucose residues in amylopectin chains are (α1→4); the branch points (occurring every 24 to 30 residues) are (α1→6) linkages (Singh et al., 2003).

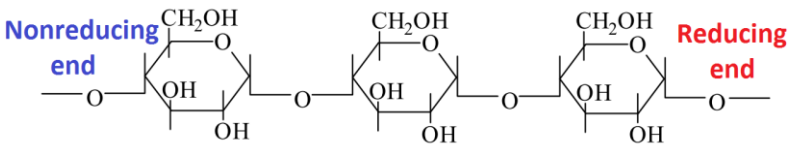

Figure 3: A short segment of amylase. (Ibrahim, 1998).

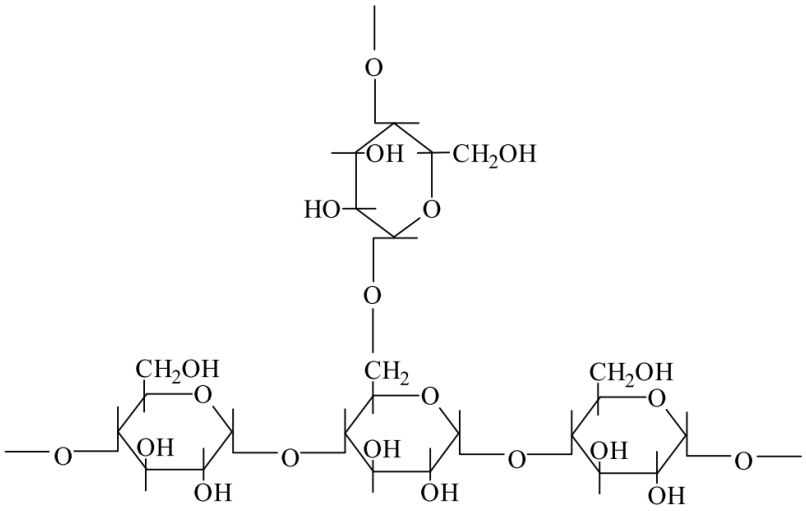

Figure 4: Branched point (α1→6) of amylopectine (Ibrahim, 1998).

Starch is an insoluble storage polysaccharide for plant cells and the main source of dietary carbohydrates. It is deposited in the cytoplasm of plant cells in the form of insoluble starch granules. Figure 5 represents the cluster of amylose and amylopectin as they are believed to occur in the starch granules. Fibers of amylopectin form double helical structures with each other or with amylose fibers (Nelson and Cox, 2004). Each granule typically containing several million amylopectin molecules accompanied by a much larger number of smaller amylose molecules. By far the largest source of starch is maize with other commonly used sources being wheat, potato, tapioca and rice. (Jobling, 2004).

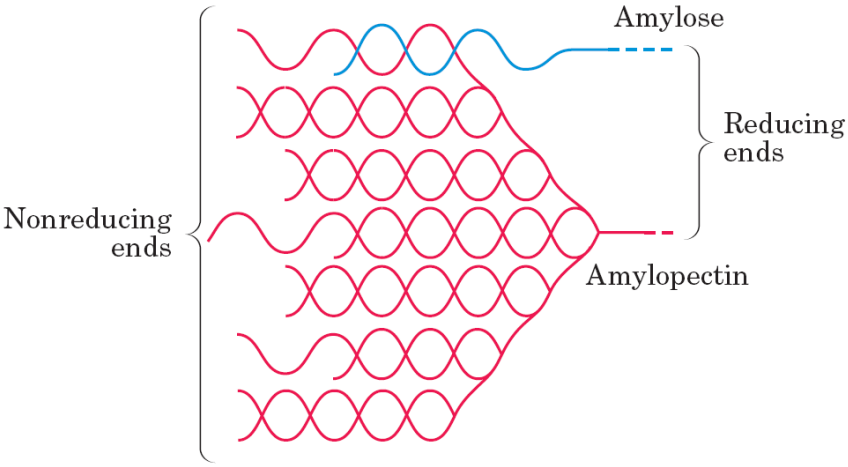

Figure 5: Cluster of amylose and amylopectine in the starch granules (Ibrahim, 1998).

Starch is a versatile and cheap, and has many uses as thickener, water binder, emulsion stabilizer and gelling agent. Many functional derivatives of starch are marketed including cross-linked, oxidized, acetylated, hydroxypropylated and partially hydrolyzed material (Copeland et al., 2009).

1.4.5 Glycogen

Glycogen is the energy storage in animal and fungi cells (Saladin, 2007). Similarly as amylopectin, glycogen is a polymer of (α1→4)-linked subunits of glucose, with (α1→6)-linked branches, but glycogen is more extensively branched (on average, every 8 to 12 residues) and more compact than starch. Glycogen is especially abundant in the liver, where it may constitute as much as 7% of the wet weight (Campbell, 2006); it is also present in skeletal muscle (Stern and Jedrzejas, 2008). In hepatocytes, glycogen is found in large granules, created by the clusters from smaller granules which are composed of single, highly branched glycogen molecules with an average molecular weight of several million Da (Nelson and Cox, 2004).

1.4.6 Dextran

It is a group of bacterial and yeast complex branched polysaccharides made up of (α1→6)-linked poly-D-glucose; all have (α1→3) branches, and some also have (α1→2) or (α1→4) branches. The molecular weight is ranging from 10 to 150kDa. Dental plaque, formed by bacteria growing on the surface of teeth, is rich in dextrans (Stern and Jedrzejas, 2008). Dextrans are used medicinally as an antithrombotic, to reduce blood viscosity, and as a volume expander in anemia. Synthetic dextrans are used in several commercial products that serve in the fractionation of proteins by size exclusion chromatography. Dextrans in these products are chemically cross linked to form insoluble materials of various porosities, admitting macromolecules of various sizes (Lewis and 2008).

1.4.7 Chitin

It is a linear homopolysaccharide composed of *N*-acetyl-D-glucosamine residues in *(β1→4)* linkage (Figure 6). Chitin forms extended fibers similar to those of cellulose, and similarly as cellulose it cannot be digested by vertebrates. In fact, chitin may be described as cellulose with one hydroxyl group on each monomer replaced by an acetylamine group, allowing for increased hydrogen bonding between adjacent polymers. This gives the polymer increased strength (Argüelles-Monal et al., 2002).

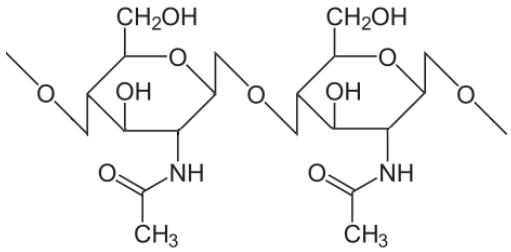

Figure 6: A short segment of chitin, a homopolymer of N-acetyl-D-glucosamine units in (β1→4) linkage (Ibrahim, 1998).

Chitin is the principal component of the hard exoskeletons of nearly a million species of arthropods (e.g. insects, lobsters, and crabs) as well as being present in the cell walls of fungi and many algae. In nature, it is probably the second most abundant polysaccharide, next to cellulose (Campbell, 2006). Chitin is used industrially in many processes. It is used in water purification, as an additive to thicken and stabilize foods, and in pharmaceuticals. It also acts as a binder in dyes, fabrics, and adhesives. Industrial separation membranes and ion-exchange resins can be made from chitin. Chitin's properties as a flexible and strong material make it favorable as surgical thread. Its biodegradibility means it wears away with time as the wound heals. Moreover, chitin has some unusual properties that accelerate healing of wounds in humans (Gupta et al., 2009). One of the most known and rich in the application chitin´s derivate is chitosan; which is produced commercially by deacetylation of the chitin. The degree of deacetylation in commercial chitosans is in the range 60–100%. In agriculture, chitosan is used primarily as a natural seed treatment and plant growth enhancer, and as an ecologically friendly biopesticide substance that boosts the innate ability of plants to defend themselves against fungal infections (Linden et al., 2000). Recently chitosan was used in bandages and other haemostatic agents because of its properties rapidly clot blood (Pusateri et al., 2003).

1.4.8 Hyaluronan

Hyaluronan (HYA) is an anionic, linear, unbranched, non-sulphated glycosaminoglycan composed of repeating disaccharides units (β-1-3 D-N-acetylglucosamine, β-1-4 D-glucuronic acid) (Figure 7).

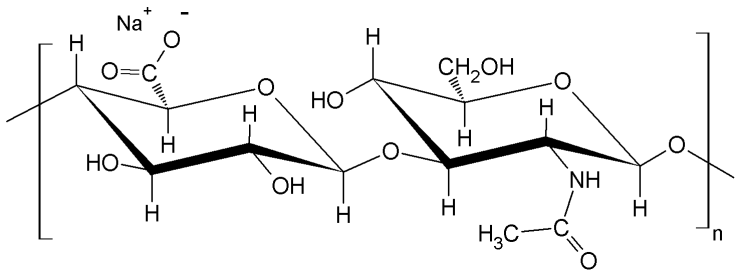

Figure 7: Hyaluronan disaccharide unit.

It is a naturally occurring biopolymer, which serves for important biological functions in bacteria and higher animals including humans. HYA in vivo exists as a polyanion and not in the protonated acid form (Hascall and Laurent, 1997). Only one kind of HYA exists, there are no sulfated, acetylated, phosphorylated or other variants of HYA. It is the archetypal glycosaminoglycan. Similar anionic glycosaminoglycans include the chondroitin, keratan and heparan sulfates. They by contrast, can exist in astronomical numbers of possible isomers, because their sulfate groups can be distributed along the polymer in many different ways (Hascall and Laurent, 1997). HYA is a water-soluble polysaccharide that produces a viscoelastic fluid (Jouon et al., 1995), but does not form a gel. HYA has a considerably greater ability to trap water than other polyelectrolyte polysaccharides. The water-binding capacity correlates with the molecular weight (Sutherland, 1998). The molecular weight of HYA covers the range from around a hundred thousand up to ten million Daltons (Kogan et al., 2007), and depends on their source and methods of isolation. Each disaccharide unit has a molecular weight of approximately 401Da (Lapcik et al., 1998). In general, depending on the HYA molecule size, it has extraordinarily wide range of biological functions. Larger matrix polymers of HYA are space-filling, anti-angiogenic, and immunosuppressive while the intermediate-sized HYA (from 25 to 50 disaccharide units) are inflammatory, immunostimulatory, and highly angiogenic; oligosaccharides are antiapoptotic. These low molecular weight oligosaccharides appear to function as endogenous danger signals and induce heat shock proteins (Kogan et al., 2007). It was suggested that all attendant properties and functions of HYA must inhere in its linear simplicity and chemical fidelity. HYA chains are simple and such perfection is unusual in biology. This suggests that, from an evolutionary point of view, it might have a protected status (Day and Sheehan, 2001). HYA is almost omnipresent however it occurs primarily in the extracellular matrix (ECM) and pericellular matrix; it is also present intracellularly, in the vitreous humour, in the umbilical cord, and in the synovial fluid. HYA together with heparin sulphate comprise the major fraction of the vertebrate ECM (Hedman

et al., 1979). Nuclear magnetic resonance confirmed the presence of extensive hydrogen-bonded structure in solution, in which each disaccharide unit is twisted through 180 degrees compared with those ahead and behind it in the chain. Two twists bring back the original orientation; thus this structure is a two-fold helix. The computer simulation study suggested that water played an important role in the structure stabilization (Scott et al., 1991). HYA is used in pharmacy, cosmetics and plastic surgery. HYA plays an important role in wound healing; it regulates the rate of epidermal proliferation and differentiation, both during the normal homeostasis in the skin as well as after cutaneous injury (Maytin et al., 2004). It is involved in tumor progression - in some cancers HYA's level correlate well with malignancy - thus it is often used as a tumor marker. It may also be used to monitor the progression of the disease. In clinical medicine HYA is used as a marker for other diseases as rheumatoid arthritis or liver pathologies (Kogan et al., 2007). Because of the HYA biocompatibility and biodegradability it is used as the biomaterial scaffold in the tissue engineering. There are other medical applications of HYA for example in ophthalmology, orthopedic surgery and rheumatology, otolaryngology, dermatology, cataract surgery, and pharmacology (Garg and Hales, 2004). HYA is also an information-rich system, its specific size fragments are informational because of the ability to interact with other cellular components (Stern et al., 2006; Stern and Jedrzejas, 2008).

1.4.9 Heparin and Heparan sulfate

The glycosaminoglycans heparin and heparan sulfate contain similar structural units in varying proportions providing considerable diversity in sequence and biological function. Both compounds are alternating copolymers of glucosamine with both iduronate- and glucoronate-containing sequences bearing *N*-sulfate, *N*-acetyl, and *O*-sulfate substitution (Mulloy and Forster, 2000; Nelson and Cox, 2004; Stern and Jedrzejas, 2008) (see Table 2).

Heparin is highly-sulfated glycosaminoglycan, with an average of 2.5 sulfates per disaccharide unit; it has the highest negative charge density of any known biological molecule (Cox and Nelson, 2004). Native heparin has molecular weight ranging from 3kDa to 50kDa (Mulloy and Forster, 2000). The main repeat unit of heparin structurally resembles the protein binding sequences in heparan sulfate, but contains higher percentage of sulfated residues. Unlike all other glycosaminoglycans, heparin is not associated with connective tissues or the ECM but is found in granules of mast cells in the mammalian tissues. When released into the blood, it inhibits clot formation by interacting with the protein antithrombin. Hence this glycosamonoglycan is also

utilized therapeutically as an anticoagulatiant. Heparin has an extended helical conformation. Charge repulsion by many negatively charged groups may contribute to this conformation. The glycosidic linkages in heparin appear relatively stiff. Heparin serves as a useful model for heparan sulfate (Humphries et al., 1999). Heparin sulfate has exactly the same component disaccharides as heparin but in different and very much more variable proportions. The unsulfated GlcA-GlcNAc sequence is the most common, with shorter IdoA-containing, sulfated *S*-regions (Lyon and Gallagher, 1998) of two to nine disaccharides separated on average by sixteen to eighteen mixed or *N*-acetylated disaccharides. It is often found embedded in cell membranes and, despite its name, is less sulfated than heparin. Further the heparin sulfate family of proteoglycans includes the syndecans (Carey, 1997), perlecans (Iozzo, 1998), glypicans (Filmus, 2001), and betaglycans (Cheifetz and Massague, 1989).

Table 2: The most common heparin and heparan sulfate disaccharides.

GlcA-GlcNAc	IdoA(2S)-GlcNS
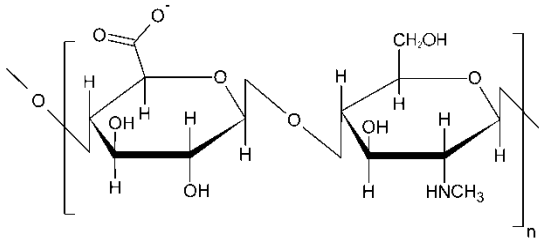	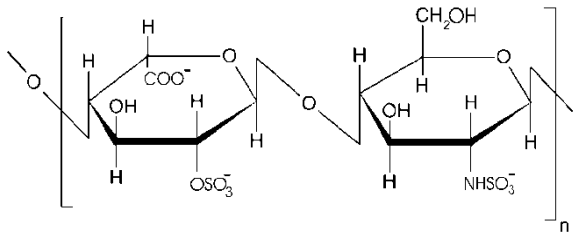
IdoA-GlcNS	**IdoA(2S)- GlcNS(6S)**
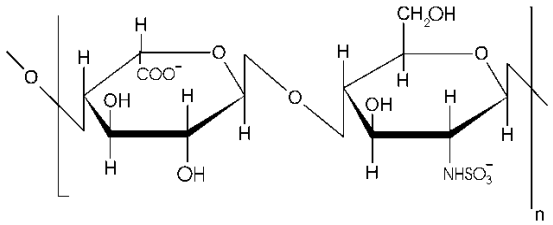	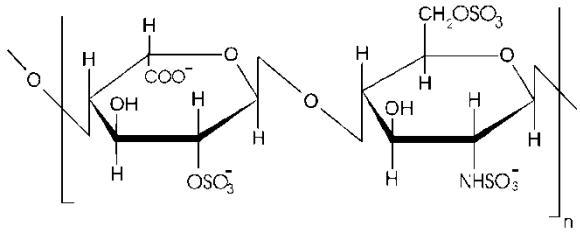
GlcA-GlcNS	**IdoA-GlcNS(6S)**
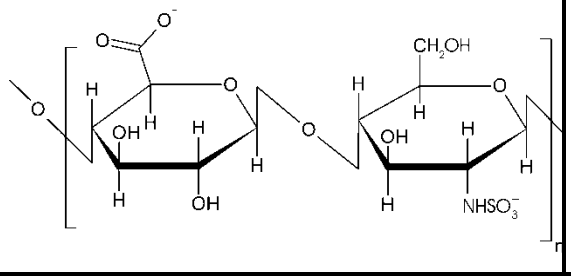	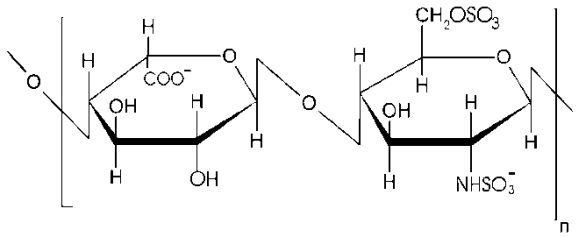

1.5 Intermolecular and intramolecular weak interactions in polysaccharides

Intermolecular interactions are as important in physics as in chemistry and the molecular biology. Weak interactions are responsible for the existence of liquids and solids in nature; determine the physical and chemical properties of gases, liquids and crystals, the stability of the chemical complexes, and the biological compounds. In the absence of intermolecular interactions our world would be a uniform ideal gas (Moore and Spencer, 2001). Certain structural characteristics such as chain conformation and intermolecular associations will influence the

physicochemical properties of polysaccharides. The native folding of polysaccharides in three dimensions follows the same principles as that governing polypeptide structure. The subunits with a more-or-less rigid structure form three-dimensional macromolecular structures that are stabilized by the weak interactions within or between the molecules. Common weak interactions are hydrogen bond, hydrophobic, and van der Waals interactions, and, for polymers with charged subunits, electrostatic interactions (Israelachvili, 1997). Because the polysaccharides have many hydroxyl groups, extensive hydrogen bonding has an especially important influence on their structure (Scott et al., 1991). Weak interactions are indistinctly classified and different authors use different subdivision. Here the most important weak interactions playing role in the polysaccharide stabilization and hydration are mentioned.

1.5.1 Electrostatic weak interactions

Electrostatic forces are in principle the classical Coulombic interactions between two charges. These interactions are the strongest of the physical forces - stronger even than some chemical binding forces (Israelachvili, 1997). Electrostatic interactions are strictly pair wise additive, highly anisotropic, and can be either repulsive or attractive (Moore and Spencer, 2001).

1.5.2 Van der Walls forces

The distortions of a molecule's charge distribution induced by the electric field of all the other molecules leads to induction forces that are always attractive and highly non-additive. These forces occur between the molecules of nonpolar covalent substances such as H_2, Cl_2, and noble gases. These forces are generally believed to be caused by a temporary dipole, or unequal charge distribution, as electrons constantly move about in an atom, ion, or molecule. At a given instant, more electrons may be in one region than in another region. The temporary dipole induces a similar temporary dipole on a nearby atom, ion, or molecule. Every instant, billions of these temporary dipoles form, break apart, and reform to act as weak electrostatic attractive van der Waals forces. It is important to note that van der Waals forces exist between all kinds of molecules. They are non-directional and hence posses only limited scope in the design of specific hosts for selective complexation of particular guests. Some molecules may have these forces, as well as other intermolecular forces. Van der Waals forces, however, are the only intermolecular bonds between nonpolar covalent molecules such as H_2, Cl_2, noble gases, and CH_4. The number of electrons in a substance increases as molecular mass (grams per mole of compound) increases. Therefore, the strength of the van der Waals forces between substances increases with increasing

molecular mass (Israelachvili, 1997; Brutschy and Hobza, 2000; Steed and Atwood, 2000; Moore and Spencer, 2001).

1.5.3 Dispersion (London) forces

The origin of this name i.e. dispersion forces, has to do with their relation to the dispersion of light in the visible and UV regions of the spectrum (Israelachvili, 1997). Dispersion interactions are always present, even between S-state atoms such as neon and krypton, carbon dioxide, and hydrocarbons. Although there are no electrostatic or induction interaction terms since all the multipole moments of both species are zero. Therefore the dispersion forces are the attractive component that results from the interactions between fluctuating multipoles (quadrupole, octupole etc.) in adjacent molecules. Dispersion forces play a role in a lot of important phenomena such as adhesion, surface tension, physical adsorption, wetting, the properties of gases, liquids, and thin films, the strengths of solids, the flocculation of particles in liquids, and the structures of condensed macromolecules such as proteins and polymers (Steed and Atwood, 2000). Dispersion forces are quantum mechanical in origin and can be described by quantum electrodynamics. Their origin may be understood intuitively as follows: consider the electronic charge cloud of an atom to be the time average of the motion of its electrons around the nucleus. The average cloud is spherically symmetric with respect to the nucleus, but at any instant of time there may be a polarization of charge giving rise to an instantaneous dipole moment. This instantaneous dipole induces a corresponding instantaneous dipole in the other atom and there is an interaction between the instantaneous dipoles. The dipole of either atom averages to zero over time, but the interaction energy does not because the instantaneous and induced dipoles are correlated and they stay in phase. Higher-order instantaneous multipole moments are also involved, giving rise to higher order dispersion terms. Dispersion forces are always present (Israelachvili, 1997). They are long-range forces and, depending on the situation, can be effective from large distances (greater than 10nm) down to interatomic spacing (about 0.2nm). Dispersion forces may be repulsive or attractive, and in general the dispersion force between two molecules or large particles does not follow a simple power law. Dispersion forces not only bring molecules together but also tend to mutually align or orient them. Further the dispersion forces are not additive; that is the force between two bodies is affected by the presence of other bodies nearby (Moore and Spencer, 2001).

1.5.4 Hydrogen bond

The hydrogen bond (Pauling, 1931) fundamental importance lies in its role in molecular associations. Its functional importance stems from both thermodynamic and kinetic reasons. The hydrogen bond is able to control and direct the structures of molecular assemblies because it is sufficiently strong and sufficiently directional (Desiraju and Steiner, 1999). The hydrogen bond plays a key role in chemistry, physics, and biology and its consequences are enormous. Hydrogen bonds are responsible for the structure and properties of water, an essential compound for life, as a solvent and in its various phases. Further, hydrogen bonds also play a key role in determining the shapes, properties, and functions of biomolecules (Scheiner, 1997; Desiraju and Steiner, 1999; Jeffrey, 2007).

The hydrogen bond is a non-covalent bond (attractive interaction) between the electron-deficient hydrogen and a region of high electron density (Hobza and Havlas, 2002). Most frequently, the hydrogen bond is of the X–H...Y type, where X is the electronegative element and Y is the place with the excess of electrons (e.g. lone electron pairs or π electrons). Hydrogen bonds having X,Y = F, O, and N are the most frequent and best studied (Scheiner, 1997; Desiraju and Steiner, 1999; Jeffrey, 2007). The X–H...π hydrogen bonds (for X = O and C) were also detected (Pribble et al., 1995; Djafari et al., 1997). The X–H...Y hydrogen bond stretches and correlates with the strength of the hydrogen bond. In the course of the X–H...Y type hydrogen bond formation the small amount of electron density (0.01–0.03*e*) is transferred from the proton-acceptor (Y) to the proton-donor molecule (X–H) (Hobza and Havlas, 2002). There are also hydrogen bonding interactions involving hydrogen atoms attached to carbon, rather than electronegative atoms such as N and O while these interactions are at the weaker end of the energy scale of hydrogen bonds, the presence of electronegative atoms near the carbon can enhance significantly the acidity of the C–H proton, resulting in a significant dipole. An elegant example of C–H…N and C–H…O hydrogen bonds is the interaction of the methyl group of nitromethane with the pyridyl crown ether (Steed and Atwood, 2000). The presence of the hydrogen bonds influences for example the Fourier transform infra-red spectra; this phenomenon is known as the red shift, the significance of this phenomenon correlates with the hydrogen bond strength (Hobza and Havlas, 2002). Hydrogen bond may be regarded as a particular kind of dipole-dipole interactions in which a hydrogen atom attached to an electronegative atom is attracted to a neighboring dipole on an adjacent molecule or functional group (Steed and Atwood, 2000). Hydrogen bonds come in an amazing range of lengths, strengths and geometries. The length of hydrogen bonds depends on

bond strength, temperature, and pressure. The bond strength itself is dependent on temperature, pressure, bond angle, and environment (usually characterized by local relative permittivity). The typical length of a hydrogen bond in water is 197pm (Legon and Millen, 1987).

Besides the intermolecular interactions of carbohydrates are dominated by extensive and cooperative O–H…O hydrogen bond networks and C–H…O hydrogen bonds are also formed in large numbers. The basic units of polysaccharides (i.e. monosaccharide) are well suited for hydrogen bonding. For example half the atoms of α-D-glucose can form strong hydrogen bonds (five –OH groups and the ring O atom) and the rest are moderately activated C–H groups. Such a molecular constitution leads to the formation of extended O–H…O hydrogen bond networks, which in general is a characteristic of all polysaccharides (Jeffrey and Saenger, 1991). In modified saccharides, hydrogen bonding groups are introduced or removed, altering the overall hydrogen bond properties. The simplest modification is a deletion of –OH groups leading to the deoxysaccharides, such as in the 2-deoxyribose of DNA. In deoxysaccharides, the O/C ratio is smaller than in the origin molecules and the average degree of C–H activation is lower. Some C–H groups may even become more or less unactivated. In the aminosaccharides, one or more –OH groups are replaced by amino or acetylamino groups. An important example is *N*-acetylglucosamine, which is the monomer building block of chitin and it is also part of hyaluronic acid disaccharide unit. Other common substituents are carboxylic acid functionalities, which are often deprotonated in the organism so that the saccharide becomes an anion. All these alterations to the strong hydrogen bonding groups also modify the characteristics of weak hydrogen bonds occurring in the system.

Using the neutron diffraction studies (Jeffrey, 2007) (Jeffrey and Saenger, 1991) the geometries of C–H…O hydrogen bonds in polysaccharides have been described. Based on 395 different C–H bonds in 30 crystal structures, it was found that about 34% of all C–H groups form intermolecular contact to O atoms with $d < 2.7$Å and $\Theta > 90°$. This high fraction is certainly associated with the high density of acceptor atoms in the system. The shortest contact occurs in sucrose, with $d = 2.27$Å and $\Theta = 166°$, and the bulk of distances d are longer than 2.4Å. This is clearly longer than the typical distances d observed with more activated C–H groups, but still it is clear that carbohydrates are rich in C–H…O hydrogen bonds. These C–H…O interactions, whatever their precise roles may be, are restricted to exist in a dense network of much stronger O–H…O hydrogen bonds and their directionality is too weak to compete successfully. Most of the

intermolecular C–H…O geometries, though, are well within the bonding regime. Because there are so many of these distorted but weakly bonding C–H…O interaction, the sum of their enthalpic contributions will be considerable and their omission is misleading (Desiraju and Steiner, 1999).

C–H…O hydrogen bonds in polysaccharides can be assumed to have dominant functions if there is a local lack of strong O–H…O competitors. An important example is the hydrophobic internal cavities of cycloamyloses. These cavities lack O–H donors and consequently, C–H…O hydrogen bonds often play significant roles in structure stabilization. Apart from weak host-guest interactions, cycloamylose also form intramolecular C–H…O hydrogen bonds. In native cycloamyloses, the orientation of neighboring glucose units is systematically stabilized by the interglucose hydrogen bond which is typical example of supportive C–H…O hydrogen bond (Desiraju and Steiner, 1999). Further in the case of cellulose where all the ring substituents are equatorial it is roughly ruler shaped, with the hydroxyl groups at the edges. The faces are formed by the axial ring H atoms and the O atoms O(4) and O(5) and are rather lipophilic in nature. Cellulose is polymorphic, but a feature common to all the polymorphs is O–H…O hydrogen bonding between the edges of the molecules and stacking of the faces. This leads to layered structures. In cellotetraose hemihydrate, a small molecule model for cellulose II, the molecules are stacked in such a way that systematic hydrogen bonds C(3) –H…O(4) and C(5) –H…O(4) are formed between the faces of molecules in adjacent layers (Gessler et al., 1995). The geometries of these hydrogen bonds are close to ideal, with the parameters d, D and Θ in the ranges 2.30–2.71Å, 3.38–3.73Å and 158–180°, respectively. The C–H…O(4) hydrogen bonds are presumably important in the fine-tuning of the stacking arrangement and it can be assumed that related interactions are formed in polymeric cellulose II (Desiraju and Steiner, 1999).

1.5.5 Hydrophobic interaction

Hydrophobic interaction is closely related to the hydrophobic effect (Steed and Atwood, 2000). In fact, it describes the unusually strong attraction between hydrophobic molecules or hydrophobic molecular moieties in water. The hydrophobic interaction is an entropic phenomenon, which arises primarily from the rearrangements of H-bonds configurations in the overlapping hydration zones as two hydrophobic species approach (Israelachvili, 1997). These interactions have also significant importance in the hydration of some polysaccharides or their parts because of the so called hydrophobic hydration, which is related to the interactions of apolar sites and water. Due to the small size of water molecules and flexibility of their spatial arrangement, an increase in the

chemical potential of the solute is achieved. Additionally, strong temperature dependence in the enthalpy of the system from exothermic at low temperatures to endothermic at high temperatures is also attained. Further, larger negative entropy of mixing as compared to the formation of a hypothetical ideal solution is obtained. The additional the decrease in the partial molar volume is achieved because the hydrophobic molecules fit into cavities in the water network (Mikheev et al., 2007). Due to the multiple van der Waals interactions between water and the hydrophobic species, the hydrophobic hydration is accompanied by reduction in density and negative enthalpy change which causes positive heat capacity change. Further, due to the increased order in the surrounding water of the hydrophobic species the negative entropy change is achieved (Gutmann, 1991).

2 STATE OF THE ART

2.1 Hydration of polysaccharides

It is generally taken as granted that water is essential for life. It is the simplest compound of the two most common reactive elements, consisting of just two hydrogen atoms attached to a single oxygen atom. Liquid water, however, is the most extraordinary substance. For example there are sixteen polymorphic forms of ice and three amorphous (non-crystalline) phases of water (Zheligovskaya and Malenkov, 2006). Even if water is that simple molecule, it is the most studied material on Earth. Understanding the behavior of water molecules interacting with the polysaccharides, or complex biological macromolecules in general, in aqueous solution has been a subject of intense research for a long time (Sherman, 1983; Fringant et al., 1996; Liu and Yao, 2001; Chaplin, 2006; Hatakeyama et al., 2010). Nevertheless, there are plenty of questions to be answered concerning this issue. In fact, the internal structure, phase transitions, and generally the physico-chemical properties of polysaccharides are affected by water molecules present in their structure. Hydration is a general term concerning the amount of water molecules affected by the polysaccharide presence, those water molecules are known as the hydration shell(s). In these water hydration shells the hydrogen bond network is locally disrupted and differs more or less significantly from those in the bulk water. There are number of approaches to describe and quantify hydration shells and affected water molecules, but in this work only some of them are mentioned. Therefore the bibliographic research is not comprehensive, but the main goal is to summarize the most important facts and studies which have been published regarding the polysaccharide hydration. Most of the analytical techniques applied to study hydration of polysaccharides have either intrinsic or practical limitations. Therefore, a combination of techniques is necessary. For this reason, in this work, the attempt is paid to combine and discuss the application of two apparently different methods such as thermal analysis and nuclear magnetic resonance (NMR) relaxometry, and bring more complex view on aspects of the polysaccharide hydration.

2.1.1 Thermal analysis

One of the simplest thermoanalytical approaches to study the polysaccharide hydration defines the hydration shells water as “non-bulk” water. Non-bulk water can be divided into “bound water”, subcategorized as being capable of freezing or not (Wolfe et al., 2002). “Unbound water” freezes at the same temperature as normal water (less than 0°C depends on the cooling rate). However

some water may take up to 24 hours to freeze since crystallization is a kinetic phenomenon. “Bound freezable water” freezes at lower temperature than normal water, being easily supercooled. It also exhibits a reduced enthalpy of fusion (melting). The inability to freeze is often used to determine the amount of bound water. Although freezing may not be a good measure of hydration as it concerns also the water content which upon cooling occurs in the glassy state. In the glassy state the conformational changes are severely inhibited and the material is metastably trapped in a solid, but microscopically disordered state (amorphous phase). The segmental motion of macromolecules occurs when the temperature increases through the glass transition temperature. The glass transition temperature value depends fairly on the method of its determination. The glass transition, unlike phase changes, occurs over a range of a few Kelvin. The non-freezing water trapped in a glassy state lowers diffusion by several orders of magnitude and hinders the crystal formation. In practical experience, the effects of water on polysaccharide and polysaccharide on water are complex and become even more complex in the presence of other materials, such as for example salts. Water competes for hydrogen bonding sites with intramolecular and intermolecular hydrogen bonding and determines the polysaccharide’s flexibility and the carbohydrate's preferred conformation(s) (Kirschner and Woods, 2001).

The most common thermoanalytical technique used in the hydration shells characterization is Differential Scanning Calorimetry (DSC); it is a technique in which the temperature or heat capacity of the sample is monitored as a function of the chosen temperature regime (Brown, 2001; Haines, 2002; Wunderlich, 2005). The DSC approach has been used by many research groups. In general, all authors are using similar nomenclature and differentiation - the first order phase transition of water fraction closely associated with the polymer matrix cannot be observed. Thus, this fraction is called “non-freezing water”. Water associated with non-freezing water - which exhibits melting/crystallization, shows considerable supercooling, and significantly smaller enthalpy than the bulk water - is referred to as “freezing-bound water”. The sum of the freezing-bound and non-freezing water fractions is the “bound water content”. It has been demonstrated that the bound water content depends on the chemical and high-order structure of each biopolymer. Water, which melting/crystallization temperature and enthalpy are not significantly different from those of normal (bulk) water, is called “free water”. This approach was used for example to investigate the interaction of hydrophilic polysaccharides with water by Hatakeyama and Hatakeyama (1998) (Hatakeyama and Hatakeyama, 1998); further in the case of ionic and neutral polysaccharides such as alginate (Fringant et al., 1996) (Nakamura et al., 1991); arabic gum

(Phillips et al., 1996); and mono-, di-, and trivalent cations in polyelectrolytes alginic acid (Hatakeyama et al., 1995); chitosan (Ostrowska-Czubenko and Gierszewska-Druzynska, 2009); cellulose (Hatakeyama et al., 1987; Berthold et al., 1994; Takahashi et al., 2000; Hatakeyama et al., 2007); lingo-cellulose (Berthold et al., 1996); polysaccharide gellan gum (Quinn et al., 1993); hyaluronan (Joshi and Topp, 1992; Yoshida et al., 1992; Yoshida et al., 1992; Takigami et al., 1993; Hatakeyama and Hatakeyama, 1998); hyaluronan derivative hylan (Takigami et al., 1993; Takigami et al., 1995); starch (Yuryev et al., 1995); xanthan hydrogels (Quinn et al., 1994). All above mentioned studies are using the same approach - simply after the melting peak integration in the DSC record, the melting enthalpy of freezable water is obtained. This obtained enthalpy of melting is normalized to the mass of the dry sample. Then the normalized enthalpy of melting is plotted as a function of the respective water content. In this way, the linear dependency is obtained and the x-intercept is equal to the non-freezing water content in the polysaccharide water system.

The water content (W_C) is defined as follows (Equation 1):

W_C = mass of water/mass of dry sample, g_{H20}/g_{HYA} (Eq1)

And follow expressions (Equation 2) is assumed:

$$W_C = W_f + W_{fb} + W_{nf}, \quad \text{(Eq2)}$$

where W_f is the amount of free water, W_{fb} is the freezing bound water amount and W_{nf} is the amount of non-freezing water. This approach was adopted and extended by Liu and Cowman (2000) (Liu and Cowman, 2000), using Temperature Modulated DSC for freezing and melting of water in semi-dilute solutions of the polysaccharide hyaluronan. The expression for the determination of non-freezing water and potentially also freezing-bound water were extended; the value of non-freezing water of $0.6g_{H20}/g_{HYA}$ and the value of freezing-bound water of $44g_{H20}/g_{HYA}$ were determined in the hyaluronan semi-diluted solution (Liu and Cowman, 2000). This approach was lately adopted by Prawitwonga et al. (Prawitwong et al., 2007) who investigated the phase transition behavior of sorbed water in Konjac mannan using DSC. Six types of adsorbed water together with glassy water were identified in Kojac mannan water system: non-freezing water, four types of freezing-bound water, and free water. Glassy water was closely related to non-freezing water and the amount of glassy water was influenced by the cooling rate. The proportion of each adsorbed water type changed with the increasing water content. The equivalent value of non-freezing water per pyranose ring was ca. 5.2 (mol/mol). Three freezing-bound water layers were influenced by interaction with the Kojac mannan matrix at lower water content regions and were

transferred to free water in the high water content regions. The last freezing-bound water was strongly bound water, maintaining interaction with Kojac mannan chains even in the high water content region; the equivalent value of this freezing-bound water per pyranose ring was ca. 1.4 (mol/mol). Most of the adsorbed water in the system with high water content was held as free-water-like behaviour.

The structure of the water molecules absorbed in different hydrophilic polymers was studied by the means of DSC and Fourier transformed infra-red (FTIR) spectroscopy (Ping et al., 2001). In that study Ping et al concluded that the average number of non-freezing water molecules per site depends on the chemical nature of the polar site - ca. 1 water molecule for a hydroxyl, and 4.2 water molecules for an amide group. For a polymer with carboxylic site, the number of the water molecules increase with increasing size of the counter-ion. It was concluded that the absorbed water in hydrophilic polymer develops two types of hydrogen bounds. One of them corresponds to water molecules directly attached to the active site of the polymer to form the first hydration layer (non-freezing water). The second one corresponds to the water molecules in the second hydration layer. It was observed that this second hydration layer is present in the polymer/water system even at low water content. Meaning that the second hydration layer can be formed on certain sites before all the polar sites are saturated with water molecules. Therefore Ping et al concluded that non-freezing water did not consist exclusively of water molecules from the first hydration layer (Ping et al., 2001).

Recently Hatakeyama et al. (Hatakeyama et al., 2010) concluded that the freezing bound water, detected as cold crystallization in DSC heating curve, plays a crucial role in blood compatibility and suggested that the presence of freezing bound water can be utilized as an index of biocompatibility for polymers. Further, after comparing the data of equilibrium water content for different biopolymers it was suggested that the amount of non-freezing water can be used as an index of the hydrophilicity (Hatakeyama et al., 2010).

Lately, the cooling/thawing DSC approach was criticized by Gemmei-Ide et al.; the criticism was mostly based on difference between the DSC and FTIR spectroscopy results. In this case poly(n-butylacrylate) was used and hydrated by exposing to air with a constant relative humidity. Authors stated that same part of water in hydrated sample cannot be in principle observed and called it thermally latent water. The authors concluded that this water condensates and sublimates

during the cooling and heating cycle respectively and the actual non-freezing water content is much smaller, than estimated from traditional DSC approach (Gemmei-Ide et al., 2010).

Another thermoanalytical approach is based on the water vaporization. The advantage of this approach is outflow of the phase transition temperature limitation. Vaporization of bound water associated with cellulose fibres of natural (cellulose I) and regenerated cellulose (cellulose II) was investigated using DSC in both dynamic and static conditions by Hatakeyama et al. It was found that vaporization peak is split into two peaks; one occurs around 60°C and the other around 120°C. The high temperature vaporization peak is related to the structural change of the cellulose amorphous chains in the course of the bound water desorption (Hatakeyama et al., 2000). Lately, the heat of water evaporation associated with cellulose fibers was studied using the traditional (Park et al., 2007) and modulated DSC (Park et al., 2006). The samples were the wood cellulose fibers at different moisture ratios. It was observed that the non-freezing bound water content was constant for moisture ratios greater than 0.3 g/g and decreased with decreasing moisture ratio below this value. This phenomenon demonstrates that freezing bound water is removed first during the drying of cellulose fibers followed by non-freezing bound water. Analysis of the pore size distribution confirms that below $0.3 g_{H20}/g_{Cellulose}$ moisture ratio only the non-freezing bound water exists (with no freezing bound water remaining). Further by the use of temperature modulated DSC, for wood cellulose fibers in the moisture ratio of $0.0–0.3 g_{H20}/g_{Cellulose}$ the steep increase in the heat of vaporization was observed. This indicates that additional energy is required to evaporate the water directly interacting with the cellulose fibres (non-freezing water). This additional energy may be attributed to energy which is required to break the mono/multilayer sorption of water molecules and also energy to overcome capillary forces in the porous geometry of the cellulose fibers (Park et al., 2007).

2.1.2 Nuclear magnetic resonance techniques

NMR spectroscopy is an analytical technique based on the phenomenon of nuclear resonance, which occurs when the nuclei are embedded in a static magnetic field and exposed to a second oscillating magnetic field (i.e. radiofrequency pulses). The interaction between the magnetic fields and matter produces spectra from which the structure and the conformation of organic and inorganic materials can be achieved (Rabenstein and Guo, 1988). Although NMR spectroscopy is very versatile for structural evaluation of organic compounds, it is not suitable for the study of the hydration water in vicinity of polysaccharides. In fact, traditional NMR requires use of diluted

solutions with deuterated solvents which prevent observation of water hydration shell. Nevertheless, such information can be acquired from the relaxation character of the observed system. In fact, if the sample is allowed to be undisturbed for a long time in the magnetic field, it reaches a state of thermal equilibrium. It means that the spins populations are given by the Boltzmann distribution at a given temperature. Obviously, radiofrequency pulses disturb the equilibrium of the spin system. Spin populations after a pulse deviate from their thermal equilibrium values and, in many cases, single-quantum coherences are created. Relaxation is the process by which equilibrium is regained, through interaction of the spin system with the molecular environment. There are two types of relaxation processes occurring simultaneously. First, spin-lattice relaxation (longitudinal relaxation) is concerned with the movement of spin populations back to their Boltzmann distribution values which in the case of spins ½ system (nuclei as ^{1}H, ^{13}C, ^{15}N etc) is characterized by spin-lattice relaxation time constant T_1 and this process has an enthalpic character. Second, spin–spin relaxation (transverse relaxation) is concerned with the decay of single-quantum coherences which in spins ½ system is characterized by transversal relaxation time constant T_2 and on the other hand this process has an entropic character (Levitt, 2007). To gain such knowledge about the observed system, essentially two types of the NMR techniques can be applied. Rather long time known time domain (TD) NMR and, an innovative NMR technique developed in the last decades, fast field cycling (FFC) NMR relaxometry. Both techniques are using relatively low magnetic fields B_0 (up to 1T) as compared to the traditional NMR spectroscopy (up to approximately 23.5T). It is important to point out the increasing of NMR signal sensitivity with increasing of applied magnetic field B_0 and vice versa. But notwithstanding the resolution-less of FFC-NMR relaxometry and TD-NMR, these techniques do not require sample dilution and deuterated solvents, thereby allowing direct observation of water hydration shells in water/polysaccharide solutions.

The TD-NMR has been used to study the proton transverse relaxation time T_2 in water systems with several polysaccharides such as dextran, schleroglucan, sodium κ-carrageenan, maltoheptose, hydrolyzed starch, and amylase (Hills et al., 1991), sucrose and xylose (Hills et al., 2001), starch (Le Botlan et al., 1998; Ritota et al., 2008) dextran sulfate, chondroitin sulfate, heparin, and xanthan (Lusse and Arnold, 1998), hyaluronan (Barbucci et al., 2006), proten-polysacharide (Ducel et al., 2008), starch (Hansen et al., 2009), methyl cellulose (Rachocki et al., 2006), hydroxyehylcellulose and carboxymethylcellulose sodim salt (Capitani et al., 2003).

While TD-NMR is operating at one proton Larmor frequency ω_L, the FFC-NMR relaxometry operates at extent range of frequencies from 10kHz up to 40MHz. As a result, dependence of T_1 longitudinal relaxation time constants (or equivalently of relaxation rates $R_1=1/T_1$) as a function of ω_L is obtained which is also referred to as nuclear magnetic relaxation dispersion (NMRD) (Redfield, 1957). Both techniques appear to be very sensitive to water molecules, because when solute interacts with the solvent (water), mainly due to dipolar interactions, translation and rotational motion of water molecules become slower and proportionally their relaxation time constants decrease. And thus the information about the structure and dynamics of solvents in proximity to solutes can be obtained (Kimmich and Anoardo, 2004).

In comparison to TD-NMR the advantage of FFC-NMR relaxometry is the possibility of isolating typical relaxation features associated with molecular processes characterized by very long correlation time τ_c. In a liquid, the correlation time τ_c corresponds to the rotational correlation time of the molecules τ_r (Levitt, 2007). The rotational correlation time is given by the average time taken for the molecules to rotate by 1rad, thus depends on the molecule size. Generally, small molecules have short rotational correlation times, whereas large molecules have long rotational correlation times.

Majority of the FFC-NMR relaxometry studies have been done on protein-water system, therefore also the nomenclature and derived theories are influenced by this fact. Indeed, in aqueous biopolymer solutions there are at least four pools of protons to be considered: (i) protons of bulk or weakly bound water molecules which is described by rotational correlation time τ_c values of the order of 10ps or less, (ii) “translationally-hindered water” characterized by τ_c, in the nanosecond time scale, (iii) irrotationally bound water with the τ_c value comparable to that of the biopolymer (from about 10μs to 10ns or less), and (iv) internal water buried inside the biopolymer with residence times in the range 1ns–0.1ms (Dobies et al., 2009). Furthermore, other two pools of proton can be define - exchangeable biopolymer protons and non exchangeable biopolymer protons (Hills, 1992). However, recently, more general nomenclature for hydration water layers was used - network water (NW) which is the water fractions closely associated with the polymer matrix, further the intermediate water (IW) representing the water molecules which are not directly interacting with the polymer and multimer water (MW) which resemble dynamics of pure water (Matteini et al., 2009). Nevertheless, FFC-NMR relaxometry and TD-NMR are techniques that, in general, do not allow easily distinguish between the different pools of protons, because each of

them is contributing to the overall decay of the signal according to its relative intensity and relaxation properties.

For NMRD profile evaluation, where the water proton relaxation is dominated by homonuclear dipole-dipole interaction, multi-Lorentzian function can be used (Equation 3):

$$J(\omega) = \sum_{n=1}^{N} A_i \frac{\tau_{c,i}}{1 + (\omega_L \tau_{c,i})^2} \qquad \text{(Eq3)}$$

Where ω_L is proton-Larmor frequency [MHz], τ_c is the correlation time [s] and A is relative amplitude. The number of terms N that can be included in eq. 3 is determined by a Merit function analysis, usually a sum of three Lorentzians is sufficient (Halle et al., 1998). On the other hand, when TD-NMR decay curves are evaluated, simple multi-exponential decay function is used (Equation 4).

$$F(t) = \sum_{i=1}^{n} A_i \exp\left(-\frac{t}{T_{2,i}}\right) \qquad \text{(Eq4)}$$

Where A is amplitude, t [s] is time and T_2 [ms] is spin-spin relaxation time. Number of components depends on statistical parameters like χ^2, standard error and R^2.

FFC-NMR relaxometry has been also used to extract the value of the hydration water correlation times in systems such as bovine serum albumin (Zhou and Bryant, 1994; Calucci and Forte, 2009), casein (Godefroy et al., 2003), bovine proteins (Van-Quynh et al., 2003) proteons (Bertini et al., 2000; Luchinat and Parigi, 2008), protein bacteriorhodopsin (Gottschalk et al., 2001), cyclic protein oxytocin and the globular protein BPTI (basic pancreatic trypsin inhibitor) (Modig et al., 2003). Further this approach has been also used to extract the value of hydration water correlation times in systems such as polysaccharide-protein conjugate vaccines (Berti et al., 2004), agarose gel (Chavez et al., 2006) and human protein HC (Dobies et al., 2009).

3 MAIN RESEARCH QUESTIONS

Principal purpose of this work is to reveal the relationship between the hydration of polysaccharides (by chosen representative hyaluronan) and their conformation, and possibly shed more light on the mechanisms of their hydration and dehydration with respect to dynamics and nature of their supramolecular arrangement. Thus the work in this thesis is centred on two main tasks.

- The first one is the hydration characteristics in terms of hydration shells quantification and characterization in semi-diluted and diluted systems. The main question is how the hydration influences the physical structure of the polysaccharide and what are the properties of the water hydration shells in hyaluronan. The most widely applied technique is DSC which has several limits associated for example with non-equlibrium experimental conditions. The open question still is if those issues are crucial in understanding of polysaccharide hydration and if results obtained with DSC are comparable with other techniques using different principles and working under equilibrium experimental conditions.
- The second task is to understand and briefly test the hypothesis which comes out from knowledge about the processes associated with dehydration (drying) of the semi-diluted polysaccharide system. It is matter of fact that the supramolecular structures of polysaccharides are significantly different in solid and liquid state. We assume that the understanding of processes occurring in semi-solid or highly concentrated solutions representing a border between solid and liquid state are crucial for designing of “intelligent” structures in solid state. Those structures might be for example systems with slower kinetics of hydration and dissolution which are traditionally accomplished with a chemical modification of native polysaccharides.

4 OVERVIEW OF RESULTS AND DISSCUSION

In this part an effort is paid to summarize and comment the data which have been either already published or submitted in form of the scientific paper. The data are mostly dealing with the hydration of hyaluronan which was chosen as a model polysaccharide because of its popularity, importance, and unique physical properties. We assume that the obtained results and developed approaches can help to understand the behaviour of other polysaccharides. In the first part, we focused our attention on the DSC traditional approach (Liu and Cowman, 2000; Hatakeyama, 2004) useful for the study of hydration of (bio)polymers or small organic molecules. This approach allows the categorization of hydrating and non-hydrating water into different classes according to its physical properties. As it has already been mentioned, the first water fraction, which is in intimate contact with HYA and does not freeze, is called “non-freezing water" (NFW). Hypothetical next hydration layer is a water fraction associated with non-freezing water, this hydration shell exhibits melting/crystallization, shows considerable supercooling, and significantly smaller enthalpy than the bulk water and it is referred to as “freezing-bound water”. The third fraction is free water which has properties resembling the bulk water. Last two water fractions can be detected as ice crystallization or melting peaks on DSC record. (See part 2.1.1) After the integration of the melting peak, the water melting enthalpy is obtained. That is first normalized dividing by the mass of the dry HYA and then plotted against the respective water content - W_C (g_{H20}/g_{HYA}). In this way, the NFW content is determined from the x-intercept of the linear dependency. It is worth mentioning that this approach is the only way how to compare all data, obtained for different water contents. Other approaches of enthalpy normalization suggested by other authors (Pekar, 2012), such as normalization to the water content would bring errors into the calculations since the amount of freezable water is not known. Similar problem would appear if obtained melting enthalpy would not be normalized; then the data would be biased by the fact that the dry mass of HYA at different water contents is not constant and it is changing irregularly. Using above-mentioned approach the amount of NFW, $0.8g_{H20}/g_{HYA}$, was obtained (Appendix 1). However, it is worth to mention that there are several factors that complicate the analysis and interpretation of data obtained with the DSC cooling/thawing traditional approach, namely the character of water which is the substance forming polymorphic and polyamorphic structures (Bai and Zeng, 2012). Therefore the resulting structure of the ice formed during DSC experiment depends on the way of the HYA solution and perhaps also on dry HYA preparation, water content and experimental conditions such as cooling/heating programme. Those problems can be partially

solved by the application of extremely slow cooling rate accompanied with very long isotherm conducted at subambient conditions. However, as suggested by other authors (Wolfe et al., 2002), such isothermal period can last for several days which is unsustainable from the experimental point of view.

Therefore, in order to avoid problems with ice heterogeneity; we extended the traditional approach by determination of the enthalpy of water evaporation from highly concentrated HYA solutions. This approach has the only limitation caused by the high evaporation enthalpy of water ($2250 Jg^{-1}$). In other words, in the case of higher water content the amount of heat necessary for water elimination can exceed the limits of the DSC instrument and give an experimental artefact. However, in the present work this limit was out of the concentration area of interest. It was shown (Appendix 1) that in the course of water evaporation from a HYA solution a linear dependency of evaporation enthalpy normalized by dry mass was abruptly interrupted at W_C=0.34g_{H20}/g_{HYA}. This revealed that at this particular water content the evaporation from HYA is compensated by another processes associated with heat release, which we assumed being the enthalpy associated with formation of weak interactions in HYA supramolecular structure. Put simply, during the drying the entropy of the system decreases, at the same time new interactions - resembling processes of crystallization - were hypothesized being formed (for details see Appendix 1). In order to understand the influence of the Na^+ ions present in the hyaluronan structure on this process, the H^+ form of hyaluronan was tested as well and showed significant influence on its value, i.e. it was detected at 0.84g_{H20}/g_{HYA}. The second factor influencing slightly the value of the linear dependency interruption was the molecular weight of hyaluronan - approximately above 1MDa the value slightly increased. The existence and value of the linear dependency interruption was confirmed in other work (Appendix 2) when the enthalpy of evaporation/desorption was determined at selected degrees of conversion for water evaporated from hyaluronan semi-diluted solutions. For this purpose the Kissinger-Akahira-Sunose integral linear isoconversional method was used. The subtraction of the baseline which was the enthalpy of evaporation of pure water showed that such a compensation process is not strong enough to overbalance the enthalpy of evaporation. This indicated that interaction between water and hyaluronan is stronger than between two water molecules which explains the good solubility of hyaluronan in water but still does not perfectly explain the character of presumed interactions. This issue was later investigated in Appendix 6. The dynamic character of molecular motion observed during the drying let us to conclusions that the way of HYA drying is crucial for the resulting HYA physical structure and

physical-chemical properties such as for example stability, water holding capacity, and solubility. Those assumptions are also tested in Appendix 6.

Further, the knowledge of the NFW content was used to determine the content of "freezable water" (FW) in each sample by simple subtracting of NFW from total water content in the sample. Than the enthalpy measured by DSC was divided by freezable water content. Finally the dependence of freezable water melting enthalpy on the W_C was obtained. It was observed that at low W_C, the melting enthalpy was significantly lower than the enthalpy of the ice (hexagonal) formed by pure water ($334 Jg^{-1}$). The value of pure water melting enthalpy was reached around W_C=2g_{H20}/g_{HYA}, for higher values of W_C the value of water melting enthalpy stayed constant at around 334 Jg^{-1}. The value of $334 Jg^{-1}$ would indicate that from the point of view of DSC measurement, in solutions with W_C>2, there exist only two kinds of water structures; non-freezing water (NFW) and freezable water (FW). This observation is in contrast to the results published by Liu and Cowman (Liu and Cowman, 2000) who assumed the existence of the third water fraction - "freezing-bound water" (FBW) as high as 44g_{H20}/g_{HYA}. Based on the results in Appendix 1 and 2, we have suggested that instead of conventional one hydration number a range of hydration numbers reflecting structural changes and dynamic conformational states of polysaccharides should be used. The reason for the lower melting enthalpy of water in semi-diluted systems (reported by some authors as freezing-bound water) can be explained by several factors. First, the surface of HYA is rich in polar functionalities which influences the water mobility and thereby hinder the formation of the "perfct" hexagonal ice crystals. Second, the presence of cavities and pores in the hyaluronan dry structure can be the reason for the water restriction (see microscopy Figures in Appendix 6). It is well known that the water structure in cavities changes its character with respect to the cavity size, geometry, and wettability of its surface (Chaplin, 2010). Thus, water distributed in different either separated or connected or both pores is assumed. The amount of water in the pore is not always high enough to form nuclei for non-disturbed water crystallization. When the critical mass of water in the sample is reached, the collapse of the pores occurs, and the water from the pores is mixed with the bulk water as reported in Appendix 2. Thus only two types of water (non-freezing water and bulk water) can be seen on the DSC record.

The hypothesis about the influence of pores and cavities on water properties was tested in the study dealing with the hydration of acylated HYA derivatives (Appendix 3). The derivative was prepared from the sodium salt HYA by acylation with the hexanoic anhydride in the dimethyl sulfoxide/water mixture. Indeed, one of the HYA derivatives showed a second ice melting peak

occurring at unusually high temperature range from 0 to 25°C. This observation was explained as the presence of two types of domains (pores) in the acylated hyaluronan derivative, i.e. with either hydrophilic or hydrophobic surfaces. In principle, the pore size, and wettability, influences the physical properties of the encapsulated water which in turn causes anomaly high melting temperature of the formed ice. It was reported that there exist two principally different ways of water binding in HYA hydrophobicized derivative reflected by two different crystallization/melting mechanisms. The first type of water binding resembles the ordinary hydration of polar sites of HYA. Second type of water binding is probably associated with the presence of confined water (Appendix 3). Nevertheless, the linear dependency of melting enthalpy (obtained from the first melting peak) normalized by dry mass was observed again similarly as in the case of native hyaluronan.

The cooling/thawing approach of hydration study was tested also on the other system which completely differed from the polysaccharide/water system, i.e. on humic, and fulvic acids/water systems (Appendix 4). Unlike other tested biopolymers, linear dependency of melting enthalpy on water content was observed only in the case of hydrophilic fulvic acids while some of humic acids, which are more hydrophobic, showed non-linear behaviour and other anomalies. In the latter case, the step-like way increase of melting enthalpy with increasing water content was observed. Such behaviour implied a preservation of original hydrophobic scaffold during the wetting and consequent swelling, and hydration of the structure. However due to existence of one broad melting peak it can be stated that the cavities are connected and not separated (unlike in the case of hydrophobicized hyaluronan, Appendix 3). The progressive decrease in the ice melting enthalpy revealed that the hydration of humic, and fulvic acids takes 21 days which is in contrast to hyaluronan which took only several hours (Appendix 4).

The results obtained by methods of thermal analysis provided data obtained under non-isothermal conditions. Depending on the experimental conditions, the hydration is a parameter which reflects the adsorption of water on the surface of a biopolymer or its condensation in the pores formed by a biopolymer. It is a matter of fact that during the hydration of HYA some conformation changes occur and these changes are altering the HYA sorption capacity. Thus the obtained hydration number cannot be related to the adsorption isotherm known from classical experiments in which the stable surface, not changing during the sorption, is assumed. It should be understood as a number reflecting the dynamic character of the conformation changes occurring in the temperature range of the experiment. Therefore the use of a technique operating at ambient and

isothermal conditions, such as nuclear magnetic resonance (NMR), was an appropriate choice. Such a technique does not require extrapolation of observations made at temperatures far from the point of interest as is often done in the case of methods of thermal analysis. Besides, it is well known that the nuclear spin relaxation times - the spin-lattice relaxation time (T_1) and the spin-spin relaxation time (T_2) - of hydrogen nuclei within water molecules are determined by the detailed dynamics and chemical and physical environment of the water (Shapiro, 2011). Consequently, the measurement of proton nuclear spin relaxation times provides information on polymer-water interactions and water dynamics in such a system. Therefore, the time domain (TD-NMR) and fast field cycling (FFC-NMR) techniques were used. TD-NMR was used to measure transversal (T_2) relaxation time in semi-diluted HYA/water system (Appendix 6) and FFC-NMR relaxometry technique was used to study water dynamics and consequently the conformational properties of HYA in diluted aqueous solutions (Appendix 5). The results reported in Appendix 5 revealed that, irrespective of the solution concentration (i.e. 10–25mg L^{-1}), three different water proton pools (hydration layers) surround HYA. Based on the determination of correlation times, the inner layer consists of water molecules strongly retained in the proximity of the HYA surface. Due to their strong interactions with HYA, water molecules in this inner hydration layer are subject to very slow dynamics and have the largest correlation times. The other two hydration layers are made of water molecules which are located progressively further from the HYA surface. As a result, decreasing correlation times caused by faster molecular motion were measured. The NMR dispersion (NMRD) profiles obtained by FFC-NMR relaxometry also showed peaks attributable to ^{1}H-^{14}N quadrupole interactions. Changes in intensity and position of the quadrupolar peaks in the NMRD profiles suggested that with increasing concentration the amido group is progressively involved in the formation of weak and transient intramolecular water bridging adjacent HYA chains (Appendix 5).

The aim of the last paper (Appendix 6) reported in this thesis was to test hypothesis developed in previous papers and to test the consistency between TD-NMR and DSC results. First, it was shown that DSC and TD-NMR provide comparable data. Further, by the use of TD-NMR, it was find out that NFW content determined with DSC consists of two water pools which are distinct in terms of relaxation rate. Second, the appearance of a new proton fraction indicated that this is the water content corresponding to the plasticisation point of HYA and clarified the process observed and discussed in Appendix 1 and Appendix 2. In fact, during the drying the glass transition temperature shifts into the lower values because water acts as plasticizer in hydrophilic polymers.

When the plasticisation point is reached the heat capacity of the system suddenly decreases which causes the break in the dependence of evaporation enthalpy. As tested in other study, using other polysaccharides, this is the only case of hyaluronan. Other polysaccharides such as chitosan, schizophyllan, cellulose, and carboxymethyl cellulose do not show the plasticisation point in the same concentration range as hyaluronan (Mlčoch and Kučerík, 2013).

Last, the hypothesis of the possibility to influence the physical structure of native hyaluronan during drying in order to obtain unique structure of native polysaccharide suggested in Appendixes 1 and 2 was tested as well (Appendix 6). The motivation is to avoid any chemical modification of native HYA in order to prepare a modified structure having adjustable properties such as wetting, hydration kinetics, and dissolution using only native biopolymers. This might be achievable by manipulation of weak interactions stabilizing the flexible and unique supramolecular structure of HYA. In this study, HYA samples were prepared under three different drying conditions yielding the original, the freeze-dried, and the oven-dried HYA sample. It was demonstrated that the oven-dried sample has the fastest hydration kinetics whereas the HYA precipitated using isopropylalcohol has the slowest hydration kinetics. Based on the glass transition temperature, it was observed that the sample prepared by freeze-drying was the most rigid while the oven-dried sample had the lowest amorphous fraction. Hence it was demonstrated that the supramolecular structure of native HYA is easily modifiable by drying conditions. It was also found out that non-freezing water fraction determined with DSC can be determined also using TD-NMR. Last but not least, by using TD-NMR it is possible to determine the hydration kinetics of HYA and also to determine the water content of an HYA sample that corresponds to the glass-to-rubbery-state transition which is a measure of the rigidity of a system.

The biocompatible and biodegradable character of polysaccharides, associated with the presence of specific interaction sites in their structure, make them very attractive for modification, especially for the use in the pharmaceutical industry. Nevertheless, past efforts to develop techniques to reprocess polysaccharides have addressed mainly the hydration problem and gave little attention to how much the native structure is compromised or physically changed. Understanding how polysaccharides interact with themselves, each other, and with water in semi-diluted systems is of great importance as it determines its final structure and physical properties. In this thesis, it was demonstrated that DSC, FFC-NMR, and TD-NMR are complementary and highly suitable techniques in terms of gaining such knowledge.

It is worth mentioning that the terminology as “hydration shell” or “hydration layer” might be misleading. As emerged from this thesis, hydration of polysaccharides cannot be understood as water absorption layer by layer. Instead it should be seen more as water sorption on polysaccharide-specific sites (e.g. hydroxyl or amido functionalities) mainly in pores (according to Kelvin and Young-Laplace equations). In the second step the water is clustering around the sorbed water molecules as suggested also by other researchers (Despond et al., 2005).

5 REFERENCES

Argüelles-Monal, W., F. M. Goycoolea, J. Lizardi, C. Peniche and I. Higuera-Ciapara (2002). Chitin and Chitosan in Gel Network Systems. *Polymer Gels* 7: 102 - 121.

Bai, J. and X. C. Zeng (2012). Polymorphism and polyamorphism in bilayer water confined to slit nanopore under high pressure. *Proceedings of the National Academy of Sciences of the United States of America* 109: 21240-5.

Barbucci, R., G. Leone, A. Chiumiento, M. E. Di Cocco, G. D'Orazio, R. Gianferri and M. Delfini (2006). Low- and high-resolution nuclear magnetic resonance (NMR) characterisation of hyaluronan-based native and sulfated hydrogels. *Carbohydrate Research* 341: 1848-1858.

Berthold, J., J. Desbrieres, M. Rinaudo and L. Salmen (1994). Types of adsorbed water in relation to the ionic groups and their counterions for some cellulose derivatives. *Polymer* 35: 5729-5736.

Berthold, J., M. Rinaudo and L. Salmeń (1996). Association of water to polar groups; estimations by an adsorption model for ligno-cellulosic materials. *Colloids and Surfaces A: Physicochemical and Engineering Aspects* 112: 117-129.

Berti, F., P. Costantino, M. Fragai and C. Luchinat (2004). Water accessibility, aggregation, and motional features of polysaccharide-protein conjugate vaccines. *Biophysical Journal* 86: 3-9.

Bertini, I., M. Fragai, C. Luchinat and G. Parigi (2000). H-1 NMRD profiles of diamagnetic proteins: a model-free analysis. *Magnetic Resonance in Chemistry* 38: 543-550.

Brown, M. E. (2001). Introduction to Thermal Analysis: Techniques and Applications, Springer.

Brutschy, B. and P. Hobza (2000). van der Waals molecules III: Introduction. *Chemical Reviews* 100: 3861-3862.

Buleon, A., P. Colonna, V. Planchot and S. Ball (1998). Starch granules: structure and biosynthesis. *International Journal of Biological Macromolecules* 23: 85-112.

Calucci, L. and C. Forte (2009). Proton longitudinal relaxation coupling in dynamically heterogeneous soft systems. *Progress in Nuclear Magnetic Resonance Spectroscopy* 55: 296-323.

Campbell, N. A. B. W. R. J. H. (2006). Biology: Exploring Life. Boston, Massachusetts, Pearson Prentice Hall.

Capitani, D., G. Mensitieri, F. Porro, N. Proietti and A. L. Segre (2003). NMR and calorimetric investigation of water in a superabsorbing crosslinked network based on cellulose derivatives. *Polymer* 44: 6589-6598.

Carey, D. J. (1997). Syndecans: Multifunctional cell-surface co-receptors. *Biochemical Journal* 327: 1-16.

Clasen, C. and W. M. Kulicke (2001). Determination of viscoelastic and rheo-optical material functions of water-soluble cellulose derivatives. *Progress in Polymer Science* 26: 1839-1919.

Copeland, L., J. Blazek, H. Salman and M. C. M. Tang (2009). Form and functionality of starch. *Food Hydrocolloids* 23: 1527-1534.

Cox, M. and D. Nelson (2004). Principles of Biochemistry, Lehninger Freeman.

Day, A. J. and J. K. Sheehan (2001). Hyaluronan: polysaccharide chaos to protein organisation. *Current Opinion in Structural Biology* 11: 617-622.

Dei, L. and S. Grassi (2006). Peculiar properties of water as solute. *Journal of Physical Chemistry B* 110: 12191-12197.

Desiraju, G. R. and T. Steiner (1999). The weak hydrogen bond. Oxford, Oxford University Press.

Despond, S., E. Espuche, N. Cartier and A. Domard (2005). Hydration mechanism of polysaccharides: A comparative study. *Journal of Polymer Science: Part B: Polymer physics* 43: 48-58.

Dickinson, E. (2003). Hydrocolloids at interfaces and the influence on the properties of dispersed systems. *Food Hydrocolloids* 17: 25-39.

Djafari, S., H. D. Barth, K. Buchhold and B. Brutschy (1997). Infrared-depletion spectroscopy study on hydrogen-bonded fluorobenzene-methanol clusters. *Journal of Chemical Physics* 107: 10573-10581.

Dobies, M., M. Kozak, S. Jurga and A. Grubb (2009). The Dispersion of Water Proton Spin-Lattice Relaxation Rates in Aqueous Human Protein HC (alpha(1)-Microglobulin) Solutions. *Protein and Peptide Letters* 16: 1496-1503.

Ducel, V., D. Pouliquen, J. Richard and F. Boury (2008). 1H NMR relaxation studies of protein–polysaccharide mixtures. *International Journal of Biological Macromolecules* 43: 359-366.

Filmus, J. (2001). Glypicans in growth control and cancer. *Glycobiology* 11: 19R-23R.

Fringant, C., J. Desbrieres, M. Milas, M. Rinaudo, C. Joly and M. Escoubes (1996). Characterisation of sorbed water molecules on neutral and ionic polysaccharides. *International Journal of Biological Macromolecules* 18: 281-286.

Fry, S. C. (1989). The Structure and Functions of Xyloglucan. *Journal of Experimental Botany* 40: 1-11.

Garg, H. G. and C. A. Hales (2004). Chemistry and Biology of Hyaluronan.

Gemmei-Ide, M., A. Ohya and H. Kitano (2010). Thermally Latent Water in a Polymer Matrix. *Journal of Physical Chemistry B* 114: 4310-4312.

Gessler, K., N. Krauss, T. Steiner, C. Betzel, A. Sarko and W. Saenger (1995). Beta-D-cellotetraose hemihydrate as a strucural model for cellulose. 2. An X-ray diffraction study *Journal of the American Chemical Society* 117: 11397-11406.

Godefroy, S., J. P. Korb, L. K. Creamer, P. J. Watkinson and P. T. Callaghan (2003). Probing protein hydration and aging of food materials by the magnetic field dependence of proton spin-lattice relaxation times. *Journal of Colloid and Interface Science* 267: 337-342.

Gottschalk, M., N. A. Dencher and B. Halle (2001). Microsecond exchange of internal water molecules in bacteriorhodopsin. *Journal of Molecular Biology* 311: 605-621.

Gupta, B., A. Arora, S. Saxena and M. S. Alam (2009). Preparation of chitosan–polyethylene glycol coated cotton membranes for wound dressings: preparation and characterization. *Polymers for Advanced Technologies* 20: 58-65.

Gutmann, V. (1991). Fundamental considerations about liquid water. *Pure and Applied Chemistry* 63: 1715-1724.

Haines, P. J. (2002). Principles of Thermal Analysis and Calorimetry, Royal Society of Chemistry.

Halle, B., H. Jóhannesson and K. Venu (1998). Model-Free Analysis of Stretched Relaxation Dispersions. *Journal of Magnetic Resonance* 135: 1-13.

Hansen, M. R., A. Blennow, I. Farhat, L. Norgaard, S. Pedersen and S. B. Engelsen (2009). Comparative NMR relaxometry of gels of amylomaltase-modified starch and gelatin. *Food Hydrocolloids* 23: 2038-2048.

Hascall, V. and T. Laurent (1997). "Hyaluronan: structure and physical properties." Glycoforum/Science of Hyaluronan Review Series. from:

http://www.glycoforum.gr.jp/science/hyaluronan/HA01/HA01E.html1997.

Hatakeyama, H. and T. Hatakeyama (1998). Interaction between water and hydrophilic polymers. *Thermochimica Acta* 308: 3-22.

Hatakeyama, H., T. Onishi, T. Endo and T. Hatakeyama (2007). Gelation of chemically cross-linked methylcellulose studied by DSC and AFM. *Carbohydrate Polymers* 69: 792-798.

Hatakeyama, T., H. Hatakeyama and K. Nakamura (1995). Non-freezing water content of mono- and divalent cation salts of polyelectrolyte-water systems studied by DSC. *Thermochimica Acta* 253: 137-148.

Hatakeyama, T., Hatakeyama, H. (2004). Thermal Properties of Green Polymers and Biocomposites.

Hatakeyama, T., K. Nakamura and H. Hatakeyama (2000). Vaporization of bound water associated with cellulose fibres. *Thermochimica Acta* 352: 233-239.

Hatakeyama, T., M. Tanaka and H. Hatakeyama (2010). Studies on bound water restrained by poly(2-methacryloyloxyethyl phosphorylcholine): Comparison with polysaccharide–water systems. *Acta Biomaterialia* 6: 2077-2082.

Hatakeyama, T., H. Yoshida and H. Hatakeyama (1987). A differential scanning calorimetry study of the phase transition of the water-sodium cellulose sulphate system. *Polymer* 28: 1282-1286.

Hedman, K., M. Kurkinen, K. Alitalo, A. Vaheri, S. Johansson and M. Hook (1979). Isolation of the pericellular matrix of human fibroblast cultures. *Journal of Cell Biology* 81: 83-91.

Heinze, T. (2005). Polysaccharides I, Springer.

Hills, B. P. (1992). The proton-exchange corss-relaxation model of water relaxation in biopolymers systems. *Molecular Physics* 76: 489-508.

Hills, B. P., C. Cano and P. S. Belton (1991). Proton NMR relaxation studies of aqueous polysaccharide systems. *Macromolecules* 24: 2944-2950.

Hills, B. P., Y. L. Wang and H. R. Tang (2001). Molecular dynamics in concentrated sugar solutions and glasses: an NMR field cycling study. *Molecular Physics* 99: 1679-1687.

Hobza, P. and Z. Havlas (2002). Improper, blue-shifting hydrogen bond. *Theoretical Chemistry Accounts* 108: 325-334.

Humphries, D. E., G. W. Wong, D. S. Friend, M. F. Gurish, W. T. Qiu, C. F. Huang, A. H. Sharpe and R. L. Stevens (1999). Heparin is essential for the storage of specific granule proteases in mast cells. *Nature* 400: 769-772.

Chaplin, M. (2006). Water structuring at colloidal surfaces. Dordrecht, Springer.

Chaplin, M. F. (2010). Structuring and Behaviour of Water in Nanochannels and Confined Spaces

Adsorption and Phase Behaviour in Nanochannels and Nanotubes. L. J. Dunne and G. Manos, Springer Netherlands: 241-255.

Chavez, F. V., E. Persson and B. Halle (2006). Internal water molecules and magnetic relaxation in agarose gels. *Journal of the American Chemical Society* 128: 4902-4910.

Cheifetz, S. and J. Massague (1989). Transforming growth factor-beta (TGF-BETA) receptor proteoglucan-cell-surface expression and ligand-binding in the absence of glycosaminoglycan chains. *Journal of Biological Chemistry* 264: 12025-12028.

Ibrahim, M. (1998). Clean fractionation of biomass-steam explosion and extraction. Blacksburg, Virginia Polytechnic Institute and State University.

Ifuku, S. and J. F. Kadla (2008). Preparation of a Thermosensitive Highly Regioselective Cellulose/N-Isopropylacrylamide Copolymer through Atom Transfer Radical Polymerization. *Biomacromolecules* 9: 3308-3313.

Iozzo, R. V. (1998). MATRIX PROTEOGLYCANS: From Molecular Design to Cellular Function. *Annual Review of Biochemistry* 67: 609-652.

Iozzo, R. V. and A. D. Murdoch (1996). Proteoglycans of the extracellular environment: Clues from the gene and protein side offer novel perspectives in molecular diversity and function. *Faseb Journal* 10: 598-614.

Isogai, A., M. Usuda, T. Kato, T. Uryu and R. H. Atalla (1989). Solid-state CP MAS C-13 NMR-study of cellulose polymorphs. *Macromolecules* 22: 3168-3172.

Israelachvili, J. N. (1997). Intermolecular and Surface Forces, London: Academic Press Ltd.

Jeffrey, G. A. (2007). An introduction to hydrogen bonding. New York, Oxford University Press.

Jeffrey, G. A. and W. Saenger (1991). Hydrogen bonding in biological strucutres. Berlin Springer-Verlag.

Jobling, S. (2004). Improving starch for food and industrial applications. *Current Opinion in Plant Biology* 7: 210-218.

Joshi, H. N. and E. M. Topp (1992). Hydration in hyaluronic-acid and its esters using differential scanning calorimetry. *International Journal of Pharmaceutics* 80: 213-225.

Jouon, N., M. Rinaudo, M. Milas and J. Desbrières (1995). Hydration of hyaluronic acid as a function of the counterion type and relative humidity. *Carbohydrate Polymers* 26: 69-73.

Kimmich, R. and E. Anoardo (2004). Field-cycling NMR relaxometry. *Progress in Nuclear Magnetic Resonance Spectroscopy* 44: 257-320.

Kirschner, K. N. and R. J. Woods (2001). Solvent interactions determine carbohydrate conformation. *Proceedings of the National Academy of Sciences of the United States of America* 98: 10541-10545.

Kogan, G., L. Soltes, R. Stern and P. Gemeiner (2007). Hyaluronic acid: a natural biopolymer with a broad range of biomedical and industrial applications. *Biotechnology Letters* 29: 17-25.

Lapcik, L., S. De Smedt, J. Demeester and P. Chabrecek (1998). Hyaluronan: Preparation, structure, properties, and applications. *Chemical Reviews* 98: 2663-2684.

Le Botlan, D., Y. Rugraff, C. Martin and P. Colonna (1998). Quantitative determination of bound water in wheat starch by time domain NMR spectroscopy. *Carbohydrate Research* 308: 29-36.

Legon, A. C. and D. J. Millen (1987). Angular geometries and other properties of hydrogen-bonded dimers - A simple electrostatic interpretation of the success of the electron-pair model. *Chemical Society Reviews* 16: 467-498.

Leppanen, K., S. Andersson, M. Torkkeli, M. Knaapila, N. Kotelnikova and R. Serimaa (2009). Structure of cellulose and microcrystalline cellulose from various wood species, cotton and flax studied by X-ray scattering. *Cellulose* 16: 999-1015.

Levitt, M. H. (2007). Spin Dynamics. Chichester, John Wiley and Sons, Ltd.

Lewin, M. (2007). Handbook of Fiber Chemistry, Taylor & Francis Group.

Lewis, S. L. and (2008). Medical Surgical Nursing, Mosby.

Linden, J., R. Stoner, K. Knutson and C. Gardner-Hughes (2000). Organic Disease Control Elicitors. *Agro Food Industry Hi-Te.*: 12–15.

Liu, J. and M. K. Cowman (2000). Thermal analysis of semi-dilute hyaluronan solutions. *Journal of Thermal Analysis and Calorimetry* 59: 547-557.

Liu, W. G. and K. D. Yao (2001). What causes the unfrozen water in polymers: hydrogen bonds between water and polymer chains? *Polymer* 42: 3943-3947.

Luchinat, C. and G. Parigi (2008). Nuclear relaxometry helps designing systems for solution DNP on proteins. *Applied Magnetic Resonance* 34: 379-392.

Lusse, S. and K. Arnold (1998). Water binding of Polysaccharides-NMR and ESR studies. *Macromolecules* 31: 6891-6897.

Lyon, M. and J. T. Gallagher (1998). Bio-specific sequences and domains in heparan sulphate and the regulation of cell growth and adhesion. *Matrix Biology* 17: 485-493.

Matteini, P., L. Dei, E. Carretti, N. Volp, A. Goti and R. Pini (2009). Structural Behavior of Highly Concentrated Hyaluronan. *Biomacromolecules* 10: 1516-1522.

Maytin, E. V., H. H. Chung and V. M. Seetharaman (2004). Hyaluronan participates in the epidermal response to disruption of the permeability barrier in vivo. *American Journal of Pathology* 165: 1331-1341.

Mikheev, Y. A., L. N. Guseva, E. Y. Davydov and Y. A. Ershov (2007). The hydration of hydrophobic substances. *Russian Journal of Physical Chemistry A* 81: 1897-1913.

Mlčoch, T. and J. Kučerík (2013). Hydration and drying of various polysaccharides studied using DSC. *Journal of Thermal Analysis and Calorimetry*.

Modig, K., E. Liepinsh, G. Otting and B. Halle (2003). Dynamics of Protein and Peptide Hydration. *Journal of the American Chemical Society* 126: 102-114.

Moore, J. H. and N. D. Spencer (2001). Encyclopedia of Chemical Physics and Physical Chemistry, Taylor & Francis.

Mulloy, B. and M. J. Forster (2000). Conformation and dynamics of heparin and heparan sulfate. *Glycobiology* 10: 1147-1156.

Nakamura, K., T. Hatakeyama and H. Hatakeyama (1991). Formation of the glassy state and mesophase in the water-sodium alginate system. *Polymer Journal* 23: 253-258.

Nelson, D. L. and M. M. Cox (2004). Principles of biochemistry.

Ostrowska-Czubenko, J. and M. Gierszewska-Druzynska (2009). Effect of ionic crosslinking on the water state in hydrogel chitosan membranes. *Carbohydrate Polymers* 77: 590-598.

Ovodov, Y. S. (2009). Current views on pectin substances. *Russian Journal of Bioorganic Chemistry* 35: 269-284.

Park, S., R. A. Venditti, H. Jameel and J. J. Pawlak (2006). Changes in pore size distribution during the drying of cellulose fibers as measured by differential scanning calorimetry. *Carbohydrate Polymers* 66: 97-103.

Park, S., R. A. Venditti, H. Jameel and J. J. Pawlak (2007). Studies of the heat of vaporization of water associated with cellulose fibers characterized by thermal analysis. *Cellulose* 14: 195-204.

Pauling, L. (1931). The nature of the chemical bond. II. The one-electron bond and the three-electron bond. *Journal of the American Chemical Society* 53: 3225-3237.

Pekar, M. (2012). A note on an alternative DSC approach to study hydration of hyaluronan. *Carbohydrate Polymers* 89: 1009-1011.

Perez, S., K. Mazeau and C. H. du Penhoat (2000). The three-dimensional structures of the pectic polysaccharides. *Plant Physiology and Biochemistry* 38: 37-55.

Phillips, G. O., S. Takigami and M. Takigami (1996). Hydration characteristics of the gum exudate from Acacia senegal. *Food Hydrocolloids* 10: 11-19.

Ping, Z. H., Q. T. Nguyen, S. M. Chen, J. Q. Zhou and Y. D. Ding (2001). States of water in different hydrophilic polymers - DSC and FTIR studies. *Polymer* 42: 8461-8467.

Prawitwong, P., S. Takigami and G. O. Phillips (2007). Phase transition behaviour of sorbed water in Konjac mannan. *Food Hydrocolloids* 21: 1368-1373.

Pribble, R. N., A. W. Garrett, K. Haber and T. S. Zwier (1995). Resonant ion-dip infrared-spectroscopy of benzene-H2O and benzene HOD. *Journal of Chemical Physics* 103: 531-544.

Pusateri, A. E., S. J. McCarthy, K. W. Gregory, R. A. Harris, L. Cardenas, A. T. McManus and C. W. J. Goodwin (2003). Effect of a Chitosan-Based Hemostatic Dressing on Blood Loss and

Survival in a Model of Severe Venous Hemorrhage and Hepatic Injury in Swine. *The Journal of Trauma* 54: 177-182.

Quinn, E. X., T. Hatakeyama, H. Yoshida, M. Takahashi and H. Hatakeyama (1993). The conformational properties of gellan gum hydrogels. *Polymer Gels and Networks* 1: 93–114.

Quinn, F. X., T. Hatakeyama, M. Takahashi and H. Hatakeyama (1994). The effect of annealing on the conformational properties of xanthan hydrogels. *Polymer* 35: 1248-1252.

Rabenstein, D. L. and W. Guo (1988). Nuclear Magnetic Resonance Spectroscopy. *Analytical Chemistry* 60: 1R-28R.

Rachocki, A., J. Kowalczuk and J. Tritt-Goc (2006). How we can interpret the T-1 dispersion of MC, HPMC and HPC polymers above glass temperature? *Solid State Nuclear Magnetic Resonance* 30: 192-197.

Redfield, A. G. (1957). On the theory of relaxation processes. *Ibm Journal of Research and Development* 1: 19-31.

Ritota, M., R. Gianferri, R. Bucci and E. Brosio (2008). Proton NMR relaxation study of swelling and gelatinisation process in rice starch-water samples. *Food Chemistry* 110: 14-22.

Saladin, K. S. (2007). Anatomy and Physiology, McGraw-Hill Education.

Scott, J. E., C. Cummings, A. Brass and Y. Chen (1991). Secondary and tertiary structures of hyaluronan in aqueous solution, investigated by rotary shadowing electron-microscopy and computer-simulation - Hyaluronan is a very efficient network-forming polymer. *Biochemical Journal* 274: 699-705.

Shapiro, Y. E. (2011). Structure and dynamics of hydrogels and organogels: An NMR spectroscopy approach. *Progress in Polymer Science* 36: 1184-1253.

Sherman, F. (1983). Microdetermination of the degree of hydration of polysaccharides and glycoproteins. *Talanta* 30: 705-707.

Scheiner, S. (1997). Hydrogen Bonding. New York, Oxford University Press.

Singh, N., J. Singh, L. Kaur, N. S. Sodhi and B. S. Gill (2003). Morphological, thermal and rheological properties of starches from different botanical sources. *Food Chemistry* 81: 219-231.

Steed, J. W. and J. L. Atwood (2000). Supramolecular Chemistry, Chichester: John Wiley and Sons Ltd.

Stern, R., A. A. Asari and K. N. Sugahara (2006). Hyaluronan fragments: An information-rich system. *European Journal of Cell Biology* 85: 699-715.

Stern, R. and M. J. Jedrzejas (2008). Carbohydrate Polymers at the Center of Life's Origins: The Importance of Molecular Processivity. *Chemical Reviews* 108: 5061-5085.

Sun, R. C., J. M. Fang, P. Rowlands and J. Bolton (1998). Physicochemical and thermal characterization of wheat straw hemicelluloses and cellulose. *Journal of Agricultural and Food Chemistry* 46: 2804-2809.

Sutherland, I. W. (1998). Novel and established applications of microbial polysaccharides. *Trends in Biotechnology* 16: 41-46.

Takahashi, M., T. Hatakeyama and H. Hatakeyama (2000). Phenomenological theory describing the behaviour of non-freezing water in structure formation process of polysaccharide aqueous solutions. *Carbohydrate Polymers* 41: 91-95.

Takigami, S., M. Takigami and G. O. Phillips (1993). Hydration characteristics of the cross-linked hyaluronan derivative hylan. *Carbohydrate Polymers* 22: 153-160.

Takigami, S., M. Takigami and G. O. Phillips (1995). Effect of preparation method on the hydration characteristics of hylan and comparison with another highly cross-linked polysaccharide, gum-arabic. *Carbohydrate Polymers* 26: 11-18.

Tolstoguzov, V. (2004). Why are polysaccharides necessary? *Food Hydrocolloids* 18: 873-877.

Tolstoguzov, V. (2004). Why were polysaccharides necessary? *Origins of Life and Evolution of Biospheres* 34: 571-597.

Van-Quynh, A., S. Willson and R. G. Bryant (2003). Protein reorientation and bound water molecules measured by H-1 magnetic spin-lattice relaxation. *Biophysical Journal* 84: 558-563.

Voet, D. V., J. G. (2004). Biochemistry. New York.

Wakelyn, P. J. (2007). Cotton fiber chemistry and technolog, Taylor&Francis Group.

Wolfe, J., G. Bryant and K. L. Koster (2002). What is 'unfreezable water', how unfreezable is it and how much is there? *Cryoletters* 23: 157-166.

Wunderlich, B. (2005). Thermal analysis of Polymeric Materials. Berlin, Springer-Verlag.

Yoshida, H., T. Hatakeyama and H. Hatakeyama (1992). Effect of water on the main chain motion of polysaccharide hydrogels. *Acs Symposium Series* 489: 217-230.

Yoshida, H., T. Hatakeyama, H. Hatakeyama, N. Maeno and T. Hondah (1992). Physics and Chemistry of Ice. *Hokkaido University Press*: 282.

Yuryev, V. P., I. E. Nemirovskaya and T. D. Maslova (1995). Phase state of starch gels at different water contents. *Carbohydrate Polymers* 26: 43-46.

Zhao, H., J. H. Kwak, Y. Wang, J. A. Franz, J. M. White and J. E. Holladay (2005). Effects of crystallinity on dilute acid hydrolysis of cellulose by cellulose ball-milling. *Energy&Fuels* 20: 807–811.

Zheligovskaya, E. A. and G. G. Malenkov (2006). Crystalline water ices. *Uspekhi Khimii* 75: 64-85.

Zhou, D. and R. G. Bryant (1994). Magnetization-transfer, cross-relaxation, and chemical-exchange in rotationally immobilized protein gels. *Magnetic Resonance in Medicine* 32: 725-732.

Zugenmaier, P. (2008). Crystalline cellulose and Cellulose Derivatives: Characterization and Structures.

6 LIST OF ABBREVIATION

DSC	Differential scanning calorimetry
Da	Dalton
EMC	Extracellular matrix
FTIR	Fourier transformed infrared spectroscopy
FFC-NMR	Fast field cycling nuclear magnetic resonance
GlcA	*β*-L-glucuronic acid
GlcNAc	2-deoxy-2-acetamido-α-D-glucopyranosyl
GlcNS	2-deoxy-2-sulfamido-α-D-glucopyranosyl
GlcNS(6S)	2-deoxy-2-sulfamido-α-D-glucopyranosyl-6-O-sulfate
HYA	Hyaluronan
IdoA	α-L-iduronic acid
IdoA(2S)	2-O-sulfo-α-L-iduronic acid
MDSC	Temperature modulated differential scanning calorimetry
NMR	Nuclear magnetic resonance
NMRD	Nuclear magnetic resonance dispersion
TD NMR	Time domain nuclear magnetic resonance
ω_L	Proton Larmor frequency

Appendix 1

Průšová, A., Šmejkalová, D., Chytil, M., Velebný, M., Kučerík, J. (2010). An alternative DSC approach to study hydration of hyaluronan. Carbohydrate Polymers 82: 498–503.

Carbohydrate Polymers 82 (2010) 498–503

Contents lists available at ScienceDirect

Carbohydrate Polymers

journal homepage: www.elsevier.com/locate/carbpol

An alternative DSC approach to study hydration of hyaluronan

A. Průšová [a], D. Šmejkalová [b], M. Chytil [a], V. Velebný [b], J. Kučerík [a,*]

[a] Brno University of Technology, Faculty of Chemistry, Purkyňova 118, Brno CZ-612 00, Czech Republic
[b] Contipro C, Dolní Dobrouč 401, 56102 Dolní Dobrouč, Czech Republic

ARTICLE INFO

Article history:
Received 7 April 2010
Received in revised form 5 May 2010
Accepted 7 May 2010
Available online 21 May 2010

Keywords:
Hyaluronan
Hydration
DSC
Water evaporation

ABSTRACT

Differential scanning calorimetry (DSC) was used to determine the number of water molecules in the hydration shell of hyaluronan of different molecular weights and counterions. First, traditional experiments including freezing/thawing of free water in semi-diluted solutions were carried out leading to the determination of melting enthalpy of freezable water. Non-freezing water was determined using extrapolation to zero enthalpy. For sodium hyaluronan within the molecular weight range between 100 and 740 kDa the hydration shell was determined as 0.74 g g^{-1} HYA. A larger hydration shell containing 0.84 and 0.82 g g^{-1} HYA was determined for hyaluronan of 1390 kDa in its sodium and protonized form, respectively. Second, melting enthalpy of freezing water was further studied applying water evaporation experiments. Resulted plot of enthalpy vs concentration indicated an additional heat evolution process which occurs at specific concentration and decreases the measured evaporation enthalpy. The heat evolution was attributed to the mutual approaching of hyaluronan molecular chains, their mutual interactions and formation of the ordered hyaluronan structure which starts immediately when the hydration water is desorbed from the hyaluronan surface. The concentration at which the process occurred was related to "non-evaporable water" which was determined as 0.31–0.38 g g^{-1} for sodium hyaluronan and 0.84 g g^{-1} for its protonized form. The second approach provides additional information enabling a deeper insight into the problem of hyaluronan hydration.

© 2010 Elsevier Ltd. All rights reserved.

1. Introduction

Hyaluronan (HYA) is a linear, unbranched, high molecular weight extracellular matrix polar polysaccharide belonging to the glycosaminoglycans class. HYA is composed of repeating polyanionic disaccharide units which consist of N-acetyl-D-glucosamine and D-glucuronic acid linked by a β 1–4 glycosidic bond. The disaccharides are linked by β 1–3 bonds to form HYA chains (Fig. 1). In vivo, it occurs exceptionally in the form of Na^+ salt. HYA polymers have extraordinarily wide range of use and often different biological functions depending on the molecular mass which can reach up to 10 MDa. Larger matrix polymers of HYA show space-filling, anti-angiogenic, immunosuppressive effects and play an important role in tissue hydration (Kogan, Šoltéz, Stern, & Gemener, 2007). In contrast, the HYA segments of lower molecular weight are well known to have pronounced biological activities playing role for example in tumour diagnose.

Hydration and/or water holding capacity is probably one of the most important aspects of the HYA function. A perusal of literature shows a lot of works dealing with the determination of hydration shells and enumeration of water molecules surrounding HYA molecules in diluted and semi-diluted HYA/water solutions (Haxaire, Marechal, Milas, & Rinaudo, 2003a, 2003b; Joun, Rinaudo, Miles, & Desbrieres, 1995; Marechal, Milas, & Rinaudo, 2003; Yoshida, Hatakeyama, & Hatakeyama, 1992) and swelling of HYA in water (Mráček, Benešová, Minařík, Urban, & Lapčík, 2007) or in salt solutions (Mráček et al., 2008). There are several techniques and approaches, both experimental and theoretical, to shed light on water behaviour in the presence of HYA molecules. In this paper we focus on the differential scanning calorimetry (DSC), a method belonging to the family of thermo-analytical techniques.

The traditional and probably the only way of differentiation of water molecules in hydration shells using DSC is based on freezing/thawing experiments in which the difference in physical properties between freezable water in form of ice and non-freezable water that is tightly bound on the HYA surface is investigated. Accordingly, the water shells are categorized into three groups, i.e. non-freezing water (NFW), freezing-bound water (FBW) and free water (FW). NFW is strongly fixed to the HYA surface through the electrostatic interactions. The motion of NFW is limited and therefore such water cannot crystallize when cooled down (Wolfe, Bryant, & Koster, 2002) or crystallizes in time period which is far beyond the time framework of the experiment. It was stated that such water molecules are directly attached especially to the hydroxyl groups of HYA (Hatakeyama, Nakamura, & Hatakeyama, 2000). FBW is located in larger distance from a HYA molecule. It is

* Corresponding author. Tel.: +420 777 633 675; fax: +420 541 211 697.
E-mail address: kucerik@fch.vutbr.cz (J. Kučerík).

0144-8617/$ – see front matter © 2010 Elsevier Ltd. All rights reserved.
doi:10.1016/j.carbpol.2010.05.022

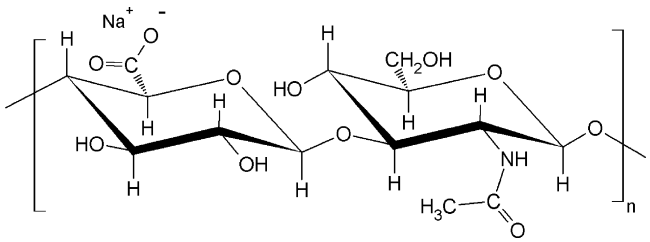

Fig. 1. Disaccharide unit of hyaluronan.

thought it freezes and melts at lower temperatures than normal, bulk water, it is easy to be supercooled and further the melting enthalpy is also lower than for the bulk water due to its different crystal morphology. In fact, while frozen FBW is thought to consist of cubic ice, the FW ice is formed by hexagonal structures (Yoshida et al., 1992). FW behaves as normal pure water, because its structure is not influenced by the presence of HYA molecules, it means that, when frozen, the melting enthalpy is 334 J g^{-1} and the melting and freezing temperature is around 0 °C (Berthold, Desbrieres, Rinaudo, & Salomen, 1994; Joshi and Topp, 1992; Joun et al., 1995; Lui & Cowman, 2000; Takahashi, Hatakeyama, & Hatakeyama, 2000; Yoshida, Hatakeyama, & Hatakeyama, 1989, 1990; Yoshida et al., 1992; Yoshida, Hatakeyama, & Hatakeyama, 1993). Lui and Cowman (2000) reviewed previously published DSC approaches and made the first attempt to describe such behaviour mathematically. They derived equations allowing a precise determination of NFW and FBW while adopting the minimum value of fusion enthalpy change of 312 J g^{-1} previously reported by Yoshida (Yoshida et al., 1992). For the native HYA they determined about 44 g g^{-1} HYA as FBW and about 0.6 g g^{-1} HYA as NFW (Lui & Cowman, 2000). When related to number of water molecules per dissacharide HYA unit, the determined amount of NFW corresponds to 13.4 molecules. This value is rather different from 4 to 5 molecules that were theoretically derived using FTIR in dry HYA film (Haxaire et al., 2003a, 2003b; Marechal et al., 2003). The reason of such difference is that there are several undisputable limits to use DSC cooling/thawing experiments for precise enumeration of water in NFW shell (Wolfe et al., 2002). The main problem is the occurrence of an unknown amount of amorphous (Wolfe et al., 2002) and low density ice (probably associated with FBW) in frozen water which can bias the determined enthalpy of ice melting which in turn may consequently result in an overestimation of NFW. In addition, there are other experimental aspects which can influence the DSC results, such as the baseline distortion, or supercooling effect (Wolfe et al., 2002).

In order to overcome some of the disadvantages mentioned above, instead of melting enthalpy, the enthalpy of water evaporation from hyaluronan solution was measured in this work. Determined data were compared with results obtained by traditional HYA hydration experiments using DSC cooling/thawing experiments. The results obtained from the two different methods provided new information regarding the hydration of hyaluronan.

2. Materials and methods

2.1. Hyaluronan (HYA)

Bacterial HYA, specifically its Na^+ form (Na^+HYA) was kindly provided by CPN Company (Dolní Dobrouč, Czech Republic). HYAs with the following molecular weights were used: 100, 254, 740 and 1390 kDa.

The protonized form of HYA (H^+HYA) was produced as follows: 1390 kDa Na^+HYA was dissolved in water, transferred into a dialysis bag (cut off 3500 Da) and dialyzed against 0.1 mol L^{-1} HCl until Na^+ free. Then, the obtained product was dialyzed against milli-Q water until it became chloride-free. Quality of final product was controlled by thermogravimetry to determine the residual ash after burning in dynamic air atmosphere at 600 °C (i.e. 0%).

2.2. Preparation of HYA/water systems

Samples of approximately 10–20 mg (weighted with an accuracy of ±0.01 mg) were placed in aluminum sample pans (TA Instruments, Tzero® technology) and the excess of water (milli-Q) was added to HYA sample. Surplus water was allowed to evaporate slowly at room temperature until the desired water content was obtained. The pans were subsequently hermetically sealed and left to equilibrate at room temperature for 26 h as recommended by Takahashi et al. (2000). It was already published that the time interval is enough to reach a constant value of NF water in the HYA sample. Similar samples were used for freezing/thawing as well as for the evaporation experiments.

Water content (W_c) was defined as follows:

$$W_c = \frac{\text{grams of water}}{\text{grams of dry sample}} \, (\text{g g}^{-1}) \quad (1)$$

2.3. Thermal analysis

Differential scanning calorimetry (DSC) was carried out using the TA Instruments DSC Q200 equipped with a cooling accessory RCS90 and assessed by the TA Universal Analysis 2000 software. The following thermal protocol was used for freezing/thawing experiments: start at 40.0 °C; cooling from 40.0 to −90.0 °C at 3.0 °C min^{-1}; isothermal at −90.0 °C for 2.0 min; heating from −90.0 to 30 °C at 3.0 °C min^{-1}. Flow rate of dynamic nitrogen atmosphere was 50 mL min^{-1}, as a sample holder was used hermetically sealed T_{zero} Al pan while sample was prepared as described above.

The following thermal protocols were used for the measurement of evaporation enthalpy: equilibration at 27.0 °C; cooling from 27.0 to −40.0 °C at 10.0 °C min^{-1}; isothermal at −40.0 °C for 2.0 min; heating from −40.0 to 250.0 °C at 3.0 °C min^{-1} and switching the flow rate of nitrogen from 50 mL min^{-1} to 5 mL min^{-1}. Immediately before the measurement, the hermetic lid (necessary for the sample preparation) was perforated using a sharp tool and the measurement was carried out straightway.

Selected samples in different concentration ranges were measured in triplicate to determine the statistical significance. Standard deviation never exceeded 7%; typically it was below 5%.

To obtain precise water content, thermogravimetry (TA Instruments, Q5000IR) was used to determine the equilibrium moisture content as a weight loss in the temperature interval 25–220 °C under dynamic atmosphere of nitrogen 25 mL min^{-1}. That information was used during the HYA/water sample preparation.

3. Results and discussion

3.1. Freezing/thawing experiments

First of all, the DSC of HYA/water systems was carried out for different water concentrations; examples of DSC records for low concentrations are given in Fig. 2. Fig. 2 shows the heating run, i.e. ice melting records for HYA (740 kDa) with various concentrations of water; the dotted line represents the hypothetical straight baseline which should only serve for a better recognition of processes occurring during the melting of ice in frozen HYA/water mixture. The determination of enthalpies presented here was carried out using a slightly different approach taking into account the cold crystallization, baseline shift and non-linearity according to the literature recommendations (Riesen, 2007).

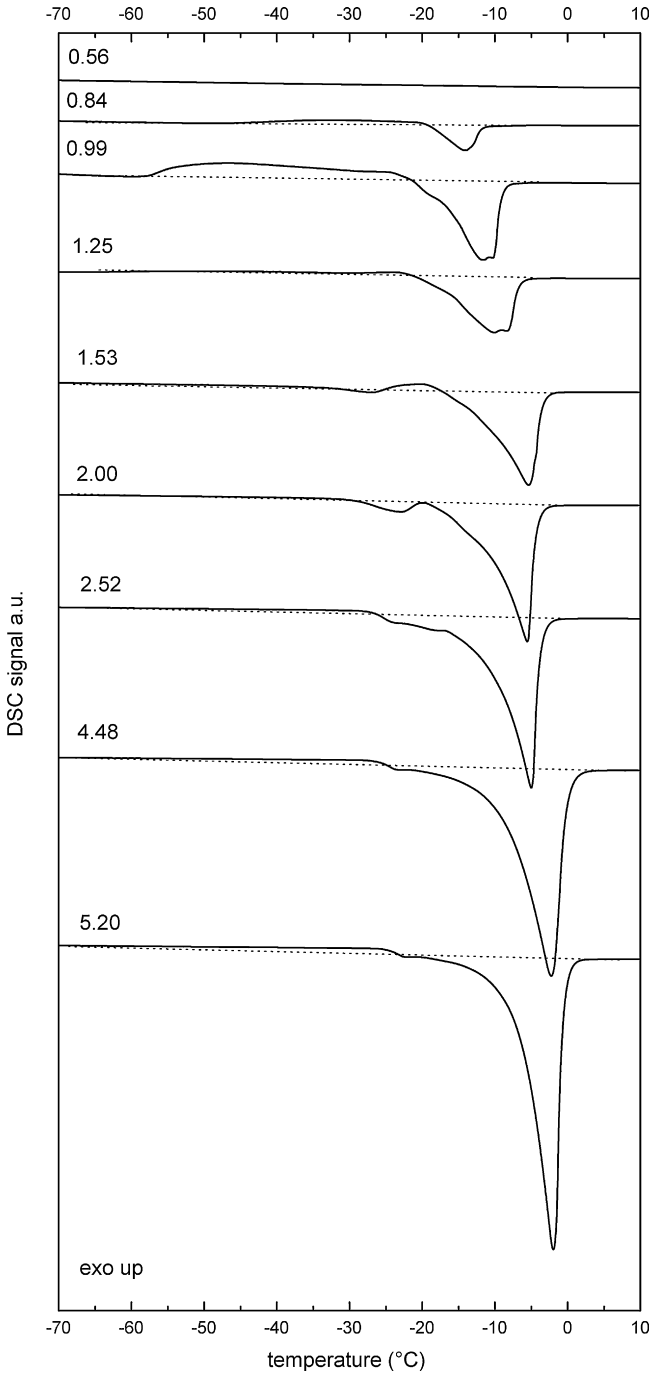

Fig. 2. DSC melting records for HYA (740 kDa).

It can be seen that around $W_c = 0.5$ no peak occurred on the heating curves. It seems that all the water molecules occurred in NFW shell. Since at this concentration the number of water molecules per HYA disaccharide unit (400 g mol^{-1}) is approximately 11, it is likely that the water molecules are strongly bound to the HYA skeleton and low temperature does not affect their mutual interactions. It means that low temperature did not cause the water desorption from HYA molecule, water molecules were not separated to form ice crystals which melt when heated up. Increase in concentration of water in HYA sample brought about the appearance of events associated with the presence of freezable water. There is a weak exothermal event that occurs at $W_c = 0.84$ and can be attributed to cold crystallization of supercooled water starting around −48 °C followed by melting around −22 °C. Increase in

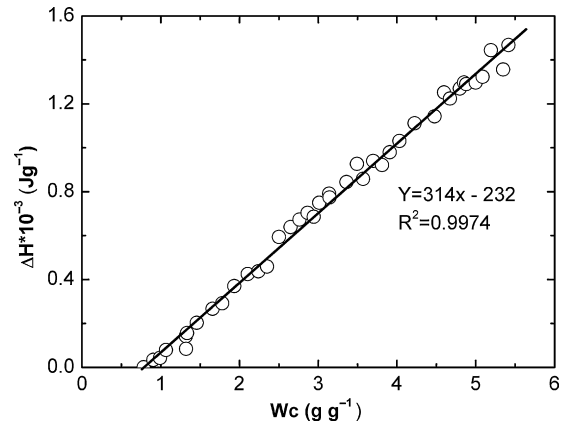

Fig. 3. Dependency of the enthalpy change associated with the melting endotherm in the HYA (740 kDa) solutions, normalized to the HYA weight, as a function of water content in HYA.

water content to $W_c = 0.99$ showed the enlargement of crystallization peak before the ice melting. Then two separate endotherms appeared at $W_c = 1.53$; first one starting at −32 °C and the other one starting at −20 °C. Those are not any longer separated at $W_c = 2.52$ and above that concentration, where again the crystallization appeared followed by a single melting peak with the onset around −30 °C. From Fig. 2 it can be further observed that there is a general tendency for the onset temperature of melting peak to slightly increase with increasing water content in the sample. Such finding is quite typical and is in accordance with the observations reported in the earlier papers (Hatakeyama & Hatakeyama, 1998); Yoshida et al., 1992). The HYA samples of molecular weight 100, 253 and 1396 kDa gave similar records and are not reported here.

As previously suggested by Liu and Cowman, the observed enthalpy of melting was first normalized dividing by the weight of the dry HYA mass and then plotted against the respective W_c (Fig. 3). In this way, the NFW content was determined from the x-intercept (Lui & Cowman, 2000). Obtained values of NFW and parameters of linearization are listed for all samples in Table 1. It can be seen that the NFW content was constant for HYA of molecular weight from 100 to 740 kDa and was always determined as 0.74 g of water per gram of HYA. A larger hydration shell consisting of 0.84 g g^{-1} NFW was found for 1390 kDA HYA.

The same experiments were carried out using H^+ form of HYA (H^+HYA). The protonized form showed different behaviour in comparison with Na^+ form. In fact, it can be easily identified in Fig. 4 that ice around H^+ HYA form melts at significantly higher temperature than that in Na^+HYA form. Although the onset of the melting is not exactly at 0 °C as for pure water, the temperature is significantly shifted to higher temperatures. Determination of NFW was carried out in the same way as suggested in Fig. 3 and brought result of about 0.82 g g^{-1}.

Table 1
Content of hydration water for HYA of different molecular weight and counterion from cooling/thawing experiments. n_{NFW} is the number of water molecules per disaccharide unit, NFW stands for non-freezing water (in g of water per 1 g of HYA) determined using the approach reported in Lui and Cowman (2000).

Sample	[a]NFW	[a]n_{NFW}	Parameters a; b	Confidence coefficient R^2
100	0.74	16.5	312; −230	0.9984
254	0.74	16.5	315; −234	0.9988
740	0.74	16.5	314; −232	0.9974
1390	0.84	18.7	302; −255	0.9976
H^+	0.82	17.2	329; −270	0.9979

[a] Recalculated to the molecular weight of Na^+ and H^+ form.

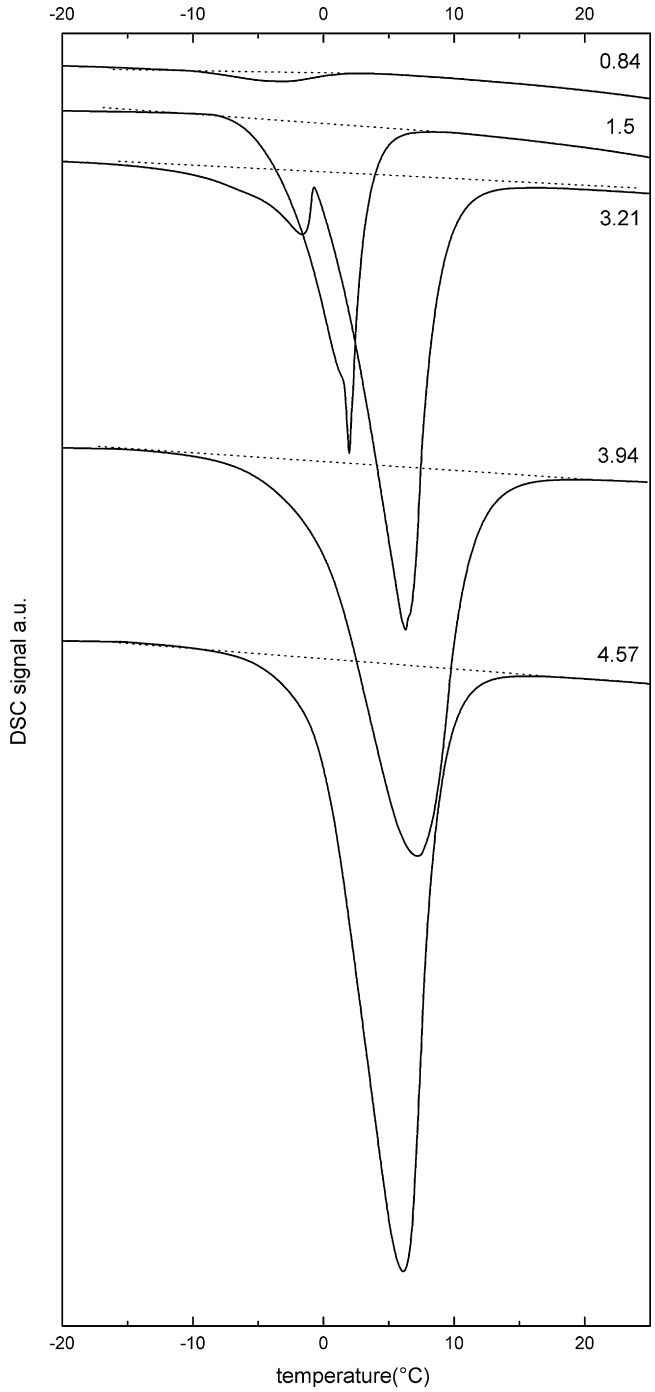

Fig. 4. DSC melting records for H^+HYA.

3.2. Evaporation experiments

Samples with the same water content as used in the freezing/thawing experiments were measured to determine the enthalpy of evaporation of water from the mixture with HYA. Simply, before the experiment was carried out, the lid was carefully perforated by a sharp pin; the sample was then cooled down and heated up to 220 °C. The reason to apply the freezing segment before the evaporation was due to easier identification of the onset of evaporation (Fig. 5).

The heating rate was chosen reasonably slow to evaporate as much as possible of the water present in the sample before its boiling. Again, the enthalpy of processes was assessed and elaborated

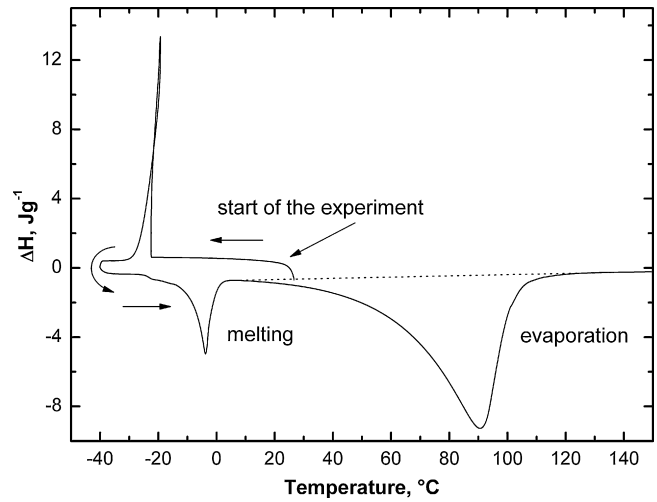

Fig. 5. DSC record for the determination of evaporation enthalpy for HYA (740 kDa), $W_c = 1.94$.

as described above. In Fig. 5 there is given a representative DSC evaporation record for HYA 740 kDa. The cooling curve, depicted in the upper part of the figure, shows an event corresponding to the freezable water crystallization. Conversely, heating curve shown at the bottom part of Fig. 5 reveals two endothermic peaks, where the first one corresponds to the melting of water in the sample while the other broad endothermic peak can be attributed to the water evaporation. Fig. 6 shows the comparison of water/HYA samples with various W_c. As expected, the peak temperature and peak area is shifted with increasing water content in the samples.

Fig. 7 shows typical dependency of evaporation enthalpy normalized to the mass of dry Na^+ forms of HYA or H^+HYA with molecular weights 101, 740 and 1390 kDa. There can be seen a linear decrease of the enthalpy with decreasing W_c; a break occurs around the value $W_c = 0.35$. Since at this concentration the water molecules are supposed to be bound more tightly to the HYA molecule, it is natural to assume that the energy necessary for its evaporation should be higher than that for bulk water. As a result, the enthalpy should be higher and the slope of the dependency should be in reverse direction to that shown in Fig. 7, i.e. more steeply decreasing. Therefore, it seems that at this concentration the consumption of energy necessary for evaporation is compensated by a process or processes in which the energy is evolved.

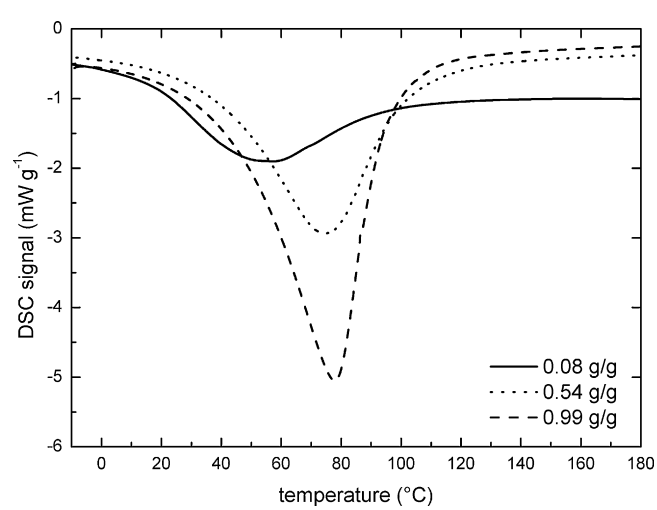

Fig. 6. Comparison of evaporation profiles of water/HYA (740 kDa) samples of different concentrations.

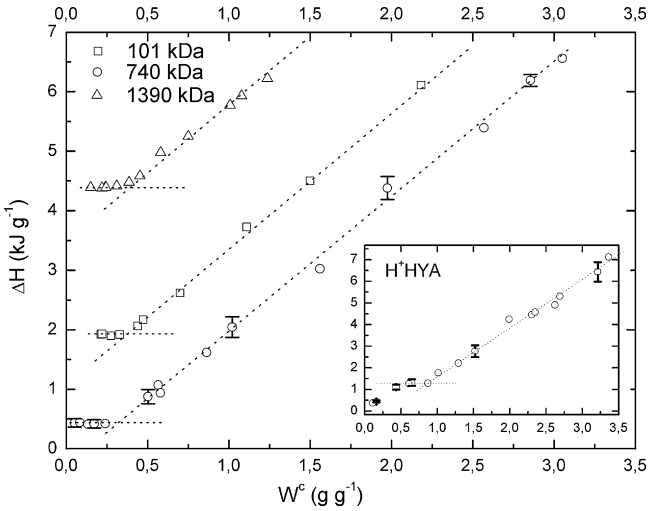

Fig. 7. Dependences of normalized enthalpy of evaporation on concentration. For better resolution, determined enthalpies of 101 and 1390 kDa HYA were shifted by 2 and 4 kJ g^{-1}, respectively.

A similar dependence was obtained also for sample of molecular weight of 254 kDa. Unlike the low molecular HYA samples, the sample of 1390 kDa did not show a perfectly clear break and instead, the dependency showed only a slow decrease of slope (Fig. 7). Nevertheless, even such a kind of dependency allowed us to proceed a rough estimation of the intersection of the two lines as suggested in Fig. 7 for low molecular weight HYA fractions. Table 2 summarizes the parameters of linear regression of points before the break occurred and the intercepts with linear region. Using those intercepts, the hydration numbers which have the meaning of "non-evaporable" water were determined (Table 2).

3.3. Comparison of methods applied

Data presented in this work confirmed earlier results that the nature and distribution of ice present in the HYA system depends on W_c (Yoshida et al., 1992). It has been also previously stated that the water-binding capacity is directly related to the molecular weight of the molecule (Sutherland, 1998). However, that statement was not confirmed in this work, where HYA having molecular weight from 101 to 740 kDa showed similar water binding capacity and different value was observed only for 1390 kDa (Table 1). A number of theories have already been reported as possible explanation for this difference such as for example influence of the molecular chain dynamics hindering the self-diffusion of water from the free movement during the nucleation (Wiggins, 1995) or occurrence and composition of glassy ice and low density ice with unknown melting enthalpy and unpredictable behaviour (Wolfe et al., 2002) In fact, in order to overcome problems associated with ice formation, the evaporation experiments were carried out. Comparison of results reported in Tables 1 and 2 shows that except for the H^+HYA the determined NFW content was substantially lower than value of non-evaporable water obtained by freezing/thawing experiment. However, some aspects should be clarified also in this case. First of all, while in general only a linear decrease of enthalpy of evaporation would be expected due to the progressively decreasing water content, in case of HYA at certain concentration the break occurs (Fig. 7). Such a break could be accounted for the appearance of a process which is associated with energy release competing with energy consumption necessary for water evaporation, or in the case of the last hydration layer, water desorption. That means that the total enthalpy measured by DSC is not linearly decreasing at lower concentration range, and instead it shows more or less constant values (except H^+HYA). Presumably, the reverse enthalpy balance should be expected since the hydration water is strongly tight on the HYA skeleton and thus would need more energy to be desorbed from the charged surface. A possible explanation could be found in the conformation and molecular movement of HYA segments. HYA was described as crowded random coil molecules in liquid state but after the evaporation of water, in solid state, it is predominantly a single helical conformation containing 3 disaccharides per helical turn. However, the number of disaccharides per helical turn and formation of single or double helix depends on the character of counter ions. Structural conformation can be understood as stretched coiled telephone cords stabilized by H-bonds linking adjacent sugar residues across both glycosidic linkages (Cowman & Matsuoka, 2005). Since the dissolution of HYA in water is accelerated by elevated temperature, it seems that the formation of some intermolecular and intramolecular H-bonds is thermodynamically slightly more favoured in comparison with water/HYA interaction. Considering this, the resulting supramolecular arrangement (entropy) in solid state is then better organized than the conformation of HYA in solution. The higher organization causes the energy release, which in turn results in the break dependence depicted in Fig. 7. Such explanation is further supported by Fig. 6 where the low water content sample $W_c = 0.08$ showed the evaporation peak at around 60 °C which is still in the temperature range, where the bulk water evaporates (Fig. 6). If the water was adsorbed on the HYA molecule, the desorption temperature would be higher than that of evaporation of bulk water. This again supports the idea of the occurrence of an additional exothermic process compensating for the enthalpy of water desorption at low water concentrations.

Assuming the monomolecular layer of water on the surface of HYA, the approaching of segments and subsequent formation of H-bonds can occur only when there is no molecule of water between two HYA segments. Accordingly, assumed reconformation process starts when the hydration water is being desorbed which means that the break necessarily indicates the desorption onset of the last hydration layer.

As it can be seen in Table 2, H^+HYA showed two times higher hydration number than HYA. The possible explanation has already been indicated in previous paragraphs (concerning the structure of HYA in solid state) and it is related to the secondary structure of HYA and H^+HYA in solid state. In fact, the presence of Na^+ ion brings about the occurrence of low-temperature melting ice when cooled down. It confirms that the presence of ions with different dimension and surface charge is crucial for the character of supramolecular structure. It seems that the Na^+ ion makes the structure more "rigid", and therefore the reported unfolding of the HYA chains during evaporation is easier when the H^+ ion is present.

Table 2
Content of hydration water for HYA of different molecular weight and counterion from evaporation experiments. n_b is the number of water molecules per disaccharide unit, NEW stands for the content of non-evaporable water in g per 1 g of HYA.

Sample	NEW	[a]n_{NEW}	[b]Parameters a; b	Confidence coefficient R^2
100	0.36	8.0	2224; −318	0.9998
254	0.36	8.0	2192; −279	0.9984
740	0.31	6.9	2251; −256	0.9981
1390	0.38	8.4	2040; −268	0.9894
H^+	0.84	17.6	2213; −609	0.9947

[a] Recalculated to the molecular weight of Na^+ and H^+ form.
[b] For the linear part of the increase.

4. Conclusion

Knowledge of HYA hydration is crucial for designing modification reactions such as crosslinking, hydrophobization etc.

In accordance with previous findings about hydration of ions (Zavitsas, 2001), the number of hydration water determined for HYA depends on the method and approach used. Nevertheless, as shown in this study, there exists an alternative approach which provides additional information enabling a deeper insight into the problem of HYA hydration when DSC technique is used. It is necessary to point out that the content of both NFW and non-evaporable water depends on the temperature since the origin of both is in the strong temperature-dependent water adsorption and therefore the content of both is different.

The evaporation approach seems to be a suitable option for the determination of hydration water in HYA or possibly also in other (bio)polymers. In our opinion, it provides more reliable results which are less biased by the unknown factors. Moreover, results published here revealed very important phenomena with interesting and exploitable consequences. In fact, during the evaporation, the concentration of water around 0.3–0.4 $g\,g^{-1}$ seems to be very important for the character of HYA in dry state. In other words, this is the moment in which the HYA supramolecular structure can be simply influenced by the external factors (such as temperature, mechanical stress etc.) in order to obtain dry, non-modified or "native" HYA with specific properties. This is in accordance with the recent comment of Hargittai and Hargittai (2008) on the work of Laurent (1957) about importance of conditions under which HYA is prepared. In addition they also stressed out the observation of Scott (1998) who put in question the randomness of HYA coiling. The influencing of HYA structure in solid state by an external factor is a similar approach as frequently used in "crystal engineering". Such issue, however, is beyond the scope of this work and it will be solved in a special study.

Acknowledgement

This work was financially supported by the Ministry of Education, Youth and Sport of the Czech Republic project No. 0021630501.

References

Berthold, J., Desbrieres, J., Rinaudo, M., & Salomen, L. (1994). Types of adsorbed water in relation to the ionic groups and their counter-ions for some cellulose derivatives. *Polymer*, *35*, 5729–5736.

Cowman, M. K., & Matsuoka, S. (2005). Experimental approaches to hyaluronan structure. *Carbohydrate Research*, *340*, 791–809.

Hargittai, I., & Hargittai, M. (2008). Molecular strcuture of hylauronan: an introduction. *Structural Chemistry*, *19*, 697–717.

Hatakeyama, H., & Hatakeyama, T. (1998). Interaction between water and hydrophilic polymers. *Termochimica Acta*, *308*, 3–22.

Hatakeyama, T., Nakamura, K., & Hatakeyama, H. (2000). Vaporation of bound water associated with cellulose fibres. *Termochimica Acta*, *352–353*, 233–239.

Haxaire, K., Marechal, Y., Milas, M., & Rinaudo, M. (2003a). Hydration of polysaccharide hyaluronan observed by IR spectrometry. I. Preliminary experiments and band assignments. *Biopolymers*, *72*, 10–20.

Haxaire, K., Marechal, Y., Milas, M., & Rinaudo, M. (2003b). Hydration of hyaluronan polysaccharide observed by IR spectrometry. II. Definition and quantitative analysis of elementary hydration spectra and water uptake. *Biopolymers*, *72*, 149–161.

Joun, N., Rinaudo, M., Miles, M., & Desbrieres, J. (1995). Hydration of hyaluronic acid as a function of the counterion type and relative humidity. *Carbohydrate Polymers*, *26*, 69–73.

Joshi, H. N., & Topp, E. M. (1992). Hydration in hyaluronic acid and its esters using differential scanning calorimetry. *International Journal of Pharmaceutics*, *80*, 213–225.

Kogan, G., Šoltéz, L., Stern, R., & Gemener, P. (2007). Hyaluronic acid: a natural biopolymer with a broad range of biomedical and industrial applications. *Biotechnology Letters*, *29*, 17–25.

Laurent, T. C. (1957). The amorphous X-ray diffractogram of hylauronic acid. *Arkiv for Kemi*, *11*, 513–518.

Lui, J., & Cowman, M. K. (2000). Thermal analysis of semi-diluted hyaluronan solutions. *Journal of Thermal Analysis and Calorimetry*, *59*, 547–557.

Marechal, Y., Milas, M., & Rinaudo, M. (2003). Hydration of haluronan polysaccharide observed by IR spectrometry. III. Structure and mechanism of hydration. *Biopolymers*, *72*, 162–173.

Mráček, A., Benešová, K., Minařík, A., Urban, P., & Lapčík, L. (2007). The diffusion process of sodium hyaluronate (Na-HA) and Na-HA-n-alkyl derivatives films swelling. *Journal of Biomedical Materials Research Part A*, *83A*, 184–190.

Mráček, A., Varhaníková, J., Lehocký, M., Grundelová, L., Pokopcová, A., & Velebný, V. (2008). The influence of Hofmeister series ions on hyaluronan swelling and viscosity. *Molecules*, *13*, 1025–1034.

Riesen, R. (2007). Choosing the right baseline. *User Com*, *25*, 1–6.

Scott, J. E. (1998). Chemical morphology of hyaluronan. In T. C. Laurent (Ed.), *The chemistry and medical applications of hyaluronan and its derivatives, Wenner–Gren international series* (pp. 7–15). London: Portland Press.

Sutherland, W. (1998). Novel and established applications of microbial polysaccharides. In *Institute of cell and molecular biology*. Edinburgh University., p. 16.

Takahashi, M., Hatakeyama, T., & Hatakeyama, H. (2000). Phenomenological theory describing the behaviour of non-freezing water in structure formation process of polysaccharide aqueous solutions. *Carbohydrate Polymers*, *41*, 91–95.

Wiggins, P. M. (1995). High and low density water in gels. *Progress in Polymer Science*, *20*, 1121–1163.

Wolfe, J., Bryant, G., & Koster, K. L. (2002). What is "unfreezeable water", how unfreezable is it and how much is there. *CryoLetters*, *23*, 157–166.

Yoshida, H., Hatakeyama, T., & Hatakeyama, H. (1989). Glass transition of hyaluronic acid hydrogel. *Kobunshi Ronbunshu*, *46*, 597–602.

Yoshida, H., Hatakeyama, T., & Hatakeyama, H. (1990). In J. F. Kennedy, G. O. Phillips, & P. A. Williams (Eds.), *Cellulose* (pp. 305–310). Chichester, UK: Horwood.

Yoshida, H., Hatakeyama, T., & Hatakeyama, H. (1992). *Polymer preprints, Japan* , p. 3026.

Yoshida, H., Hatakeyama, T., & Hatakeyama, H. (1993). Characterization of water in polysaccharide hydrogels by DSC. *Journal of Thermal Analysis*, *40*, 483–489.

Zavitsas, A. A. (2001). Properties of water solutions of electrolytes and nonelectrolytes. *Journal of Physical Chemistry B*, *105*, 7805–7815.

Appendix 2

Kučerík, J., Průšová, A., Rotaru, A., Flimel, K., Janeček, J., Conte, P. (2011). DSC study on hyaluronan hydration and dehydration. Thermochimica acta 523: 245–249.

Thermochimica Acta 523 (2011) 245–249

Contents lists available at ScienceDirect

Thermochimica Acta

journal homepage: www.elsevier.com/locate/tca

Short communication

DSC study on hyaluronan drying and hydration

J. Kučerík[a,*], A. Průšová[a], A. Rotaru[b], K. Flimel[a], J. Janeček[c], P. Conte[d]

[a] Brno University of Technology, Faculty of Chemistry, Purkyňova, 118, 612 00 Brno, Czech Republic
[b] INFLPR – National Institute for Laser, Plasma and Radiation Physics, Laser Department, Bvd. Atomistilor, Nr. 409, PO Box MG-16, 077125 Magurele, Bucharest, Romania
[c] ENSTA - École Nationale Supérieure de Techniques Avancées, 32 boulevard Victor, 75739 Paris Cedex 15, France
[d] Università degli Studi di Palermo, Dipartimento di Ingegneria e Tecnologie Agro-Forestali, Viale delle Scienze 13, ed. 4, 90128 Palermo, Italy

ARTICLE INFO

Article history:
Received 26 November 2010
Received in revised form 27 April 2011
Accepted 30 April 2011
Available online 7 May 2011

Keywords:
Evaporation kinetics
Hyaluronan
Hydration
Drying
Isoconversional methods
KAS

ABSTRACT

The processes of hyaluronan (HYA) drying and hydration were studied using differential scanning calorimetry. In the first approach the isoconversional Kissinger–Akahita–Sunose (KAS) method was applied in order to determine actual activation energies of evaporation of pure water and water from concentrated HYA solutions. Since the evaporation is a single-step process, the activation energies for pure water provided results consistent with tabulated values of evaporation enthalpies. In the course of water evaporation from hyaluronan solution a break in increasing enthalpy followed by a decrease below 0.34 g of water per 1 g of HYA was observed. This result confirmed earlier observation that at this particular water content evaporation from hyaluronan is compensated by heat evolution associated with the formation of new bonds in hyaluronan supramolecular structure. Subtraction of water evaporation enthalpy from enthalpies obtained for HYA concentrated solution provided a possibility to extrapolate the evaporation enthalpies to the concentration (approximately 2 g of water per 1 g of HYA) at which free water is not present any longer and only bound water starts being evaporated from the HYA solution. Similar results were obtained in the second approach in which using slightly modified "traditional" freezing/thawing experiment, melting enthalpy of ice was plotted against water fraction in HYA. It was found out that the melting enthalpy of ice exponentially increases from 0.8 up to 2 g of water per g of hyaluronan where it reaches and keeps the melting enthalpy of hexagonal ice. It was shown that both approaches can serve as alternatives providing an additional insight into the state of water and biopolymers in highly concentrated solutions.

© 2011 Elsevier B.V. All rights reserved.

1. Introduction

Hyaluronic acid, also known as hyaluronan (HYA), is currently a compound of a special importance and interest mainly for medicinal and cosmetic applications [1–4]. It is a naturally occurring biopolymer that serves for several important biological functions in mammals bodies. From the chemical point of view, it is a high molecular weight (10^5–10^7 Da) unbranched glycosaminoglycan composed of repeating disaccharides (β-1-3-D-*N*-acetylglucosamine, β-1-4-D-glucuronic acid). HYA in aqueous solution forms tertiary structures β sheets based on 2-fold helixes anti-parallel HYA chains. Sphere occupied by HYA molecule is quite large, but not impenetrable, and therefore HYA forms specific overlapping domains creating meshwork which is stabilized by specific H-bonds, water bridges and hydrophobic interactions. This is thought, together with its polarity, as a potential reason for higher osmotic pressure in the solution causing high water-retention capacity of HYA [5]. In fact, hydration and/or water retention capacity is probably one of the most important aspects of the hyaluronan biological functions.

HYA hydration was studied by using several approaches among which NMR [6], viscosimetry [7], ultrasonic and densitometry analyses [5] and thermal analyses (mainly differential scanning calorimetry, DSC) played an important role [8,9].

The application of DSC is mostly based on a relatively simple principle; water present in concentrated (semi-diluted) solutions is frozen and the enthalpy of ice melting obtained during the heating run is used to determine the hydration number [10]. Accordingly, water surrounding HYA molecule in the solution is categorized into three groups: non-freezing water (NFW) also called hydration number, freezing-bound water (FBW) and free water (FW) [11]. Such approach is frequently criticized since experimental arrangement and conditions can cause some errors and thus the value of the NFW obtained from those experiments does not perfectly fit to the theoretically calculated values of hyaluronan hydration [12]. In fact, a problem with the presence of so-called glassy (amorphous) water may occur. Amorphous water develops during the freezing when segments of hyaluronan hinder the self-diffusion of water

* Corresponding author. Tel.: +420 777 633 675; fax: +420 541 211 697.
E-mail address: kucerik@fch.vutbr.cz (J. Kučerík).

0040-6031/$ – see front matter © 2011 Elsevier B.V. All rights reserved.
doi:10.1016/j.tca.2011.04.034

and ice crystals cannot be formed. The experimental conditions used in thermal analysis cannot avoid the appearance of supercooling effect and thus the perfect crystallization of all freezable water is not guaranteed even after several days of intensive cooling [13]. Despite to the criticism, recent comparison of DSC measurements with NMR relaxometry brought quantitative agreement for hydroxyethylcellulose and sodium salt of carboxymethylcellulose cross-linked with divinyl sulfone, which confirms the applicability and validity of such approach (at least in specific cases) [14]. DSC technique based on cooling/thawing approach was used several times to investigate the interaction of neutral polysaccharides (e.g. Ref. [15]) or hydrophilic polysaccharides (including hyaluronan, e.g. Refs. [8–10]) with water. These approaches were lately adopted by Prawitwonga et al. [16] who investigated the phase transition behavior of sorbed water in Konjac mannan and six types of adsorbed water were identified. Another alternative DSC approach based on the water vaporization of bound water associated with cellulose fibers was used as well [17].

The first aim of this study is to continue and extend the research focused on evaluation of processes taking part during HYA dehydration and state of the hyaluronan in highly concentrated solutions. In our previous study, during the gradual drying of HYA, the evolution of enthalpy was observed at water fraction 0.34 which was in contrast to energy consumption necessary for HYA dehydration. Based on those results, in order to determine the hydration number of hyaluronan, an alternative DSC approach was suggested and new term "non-evaporable water" water was introduced [18]. Non-evaporable water content was defined as the water fraction in HYA at which, during the drying process, energy necessary for the evaporation starts to be partly compensated by the energy evolution caused by a formation of intermolecular interactions between adjacent HYA segments [18]. Based on those results, in this work isoconversional kinetic methods are applied to determine the actual enthalpy of vaporization in the course of HYA drying. With this respect, the single-step process of water evaporation H_2O (l) → H_2O (g) is assumed at every moment of progressive evaporation (conversion) and the activation energy of process is determined. Essentially, taking into account the above-mentioned single-step condition, for free water this activation energy has the meaning of the enthalpy of water evaporation. This was already demonstrated for example for evaporation enthalpy of pure caprylic acid [19]. In reference [19], the Vyazovkin method [20] was used and the obtained enthalpies of vaporization determined for conversion degree (α) around 0.5 gave a good compliance with tabulated values. Accordingly, in pure water or in diluted solutions, when free water is being evaporated, values determined by isoconversional methods are equal to the evaporation enthalpy which is the nomenclature used in this study. It is necessary to point out that in highly concentrated HYA solutions the determined enthalpy can involve also energy demands for water diffusion through the HYA structure. Further, when free water is completely evaporated, only last layer of water which is in intimate contact with the surface of HYA remains; in this case, the removing water processes should be called "desorption" (i.e. reverse process to adsorption) and thus in this case the desorption enthalpy is obtained; again the same nomenclature is used in this work. Also in this case, the obtained enthalpy can represent a sum of enthalpies associated with desorption of water from HYA surface, water diffusion thought the HYA mass and possible also reorganization of HYA physical structure itself. Therefore, both kinds of enthalpies obtained from concentrated solutions presented in this work should be considered more as apparent values. As also confirmed in this work, the value of pure water evaporation enthalpy at standard pressure is slowly and steadily decreasing in the temperature interval 0–100 °C. That implies that the possible fluctuation of enthalpy in the course of dehydration can reveal possible competitive processes with regard to the evaporation. Further, in accordance with literature data [21] it is assumed that the enthalpy needed for the evaporation of free water from HYA solution should be different in comparison with the desorption of water tightly bounded on the polar surface of HYA. Therefore, this represents an important tool for elucidation of processes which are HYA and other biopolymers exposed to in the course of their processing and further for development of native HYA-based materials with desired properties. Presented data shows the possibility of application of isoconversional methods to follow simple processes occurring during evaporation of water from a biopolymer and use them to bring some new information on the conformation of HYA in semi-diluted solutions.

The second aim of the study is to extract more information from the above-mentioned traditional freezing/thawing DSC approach. As a rule, only non-freezing water is determined from plot melting enthalpy vs. water fraction. However, we assume that this dependency can be used for distinguishing of bound and free water which is information which can be, in an ideal case, extracted also from previous approach.

2. Experimental

2.1. Sample preparation

Bacterial HYA with molecular weight of 650 kDa (measured by size-exclusion chromatography, results not reported) was kindly provided by CPN Company (Dolní Dobrouč, Czech Republic). Approximately 2 mg of the sample was placed in an aluminum pan (Tzero® Technology), excess of water (milli-Q) was added and allowed to evaporate slowly at room temperature until the desired water content was reached. The pan was subsequently hermetically sealed and left to equilibrate at room temperature for 26 h as previously recommended [17]. Water fraction (W_c) in hyaluronan samples was defined as follows: W_c = (mass of water)/(mass of dry sample).

In order to obtain the precise water content, thermogravimetric analysis (Q5000IR TA Instruments) was additionally used to determine the equilibrium moisture content as a mass loss in the temperature interval 25–220 °C under dynamic atmosphere of nitrogen 25 mL min^{-1}.

2.2. DSC evaporation measurements

Differential scanning calorimetry (DSC) measurement was performed using a TA Instruments DSC Q200 equipped with a cooling accessory RCS90. The temperature and enthalpy calibration of the device were carried out using In, Sn and pure water standards.

2.2.1. Desorption enthalpy determination by DSC

The purpose of this experiment was to obtain the evaporation peaks of water from samples of W_c = 0.3 and W_c = 1.5 at different heating rates and to use them for the determination of evaporation and/or desorption enthalpies.

Prior to the measurements, the lid covering the pan was carefully perforated using a sharp tool; the pan was immediately placed into DSC and the experiments were carried out. In order to reduce the influence of nitrogen flow on DSC record, the nitrogen flow rate was reduced to 5 mL min^{-1}; heating rates β = 1, 2, 3, 5 and 10 K min^{-1} were used in the temperature range −50 °C to 250 °C. Similarly, the enthalpies of pure water during evaporation were also determined. However, due to the experimental limitations, the heating rates β = 0.1, 0.5, 1, 2 and 3 K min^{-1} were used in this case. The kinetic calculations for the water elimination (sample 1.5 and sample 0.3) were performed by using the TKS-SP 2.0 software

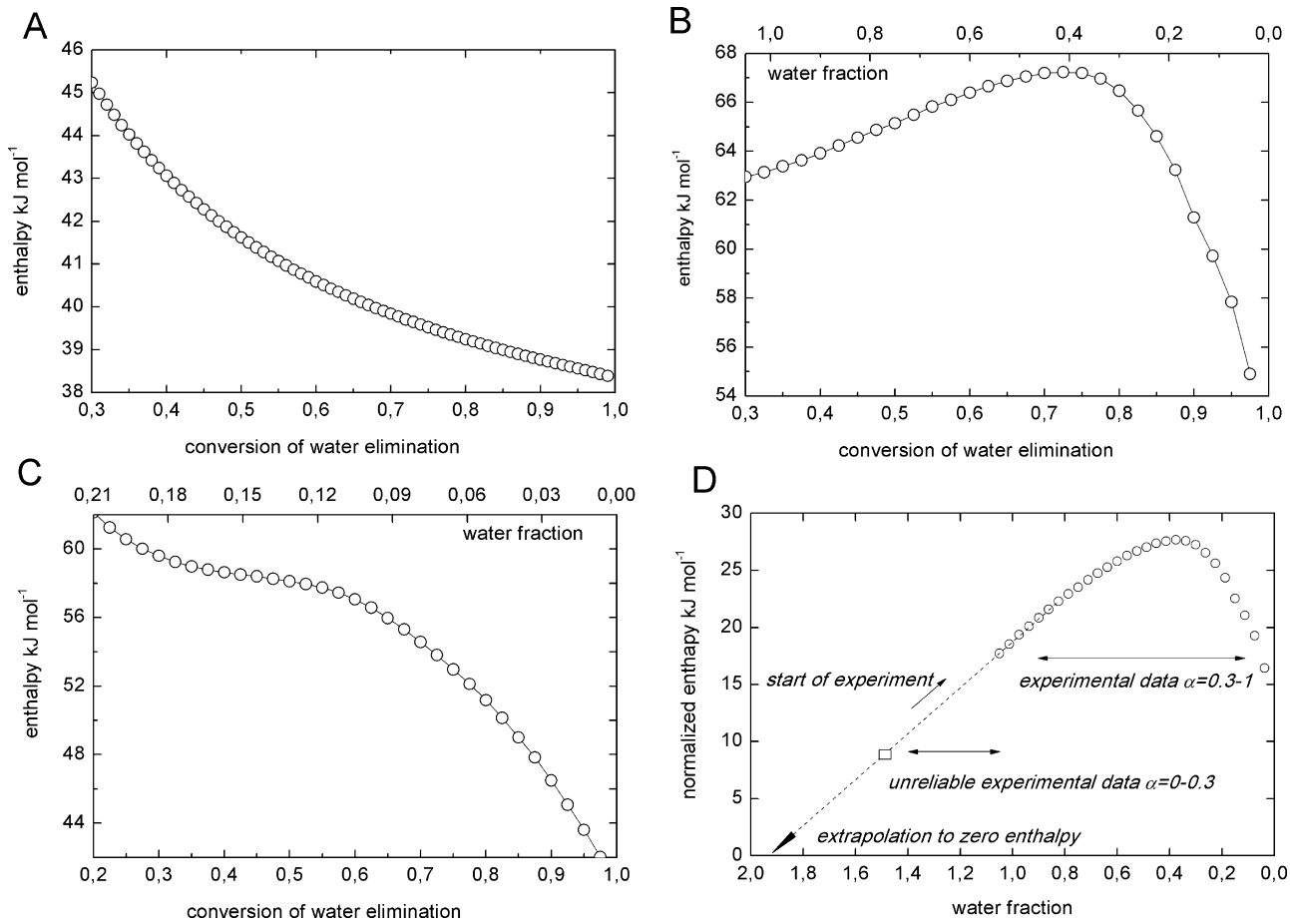

Fig. 1. Evaporation enthalpy change as a function of the degree of evaporation in: pure water (A), HYA aqueous solutions with starting water mass fraction $W_c = 1.5$ (B) and $W_c = 0.3$ (C). Difference of evaporation enthalpies (D), obtained by subtracting, at each degree of evaporation, the values referred to pure water (A) from those referred to HYA aqueous solutions with $W_c = 1.5$ (B).

package [22,23]. In this paper, the Kissinger–Akahira–Sunose (KAS) integral linear isoconversional method [24,25] was used (Eq. (1)):

$$\ln\left(\frac{\beta_i}{T_{\alpha,i}}\right) = Const - \left(\frac{E_\alpha}{R}\right) \cdot \left(\frac{1}{T_{\alpha,i}}\right) \quad (1)$$

where the subscripts α and i indicate the selected values of the degree of evaporation and heating rate, respectively, E is the activation energy, T is the absolute temperature, and R is the universal gas constant. Conversion degree (α) is taken from the partial DSC peak. KAS method uses the Coats–Redfern approximation of the temperature integral [26], which is considered to be the best among approximations of temperature integral when using Arrhenius-type theory. Thus, for fixed values of α, the plots $\ln(\beta/T^2)$ vs. $(1/T)$ obtained from the experimental DSC curves recorded for several constant-heating rates, should be straight lines with the slope proportional to the activation energy which, as stated in the Introduction, has the meaning of evaporation or desorption enthalpy (in dependency on water fraction). The standard deviation of activation energy calculations are not plotted in figures since they are such small that they would be covered by the size of symbols. Instead, the linearity of plots $\ln(\beta/T^2)$ vs. $(1/T)$ was tested by least square method, appropriate values of correlation coefficients are reported in the text. The conversion degree was calculated as partial peak areas, i.e. whole peak area obtained for particular heating rate represented 100% of the evaporation process. Plots of determined enthalpies are reported in dependency on the water fraction and the same time as a function of conversion, e.g. if 30% (conversion 0.3) of water was evaporated from sample $W_c = 1.5$, the actual water content was $W_c = 1.05$ etc.

2.2.2. DSC freezing/thawing experiments

Freezing/thawing experiments were carried out in order to determine the enthalpy of ice melting, which was formed from the freezable water present in the sample. The enthalpy was determined from the area of the endothermic peak occurring in the temperature interval from −40 °C to 0 °C. Samples used in these DSC experiments included the same way of preparation as used in the first type of evaporation experiment, but without the lid perforation. A concentration line within W_c from 0.2 to 20 water/HYA was prepared. The following thermal protocol was used: start at 40 °C; cooling from 40 °C to −90 °C at 3 K min^{-1}; keeping the samples isothermally at −90 °C for 2 min; heating with 3 K min^{-1} from −90 °C to 30 °C. The flow rate of dynamic nitrogen atmosphere was 50 mL min^{-1}.

3. Results and discussion

3.1. Determination of desorption enthalpy

Fig. 1A reports the results from application of KAS model-free kinetic approach to determine the enthalpy of pure water evaporation. Kinetics analysis rarely provides reliable data in the interval from $\alpha = 0$ to approximately 0.2 or 0.3 and therefore, only values from $\alpha = 0.3$–1.0 are reported (Fig. 1A). It can be seen that the determined values are in a good agreement with the tabulated val-

ues reported for instance in Ref. [27]. In fact, under atmospheric pressure conditions, the standard values are decreasing as follows: 45.04, 43.35 and 41.58 kJ mol^{-1} for 0, 40 and 80 °C, respectively, while in this work they decrease from 45 to 39 kJ mol^{-1} within α = 0.3–1 range. The decrease in value reflects the conditions of DSC experiment; in fact, the water was evaporated within the temperature interval 0–80 °C and under unknown pressure. Correlation coefficients for calculation of enthalpies reported in Fig. 1A gave values around 0.992 in the whole interval of conversions.

Fig. 1B shows the evaporation/desorption enthalpy for sample W_c = 1.5 within the conversion degree interval α = 0.3–1.0, i.e. water evaporation from HYA at W_c from 1.05 to 0. As it can be seen from the activation energy trend, in the conversion range of α = 0.3–0.75, the enthalpy slightly increases and after α = 0.75 steeply decreases (r > 0.998 over the entire conversion degree range). In order to confirm such a decrease in enthalpy additional measurements were carried out using the sample with W_c = 0.3. That means that water content in the sample was lower than the W_c under which the steep enthalpy decrease occurred. Results of the experiment are depicted in Fig. 1C. The respective correlation coefficients confirm the good data compliance (r > 0.990). The decreasing tendency of enthalpies confirms the previously obtained decrease reported in Fig. 1B. It is worth to point out that the value of enthalpy in Fig. 1C corresponds quite well to that depicted in Fig. 1B.

HYA was described as molecule of 2-fold helix shape interacting with adjacent HYA chains creating meshwork in liquid state, in the solid state, after the evaporation of water, HYA is believed to be composed predominantly by single helical structures containing 3 disaccharides per helical turn [7]. For this reason, during dehydration, the molecules are better organized (a decrease in entropy), stabilized also by some new inter and intra molecular interactions whose formation is associated with enthalpy evolution (break of the dependency in Fig. 1B).

The evaporation data obtained for pure water (Fig. 1A) represents kind of "baseline" for data obtained for W_c = 1.5 (Fig. 1B), since both dependencies were obtained in a similar temperature range; Fig. 1D reports the results obtained by subtraction of enthalpies reported in Fig. 1C from enthalpies reported in Fig. 1A, i.e. from enthalpies obtained from evaporation of water from HYA solution the contribution of pure water was subtracted. Subtraction of both dependencies provides more detailed view on the processes occurring in the course of water evaporation from HYA. Mainly, values different from zero represent additional enthalpies with respect to the enthalpies necessary for the free water evaporation; zero is in this case equal to the free water evaporation and therefore the chart illustrates the behavior of HYA molecule and bound water in the course of the water elimination. Adsorbed (bound) water has different physical properties in comparison with the free or unbound water. The increase in enthalpy profiles starts when the physical character of water layer is changed, i.e. when the unbound water is completely eliminated. Unfortunately, the experimental conditions do not permit measurement of water evaporation from samples with higher water content, i.e. approximately at W_c > 2, because when free water is evaporated (boiled) at 100 °C, the enthalpy is consumed (infinite heat capacity) and the DSC measuring system cannot keep the programmed temperature regime.

The only option left to estimate the concentration at which water changes its character is the extrapolation of obtained results, as reported in Fig. 1D. It is necessary to point out that the extrapolation may not be linear as used in our case. As shown in Fig. 1D the free water can be seen above approximately W_c = 1.95 while below this value only bound water is present. W_c = 1.95 corresponds to 43 molecules of water per HYA disaccharide unit, and reaches values as low as W_c = 0.34 (7.6 water molecules). All the enthalpies are above zero in Fig. 1D which means that the interactions between HYA segments are weaker than the interactions between HYA and water. Nevertheless, the H-interactions bond energy are strongly geometry- and distance-dependent, therefore the development of less soluble native HYA suggested in [18] can be carried out by an appropriate design of HYA dehydration conditions.

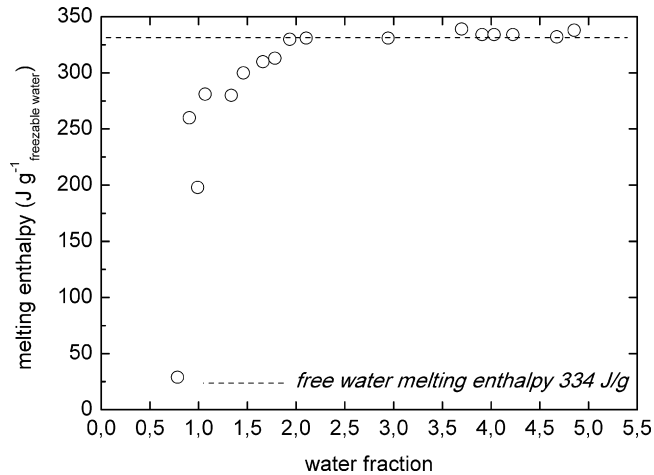

Fig. 2. Dependency of the melting enthalpy of ice formed by freezable water on the water fraction W_c.

3.2. Dependence of ice melting enthalpy on concentration

Freezing/thawing DSC experiment is one of the most frequently applied methods to study hydration of hyaluronan and of other biopolymers [8–11]. In this work, this approach was used to determine the enthalpy of melting in order to calculate non-freezing water (NFW) and consequently freezing bound water (FBW). Simply, for a set of samples with different water fractions melting enthalpy of bound water were determined and plotted against respective values of water fractions [8–11]. The extrapolation of melting enthalpy to zero showed that the NFW is 0.8 g of water per g of HYA. Obtained results are in accordance with the data reported in the earlier papers [8,10]. In the next step, the NFW content (W_{NFW}) was used to determine the content of freezable water (W_{FW}) in each sample according to following relationship (W_{total} is the total water content.):

$$W_{FW} = W_{total} - W_{NFW} \quad (2)$$

Since both W_{total} and W_{NFW} content are known, the enthalpy measured by DSC was divided by freezable water content W_{FW}. Fig. 2 reports the dependence of freezable water melting enthalpy on the water content. It can be seen that at low concentrations, the melting enthalpy is significantly lower than the enthalpy of ice (hexagonal) formed by pure water (334 J g^{-1}). This value is reached around W_c = 2. The constant value 334 J g^{-1} continued for W_c up to 20 (results not shown).

Fig. 2 reveals several important facts deserving attention and discussion. First, it is noteworthy that the normalized enthalpy of ice melting slowly reached the 334 J g^{-1} value, i.e. the enthalpy of hexagonal ice melting. Low enthalpy values at concentrations below W_c = 2 indicate the presence of ice which was formed under restricted water self-diffusion conditions. Those can involve either presence of confined water in pores of HYA physical structure or the influence of charged groups or molecular segments restricting mechanically free water diffusion or both. The value 334 J g^{-1} would indicate that in solutions with W_c > 2, there exist only two kinds of water structures; NFW and FW. However, this is in contrast with results of other authors. It is a general observation that at least three types of water structures are present in HYA solution at W_c > 2 [9,28]. This indicates that the NFW content probably

increases with increasing water content in the HYA sample in order to compensate the total enthalpy measured by DSC to reach the values of 334 J g^{-1}. This can be explained by processes of HYA dissolution and progressive dilution, increasing content of water causes the solvation of HYA molecular segments, swelling [4] (physical structure of HYA is slightly corrupted, water is still confined in a temporary pore system) and liberated (segments are free); possibly also some changes in conformation occur [29]. Similar increase in melting enthalpy was also observed for molecules of ibuprofen packed in mesoporous silicon microparticles in dependency on the pore diameter [30]. Unlike silicon, hyauluronan is a water soluble biopolymer and increasing water content is supposed to destruct the metastable pores and vacancies formed during the drying. It appears that also in this kind of experiment, W_c around 2 represents the border concentration at which the water content is high enough to allow to the hyaluronan segments to be perfectly separated. It indicates that in the concentration W_c interval between 0.34 and approximately 2 (depending on external conditions such as for example temperature), the hyaluronan physical structure is still compact but progressively weakening with water content increase. As a result water molecules cannot freely move and hyaluronan chains are stabilized by mutual intermolecular interactions. At $W_c > 2$, the restriction of self-diffusion of water molecules is much lower (appearance of free water). Interestingly enough W_c around 2 is similar for both evaporation/desorption and freezing/thawing approaches, which implies the mutual complementarity of both techniques.

4. Conclusions

In this work, the new approach useful for study of hyaluronan hydration based on the determination of evaporation/desorption enthalpy was introduced. It was shown that this approach has a potential to study structural changes of selected materials in the course of their drying and possibly also reversibility of their rehydration. Obtained results were comparable with calculations from a slightly modified "classical" approach. The obtained results suggest that the hydration number of HYA and possibly of other biopolymers as well, should not be reported simply as one value; rather it should be reported as a concentration range in which the hydration number varies when a biopolymer is being dissolved and change in a physical structure caused by water content should be taken into account as well. In fact, such value range would cover the distribution of wettable and available surface charge on the biopolymer surface, which can significantly differ in dry and wet state of a biopolymer and can be drying-method-dependent. That approach should be also more useful for further considerations concerning the designing of the HYA applications. For example, the experiments published in this work support the possibility to influence the structure of native HYA with respect to conditions during the drying. If an additional factor is introduced, either physical or chemical (or both), the resulting native HYA structures would significantly differ in their supramolecular arrangement, providing a relatively wide range of physical properties. This idea is not completely new; it just reflects the notion which was firstly published and probably forgotten almost five decades earlier [31]. Last but not least, results in Fig. 2 directly show the occurrence of ice with lower melting enthalpy in biopolymers which was frequently reported only for water confined in solid porous materials such as for example silica [32].

Acknowledgements

This work was financially supported by the Ministry of Education, Youth and Sport of the Czech Republic project no. 0021630501. Authors would like to thank Dr. Vladimír Velebný from CPN Company, Dolní Dobrouč, Czech Republic for providing of HYA samples.

References

[1] P. Mlčochová, V. Hájková, B. Steiner, S. Bystrický, M. Koóš, M. Medová, V. Velebný, Preparation and characterization of biodegradace alkylether derivatives of hyaluron, Carbohyd. Polym. 69 (2007) 344–353.
[2] Z. Bezáková, M. Hermannová, E. Dřímalová, A. Malovíková, A. Ebringerová, V. Velebný, Effect of microwave irradiation on the molecular and structural properties of hyaluronan, Carbohyd. Polym. 73 (2008) 640–646.
[3] E. Dřímalová, V. Velebný, V. Sasinková, Z. Hromádková, A. Ebringerová, Degradation of hyaluronan by ultrasonication in comparison to microwave and conventional heating, Carbohyd. Polym. 61 (2005) 420–426.
[4] A. Mráček, K. Benešová, A. Minařík, P. Urban, L. Lapčík, The diffusion process of sodium hyaluronate (Na-HA) and Na-HA-n-alkyl derivatives films swelling, J. Biomed. Mater. Res. A 83 (2007) 184–190.
[5] A. Davies, J. Gormally, E. Wyn-Jones, A study of hydration of sodium hyaluronate from compressibility and high precision densitometric measurements, Int. J. Biol. Macromol. 4 (1982) 436–438.
[6] S.G. Harding, O. Wick, A. Helander, N.-O. Ahnfelt, L. Kenne, NMR velocity imaging of the flow behaviour of hyaluronan solutions, Carbohyd. Polym. 47 (2002) 109–119.
[7] M.K. Cowman, S. Matsuoka, Experimental approaches to hyaluronan structure, Carbohyd. Res. 340 (2005) 791–809.
[8] H. Hatakeyama, T. Hatakeyama, Interaction between water and hydrophilic polymers, Thermochim. Acta 308 (1998) 3–22.
[9] J. Lui, M.K. Cowman, Thermal analysis of semi-dilute hyaluronan solutions, J. Therm. Anal. Calorim. 59 (2000) 547–557.
[10] H. Yoshida, T. Hatakeyama, H. Hatakeyama, Characterization of water in polysaccharide hydrogels by DSC, J. Therm. Anal. 40 (1993), 483- 439.
[11] T. Hatakeyama, H. Hatakeyama, K. Nakamura, Non-freezing water content of mono- and divalent cation salts of polyelectrolyte–water systems studied by DSC, Thermochim. Acta 253 (1995) 137–148.
[12] K. Haxaire, Y. Marechal, M. Milas, M. Rinaudo, Hydration of polysaccharide hyaluronan observed by IR spectrometry. I. Preliminary experiments and band assignments, Biopolymers 72 (2003) 10–20.
[13] J. Wolfe, G. Bryant, K.L. Koster, What is unfreezable water, how unfreezable is it and how much is there? Cry Lett. 23 (2002) 157–166.
[14] D. Capitani, G. Mesitieri, F. Porro, N. Proietti, A.L. Segre, NMR and calorimetric investigation of water in a superabsorbing crosslinked network based on cellulose derivatives, Polymer 44 (2003) 6589–6598.
[15] C. Fringant, J. Desbrieres, M. Milas, M. Rinaudo, C. Joly, M. Escoubes, Characterisation of sorbed water molecules on neutral and ionnic polysaccharides, Int. J. Biol. Macromol. 18 (1996) 281–286.
[16] P. Prawitwonga, S. Takigamia, G.O. Phillipsb, Phase transition behavior of sorbet water in Konjac mannan, Food Hydrocolloids 21 (2007) 1368–1373.
[17] M. Takahashi, T. Hatakeyama, H. Hatakeyama, Phenomenological theory describing the behaviour of non-freezing water in structure formation process of polysaccharide aqueous solutions, Carbohyd. Polym. 41 (2000) 91–95.
[18] A. Průšová, D. Šmejkalová, M. Chytil, V. Velebný, J. Kučerík, An alternative DSC approach to study hydration of hyaluronan, Carbohyd. Polym. 82 (2010) 498–503.
[19] S. Arias, M.M. Prieto, B. Ramajo, A. Espina, J.R. Garcia, Model-free kinetics applied to the vaporization of caprylic acid, J. Therm. Anal. Calorim. 98 (2009) 457–462.
[20] S. Vyazovkin, N. Sbirrazzuoli, Confidence intervals for the activation energy estimated by few experiments, Anal. Chim. Acta 355 (1997) 175–180.
[21] T. Hatakeyama, K. Nakamura, H. Hatakeyama, Vaporization of bound water associated with cellulose fibres, Thermochim. Acta 352–353 (2000) 233– 239.
[22] A. Rotaru, M. Gosa, P. Rotaru, Computational thermal and kinetic analysis software for non-isothermal kinetics by standard procedure, J. Therm. Anal. Calorim. 94 (2008) 367–371.
[23] A. Rotaru, M. Gosa, Computational thermal and kinetic analysis, J. Therm. Anal. Calorim. 97 (2009) 421–426.
[24] H.E. Kissinger, Reaction kinetics in differential thermal analysis, Anal. Chem. 29 (1957) 1702–1706.
[25] T. Akahira, T. Sunose, Trans 1969 joint convention of four electrical institutes, Res. Rep. Chiba Inst. Technol. 16 (1971) 22–31.
[26] A.W. Coats, J.P. Redfern, Kinetic parameters from thermogravimetric data, Nature 201 (1964) 68–69.
[27] K.N. Marsh (Ed.), Recommended Reference Materials for the Realization of Physicochemical Properties, Blackwell, Oxford, 1987.
[28] A. Průšová, P. Conte, J. Kučerík, G. Alonzo, Dynamics of hyaluronan aqueous solutions as assessed by fast field cycling NMR relaxometry, Anal. Bioanal. Chem. 397 (2010) 3023–3028.
[29] P. Matteini, L. Dei, E. Carretti, N. Volpi, A. Goti, R. Pini, Structural behavior of highly concentrated hyaluronan, Biomacromolecules 10 (2009) 1516–1522.
[30] J. Riikonen, E. Mäkilä, J. Salonen, V.P. Lehto, Determination of the physical state of drug molecules in mesoporous silicon with different surface chemistries, Langmuir 25 (2009) 6137–6142.
[31] T.C. Laurent, The amorphous X-ray diffractogram of hyaluronic acid, Ark Kemi 11 (1957) 513–518.
[32] K. Morishide, H. Yasunaga, Y. Matsutani, Effect of pore shape on freezing and melting temperatures of water, J. Phys. Chem. C 114 (2010) 4028–4035.

Appendix 3

Šmejkalová, D., Hermannová, M., Šulánková, R., Průšová, A., Kučerík, J., Velebný, M. (2012) Structural and conformation differences of acylated hyaluronan modified in protic and aprotic solvent system. Carbohydrate Polymers 87: 1460–1466.

Carbohydrate Polymers 87 (2012) 1460–1466

Contents lists available at SciVerse ScienceDirect

Carbohydrate Polymers

journal homepage: www.elsevier.com/locate/carbpol

Structural and conformational differences of acylated hyaluronan modified in protic and aprotic solvent system

Daniela Šmejkalová[a,*], Martina Hermannová[a], Romana Šuláková[a], Alena Průšová[b], Jiří Kučerík[b], Vladimír Velebný[a]

[a] Contipro C, Dolní Dobrouč 401, 561 02 Dolní Dobrouč, Czech Republic
[b] Brno University of Technology, Faculty of Chemistry, Purkyňova 118, 612 00 Brno, Czech Republic

ARTICLE INFO

Article history:
Received 7 July 2011
Received in revised form 2 September 2011
Accepted 12 September 2011
Available online 29 September 2011

Keywords:
Hyaluronan
Acylation
NMR
DSC
UV–vis
Mass spectrometry

ABSTRACT

Acylated hyaluronan (HA) in aqueous (DMSO/H_2O) and nonaqueous (DMSO) solutions was studied by means of nuclear magnetic resonance, differential scanning calorimetry (DSC), mass spectrometry and UV/vis spectroscopy. It has been demonstrated that structural and conformational properties of the acylated hyaluronan derivates are strongly dependent on the nature of reaction solvent. Acylation in DMSO was more selective than that carried out in DMSO/H_2O, though in both cases in average a maximum of one acyl chain was detected per HA dimer. The hydrophobic functionalization of hyaluronan induced its interaction with hydrophobic dye as a consequence of acyl chain aggregation. The higher the degree of acylation the more hydrophobic dye was interacting with HA. For concentrated samples, aggregation was more evident in case of acylated HA in aqueous solution. This phenomenon was explained by its different conformational arrangement in solution which was further supported by DSC data indicating an existence of hydrophobic cavities. The formation of self-aggregated assemblies indicates potential applications of this type of HA derivate as drug delivery system.

© 2011 Elsevier Ltd. All rights reserved.

1. Introduction

Carbohydrate fatty acid esters are an important class of biodegradable and non-toxic surfactants with broad applications in food, cosmetics and pharmaceutical industries as detergents, oral care products and medical supplies (Hill & LeHen-Ferrenbach, 2008). They were also reported to be applicable as antibiotics and antitumorals (Deleu & Paquot, 2004). In addition, non-toxic and biodegradable polysaccharide surfactants are considered to be attractive drug delivery systems. Among polysaccharides, a great attention is focused on esterification of hyaluronan (HA) (Kawaguchi, Matsukawa, & Ishigami, 1993; Kong, Chen, & Park, 2011; Taglienti, Valentini, Sequi, & Crescenzi, 2005).

HA is a linear polysaccharide consisting of alternating β-1,4-linked units of β-1,3-linked glucuronic acid and *N*-acetyl-D-glucosamine (Laurent, 1998; Scott, 1998). HA is a main component of the extracellular matrix in connective, epithelial, and neural tissues and is known to play an important role in organ development, cell proliferation and migration. Additionally, HA contributes to the lubrication and maintenance of cartilage, where it is a major component of synovial fluid and forms a coating around chondrocytes (Collis et al., 1998; Entwistle, Hall, & Turley, 1996; Laurent, 1998). Except for being biodegradable and non-toxic, HA is biocompatible and renewable, which is important on industrial scale production of HA derivates.

The major advantage of modified HA over the native HA is the higher resistance against enzymatic degradation (Abatangelo, Barbucci, Brun, & Lamponi, 1997; Prestwitch, Marecak, Marecek, Vercuysse, & Ziebell, 1998; Šoltés et al., 2006). In addition, besides retaining its inherently superior properties, HA derivates acquire additional physicochemical characteristics that can be tailored according to the desired requirements. For example, HA having desired amount of hydrophobic functional groups may be achieved varying the degree of substitution. In case of esterification, the degree of substitution and the length of attached carbon chain are directly related to conformational behavior of the substituted molecule in solution and the possibility of forming supramolecular assemblies (Akiyoshi & Sunamoto, 1996). Formation of supramolecular assemblies is than in turn related to the possibility of carbohydrate interaction with non-polar compounds and therefore directly affects its pharmaceutical and industrial applications. Modified HA is therefore also considered to have a great potential as a novel drug carrier in form of conjugates. Despite its excellent biocompatible and biodegradable properties, HA based drug delivery systems have been reported to work as an efficient depot for sustained release of protein drugs without denaturation (Oh et al., 2010; Prestwitch & Vercruysse, 1998). Moreover, the absence of positive charge on HA surface alleviate the problems

* Corresponding author. Tel.: +420 465519569; fax: +420 465543793.
E-mail address: smejkalova@contipro.cz (D. Šmejkalová).

0144-8617/$ – see front matter © 2011 Elsevier Ltd. All rights reserved.
doi:10.1016/j.carbpol.2011.09.057

with severe cytotoxicity and aggregations with serum proteins in the body found for cationic liposomes and polymers investigated as drug carriers (Oh et al., 2010).

In this study, we followed the structural and conformational changes of HA induced after acylation with hexanoic anhydride in DMSO and DMSO/H_2O solvent. The main attention was focused on the comparison of reaction selectivity and conformational changes of HA followed after acylation. The structural changes were studied by NMR, ESI-MS/MS and DSC. Formation of hydrophobic domains was examined by comparing the ability of acyl derivates to dissolve a hydrophobic dye.

2. Experimental

2.1. Materials

Hyaluronic acid sodium salt (200 kDa, 155 kDa and 34 kDa) was provided by CPN Dolní Dobrouč, Czech Republic. Hexanoic anhydrides, triethylamine, dimethylsulfoxide, dimethylaminopyridine (DMAP), Oil Red O (Solvent Red 27, Sudan Red 5B, C.I. 26125, $C_{26}H_{24}N_4O$), and deuterated water were of analytical grade and purchased from Sigma–Aldrich.

2.2. Preparation of hyaluronan acid form and hyaluronan sodium salt

Hyaluronan (M_w = 200 kDa, 15 g) was dissolved in 600 mL of demineralized water and then Amberlite IR 120 Na exchange resin (wet state, 100 g) was added to the mixture. The mixture was kept at room temperature with occasional stirring. Cation exchange resin was removed by centrifugation at 5000 rpm for 5 min and the resulting solution was lyophilized. About 13 g of hyaluronan acid form M_w = 50 kDa was obtained.

Since each transformation of hyaluronan into its acid form causes HA degradation, it was necessary to have a comparable starting M_w of both HA sodium salt and HA acid form as both materials were used as substrates for acylation reaction. For this reason, the obtained hyaluronan acid form was divided into two parts. One part of the material was used for acylation reaction in its acid form. The second half of hyaluronan acid form was returned into its initial sodium salt state in a following way. Hyaluronan acid form was diluted in water, neutralized to pH 6.5 and precipitated off with absolute 2-propanol. The precipitate was washed three times with 80% 2-propanol, twice with absolute 2-propanol and dried at 40 °C.

2.3. Acylation of hyaluronan sodium salt (Ac-HA-Na)

HA sodium salt (5 g) was first dissolved in 50 mL of demineralized water and then diluted with 50 mL of DMSO. Hexanoic anhydride (2.5 equiv./HA dimer), triethylamine (2.5 equiv./HA dimer) and DMAP (0.05 equiv./HA dimer) were added into the mixture and the mixture was stirred at room temperature for 2 h. At the end of reaction, the mixture was diluted with 100 mL of water followed by the addition of 15 mL of saturated NaCl solution. The product Ac-HA-Na (acylated HA-Na^+ in its Na^+ form) was precipitated with another 200 mL of absolute 2-propanol. The precipitate was first washed three times with 80% 2-propanol in water and then with absolute 2-propanol. The solid was filtered and dried in oven at 40 °C. The yield of final product was 5.4 g. The degree of substitution (DS) calculated from NMR spectra was 70%.

2.4. Acylation of hyaluronan acid form (Ac-HA-H)

Hyaluronan acid form (5 g) was dissolved in 100 mL of DMSO. Hexanoic anhydride (1.5–3.0 equiv./HA dimer), triethylamine (1.5, 2.5 and 3.0 equiv./HA dimer) and DMAP (0.05 equiv./HA dimer) were added into the mixture and the mixture was stirred at room temperature for 2 h. At the end of reaction, the reaction was quenched with 100 mL of water and the pH was adjusted with 0.1 M NaOH to pH 6, followed by the addition of 15 mL of saturated NaCl solution. The product Ac-HA-H (acylated HA-H^+ in its Na^+ form) was precipitated with 200 mL of absolute 2-propanol. The precipitate was washed three times with 80% 2-propanol in water and then absolute 2-propanol. The solid was filtered and dried in oven at 40 °C. The yield of final product was between 4.5 and 4.8 g. The degree of substitution (DS) calculated from NMR spectra was 33%, 60% and 70% for 1.5, 2.5 and 3.0 equiv. of triethylamine/HA dimer, respectively.

2.5. NMR analyses

HA acyl derivates (10 mg) were solubilized in 750 μL of D_2O, transferred into NMR tubes and directly analyzed.

The NMR analyses were performed on Bruker Avance™ 500 MHz equipped with BBFO plus probe. The ^1H and ^{13}C chemical shift were referenced to 3-trimethylsilylpropanoic acid sodium salt (TSPA) used as an internal standard. ^1H–^1H TOCSY spectra were recorded with 2048 data points, 80 scans per increment and 128 increments. TOCSY mixing time was set at 80 ms. ^1H–^{13}C HSQC spectra were acquired using gradient pulse sequences and 2048 data points, 80 scans per increment, 256 increments, and heteronuclear scalar coupling C–H set at 145 Hz. DOSY (diffusion ordered spectra) were obtained using a stimulated echo pulse sequence with bipolar gradients (STEBPGP). Scans (32) were collected using 2.5 ms sine-shaped pulses (5 ms bipolar pulse pair) ranging from 0.674 to 32.030 G cm^{-1} in 24 increments with a diffusion time of 200–600 ms, and 8192 time domain data points. Apodization was made by multiplying the data with a line broadening of 1.0 Hz, spike suppression factor of 4.0, maximum interactions number set to 100, noise sensitivity factor of 2, and number of components set to 1.

^1H NMR spectra were used for the calculation of the degree of substitution (DS) of acylated HA. DS (in %) was determined as relative integral of signal at 2.4 ppm, when the integration of signal at 2.0 ppm was normalized to 150. Explanation of resonating signals is given in the text.

2.6. MS analyses

Powdered hyaluronan (100 mg) was first dissolved in 10 mL of 0.1 M sodium acetate with 0.15 M NaCl (pH 5.3, adjusted with glacial acetic acid), and then incubated with 2000 IU of hyaluronidase (Finepharm) at 37 °C for 2 days. The enzyme was removed by short boiling of the solution at the end of incubation. The sample was filtered through 0.2 μm Nylon syringe filter. Filtered solution (2 mL) was transferred into the Vivaspin 15R concentrator (2000 MWCO Hydrosart, Sartorius) and centrifuged at 9000 rpm for 15 min. After preconcentration of the sample, the concentrator was filled with 10 mL of deionized water and centrifuged at 9000 rpm for 30 min. 4 wash cycles were used to remove the initial salt content. The sample was recovered from the bottom of the concentrator, diluted with 0.1% HCOOH:methanol = 1:1 to a final concentration of 1 mg mL^{-1} and directly injected into mass spectrometer.

Mass spectroscopic analyses of digested and desalted derivates were performed using a Synapt HDMS mass spectrometer (Waters), equipped with an electrospray ionization source operating in negative ion mode. The effluent was introduced into an electrospray source with a syringe pump at a flow rate of 10 μL min^{-1}. Nitrogen was used as cone gas (100 L h^{-1}) and desolvation gas (800 L h^{-1}). Capillary voltage was set at 3 kV. Sampling cone was set at 100 V. Extraction cone was set at 5 V. The source block temperature was set at 100 °C, while the desolvation temperature was 250 °C. For

each sample full MS and MS/MS scans from m/z 50 to 2000 were acquired for 2 min. For MS/MS measurements, argon was used as a collision gas. The collision energy was optimized to fragment the ion of interest, typically 55 eV for the ions with higher m/z and 25 eV for the ions with lower m/z. Data were collected at 1 scan s^{-1} and elaborated using MassLynx software.

2.7. UV–vis analyses

Powdered HA (10–200 mg) HA 34 kDa, HA 155 kDa, Ac-HA-H and Ac-HA-Na was first soaked with 750 μL of H_2O and then left dissolving overnight under constant stirring. Then 200 μL of Oil Red O solution (20 mg mL^{-1} in hexane) was added to the dissolved HA samples, the mixtures were heated up to 50 °C and shaken for 2 h at 50 °C, and for 2 days at room temperature. The experiments were repeated in two independent series, each consisting of replicate samples. Absorbances (522 nm) of the water phase were measured with UV-Vis Carry 100 (Varian).

2.8. Thermal analyses

HA samples of approximately 2 mg (weighted with an accuracy of ±0.01 mg) were placed in aluminum sample pans (TA Instruments, Tzero® Technology) and the excess of water (milli-Q) was added. Surplus of water was allowed to slowly evaporate at room temperature until the desired water content (W_c = mass of water (g)/mass of dry sample (g); [W_c] = g g^{-1}) was obtained. Several samples having W_c between 0.1 and 3 g g^{-1} were prepared for each HA material. The pans were subsequently hermetically sealed and left to equilibrate at room temperature for 72 h. Similar way of samples preparation was used for freezing/thawing as well as for the evaporation experiments.

Differential scanning calorimetry (DSC) was carried out using the TA Instruments DSC Q-200 equipped with a cooling accessory RCS-90 and assessed by the TA-Universal Analysis 2000 software.

The following thermal protocol was used for freezing/thawing experiments: start at 40.0 °C; cooling from 40.0 to −70.0 °C at 3.0 °C min^{-1}; isothermal at −70.0 °C for 1.0 min; heating from −70.0 to 40 °C at 5.0 °C min^{-1}. Flow rate of dynamic nitrogen atmosphere was 50 mL min^{-1}.

The following thermal protocol was used for the measurement of evaporation enthalpy: equilibration at 27.0 °C; cooling from 27.0 to −50.0 °C at 10.0 °C min^{-1}; isothermal at −50.0 °C for 1.0 min; heating from −50.0 to 200.0 °C at 5.0 °C min^{-1} and switching the flow rate of nitrogen from 50 mL min^{-1} to 5 mL min^{-1}. Immediately before the measurement, the hermetic lid (necessary for the sample preparation) was perforated using a sharp tool and the measurement was carried out straightway (Průšová, Šmejkalová, Chytil, Velebný, & Kučerík, 2010).

To obtain precise water content, thermogravimetry (TA Instruments, Q500 IR) was used to determine the equilibrium moisture content as a mass loss in the temperature interval 25–220 °C under dynamic atmosphere of nitrogen 25 mL min^{-1}.

2.9. Size exclusion chromatography coupled to multi-angle light scattering (SEC-MALS)

SEC was performed using an Agilent 1100 series liquid chromatograph equipped with a degasser (Model G1379A), an isocratic HPLC pump (Model G1310A), an automatic injector (Model G1313A), a column thermostat (Model G1316A), a DAWN EOS multi-angle light scattering photometer followed by an Optilab rEX differential refractometer (both from Wyatt Technology Corporation, USA). The injection volume was 100 μL of 0.1–1.0% (w/v) solutions. The separation was carried out using PL aquagel-OH 40 (300 mm × 7.5 mm; 8 μm) and PL aquagel-OH 20 (300 mm × 7.5 mm; 5 μm) columns connected in series. Columns were thermostated at 40 °C. The mobile phase was 0.1 M sodium phosphate buffer (pH adjusted to 7.5) + 0.05% NaN_3 at a flow rate 0.8 mL min^{-1}. Data acquisition and molecular weights calculations were performed using the ASTRA V software (Wyatt Technology Corporation, USA). The specific refractive index increment dn/dc was determined at 690 nm using the Optilab rEX refractometer for all samples according to procedure described elsewhere (Podzimek, Hermannová, Bílerová, Bezáková, & Velebný, 2010). The mean value of 9 dn/dc measurements was 0.155 ± 0.003 mL g^{-1}.

Each sample was filtered through Acrodisc Syringe Filter 0.45 μm 25 mm diameter with the Supor membrane (Pall). All reagents for SEC were HPLC grade and the mobile phase was filtered through Nylaflo Nylon Membrane Filter 0.2 μm (Pall).

3. Results and discussion

3.1. Acylation of hyaluronan

One of the main problems related to chemical modification of hyaluronan is its insolubility in organic solvents. For this reason, hyaluronan is mostly transformed prior modification into its acid form which is soluble in polar organic solvents such as DMSO (Oudshoorn, Rissmann, Bouwstra, & Hennink, 2007). However, the major disadvantage of this procedure is the contemporary degradation of HA during cation exchange step. For example, in this work a starting HA material was having M_w = 200 kDa, while after transformation into its acid form the M_w was reduced to about 50 kDa. For this reason, we tried to overcome this disadvantage by a direct acylation of hyaluronan as sodium salt in DMSO/H_2O solution. The acylation reactions are shown in Fig. 1. Regardless of the starting material and solvent choice, sodium salt of acylated HA was formed in both cases (Fig. 1). However, since the choice of reaction solvent may affect substitution position on HA chain, modified HA products received after acylation in DMSO (Ac-HA-H) and DMSO/H_2O (Ac-HA-Na) were further analyzed and compared by NMR, LC–MS, UV–vis and thermal analysis.

3.2. NMR analyses

^{1}H NMR spectra of HA, Ac-HA-H and Ac-HA-Na are shown in Fig. 2. All of the spectra show typical proton chemical shifts of HA involving signal at 2.0 ppm belonging to $COCH_3$ group, skeletal signals at 3.4–3.9 and anomeric resonances at 4.4–4.6 ppm. Remaining signals detected in modified HA at 0.8, 1.2, 1.5 and 2.4 ppm were attributed to the CH_2 in acyl chain as shown in Fig. 2. Relative integration of signals at 2.0 and 2.4 ppm were used for the determination of degree of substitution (DS). A comparable DS = 70% was determined for both acylated products shown in Fig. 2. A downfield chemical shift of one of the HA skeletal signals is evident in Ac-HA-Na at 3.1 ppm. Less significant is the appearance of a new signal at 3.3 ppm in Ac-HA-H. The new signals detected after HA modification are different for Ac-HA-Na and Ac-HA-H, and thus suggest that acylation reaction in DMSO yielded structurally different reaction outcome as compared to DMSO/H_2O reaction.

The linkage between hexyl chain and HA was established in both derivates by DOSY experiment (data not shown). Because of the marked difference between the diffusion coefficients of hexanoic acid and HA, the DOSY map can easily establish the presence of non-attached hexanoic acid to HA, which obviously is much faster than the diffusion of the bound acyl chain. In both cases, DOSY experiments showed similar diffusion behavior for all signals between 0.8 and 4.6 ppm (except for isopropanol and HDO signal) and thus indicated that all of the proton resonances in this region belonged to one structural complex.

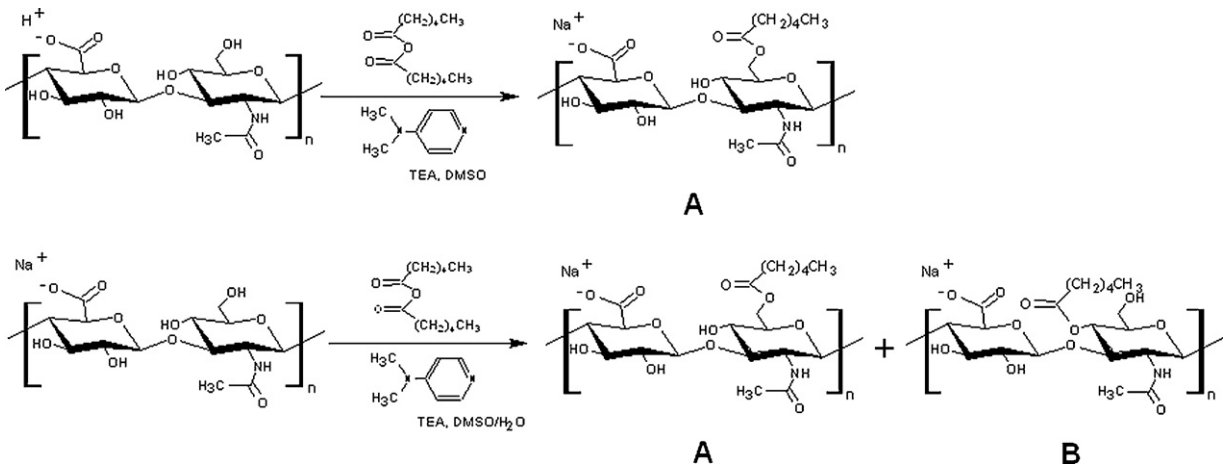

Fig. 1. Synthesis of Ac-HA-H (upper scheme) and Ac-HA-Na (lower scheme).

The structural diversity between Ac-HA-H and Ac-HA-Na was further evidenced in HSQC spectra (Fig. 3). These NMR spectra were detected in edited mode, enabling the recognition of CH and CH_3 signals (positive) from those of CH_2 (negative). The CH_2 group in HA possesses two protons that are diastereotopic (magnetically nonequivalent), and for this reason instead of one, there are two proton signals at 3.8 and 3.9 ppm correlating with one carbon shift (Fig. 3). Since there is only one CH_2 in HA it is easily recognizable in edited HSQC spectra of pure hyaluronan (spectrum not shown) as well as there is recognizable any chemical shift of this functional group resulting from the HA chemical modification in the close environment of the CH_2 group. Comparing HSQC spectra of Ac-HA-H and Ac-HA-Na there is in both cases a clear downfield shift of both C6 and H6, specific for the esterification of CH_2OH group in *N*-acetyl-D-glucosamine (product A in Fig. 1). In addition, in HSQC spectrum of Ac-HA-Na there is another shifted CH_2 correlation upfield to 3.6 and 3.7 ppm together with some extra downfield shifted CH crosspeaks in skeletal and anomeric region. The upfield shift of C6 in Ac-HA-Na may indicate esterification of OH group of *N*-acetyl-D-glucosamine in position 4 (product B in Fig. 1). Thus acylation in DMSO/H_2O is not as selective as that carried out only in DMSO.

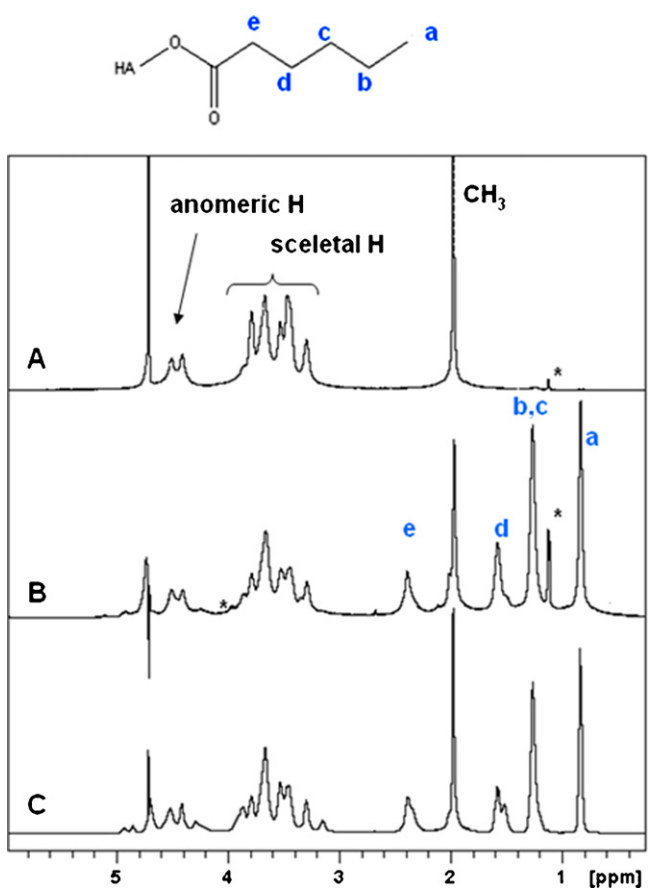

Fig. 2. ^{1}H NMR spectra of HA 155 kDa (A), Ac-HA-H (B), and Ac-HA-Na (C).

Lower reaction selectivity in DMSO/H_2O environment was also evidenced in TOCSY spectra (data not shown), where an extra spin system detected at 3.1–3.5–4.4 ppm was attributed to glucuronic acid belonging to the acylated HA in position 4 of *N*-acetyl-D-glucosamine (product B in Fig. 1). No such correlations were found for Ac-HA-H, where the reaction was carried out in DMSO only. Therefore, both products A and B (Fig. 1) were formed when acylation was carried out in DMSO/H_2O while product A (Fig. 1) was received as the major product when the same reaction was performed in DMSO.

3.3. MS analyses

ESI-MS and ESI-MS/MS analyses were carried out in order to confirm the structural differences between Ac-HA-H and Ac-HA-Na previously suggested from NMR spectra. ESI-MS spectra of both acylated products with DS = 70% after enzymatic degradation are reported in Fig. 4. There is no significant difference between the two spectra (Fig. 4), suggesting that the number of acyl chains per dimer unit in HA was comparable in both solvents. The spectra indicated the presence of unmodified HA dimer (m/z = 396), HA tetramer (m/z = 775), HA hexamer (m/z = 1154), HA octamer (m/z = 1533), and modified HA mers with one or two acyl chains (m/z is increased by 98 or 196, respectively) in case of HA tetramer and hexamer, three acyl chains (m/z is increased by 294) in case of HA hexamer and octamer, and four acyl chains (m/z is increased by 392) in case of HA octamer.

To compare the way of substitution, MS/MS spectra were collected for the most intensive peaks detected in ESI-MS spectra. The fragmentation pattern of both acylated products is similar and includes ions corresponding to the loss of acyl chain, glucuronic acid, and *N*-acetyl-D-glucosamine (Fig. 5). However, a clear difference may be noticed in the intensity of m/z = 291, corresponding to the modified glucuronic acid with hexyl chain. Being this intensity about 20% in Ac-HA-H sample, while less than 5% in Ac-HA-Na, there is hardly any modification of any OH group of glucuronic acid

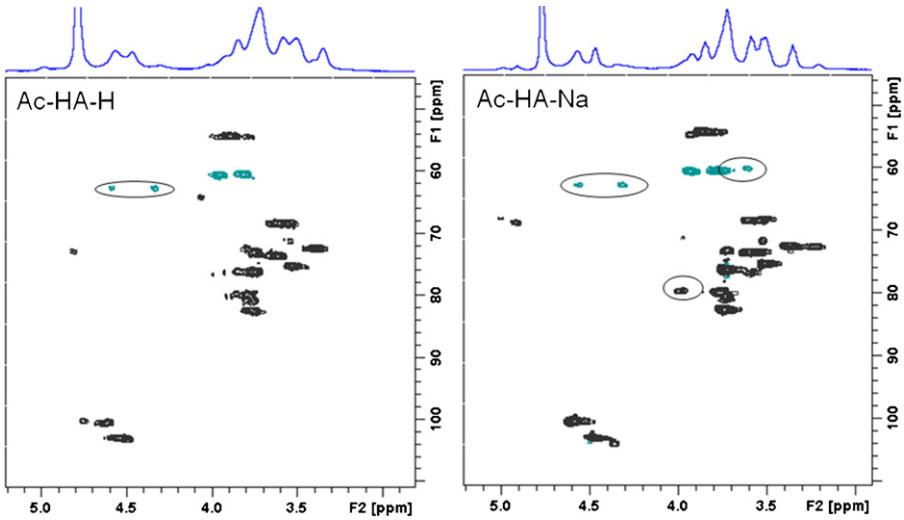

Fig. 3. 2D HSQC NMR spectra of Ac-HA-H and Ac-HA-Na. Structural differences are indicated by circles.

in Ac-HA-Na. This finding which was observed in all other MS/MS spectra (not shown), confirms the previous interpretation of NMR data, where the mixture of products A and B (Fig. 1) substituted with acyl chain in different positions on *N*-acetyl-D-glucosamine were suggested as the major products in DMSO/H_2O. Although product A was suggested as the major product in the case of Ac-HA-H, according to the results from MS spectra, acyl substitution of glucuronic acid cannot be excluded.

3.4. UV–vis analyses

In order to determine a possible hydrophobic aggregation of acyl chains in HA derivates, Ac-HA-H (DS from 33 to 70%) and Ac-HA-Na (DS = 70%) were mixed with Oil Red O which is a hydrophobic dye commonly used for staining of neutral triglycerides and lipids on froze sections and some lipoproteins on paraffin sections. Therefore, it is expected that Oil Red O will dissolve only in hydrophobic domains of HA. The results of Oil Red O absorption by two different HA concentrations are reported in Fig. 6. The lowest absorbance $A = 0.06–0.08$ of hydrophobic dye at hyaluronan concentration $c = 10\ \mathrm{mg\,mL^{-1}}$ was observed for unmodified 34 kDa and acylated Ac-HA-H with DS = 33%, followed by unmodified HA 155 kDa ($A = 0.1$). Thus low degree of acylation did not induce any significant formation of hydrophobic domains. This situation changes for acylation degree of 60 and 70%, where the presence of hydrophobic domains is indicated by a 3.5 times higher absorbance ($A = 0.5$) as compared to control unmodified samples. In fact, in this case it seems that higher DS indicates larger amounts of hydrophobic domains in HA samples and for this reason also higher affinity towards hydrophobic compounds.

However, a completely different absorption behavior was observed at hyaluronan concentration $c = 15\ \mathrm{mg\,mL^{-1}}$. Here, again the lowest absorbances ($A = 0.1–0.2$) were measured for HA 34 kDa and Ac-HA-H (DS = 33%). But then unlike the previous case, HA 155 kDa showed a two fold absorbance increase to $A = 0.4$, which was comparable to $A = 0.4$ and 0.5 observed for acylated samples Ac-HA-H with DS of 60 and 70%. The detected absorbance increase in 155 kDa HA is in agreement with the observation of hydrophobic patches in aggregated HA (Scott, Cummings, Brass, & Chen, 1991; Scott et al., 1990). No such observation was made in case of 34 kDa HA probably due to its lower molecular size. A significant change was found for Ac-HA-Na (DS = 70%) sample whose absorbance is a double from that of Ac-HA-H (DS = 70%). Since DS of the acylated HA in this last case is comparable, the amount of acyl chains attached to HA is not the only driving force influencing the amount of bound hydrophobic dye. The data suggest that except for DS, it is also important which OH group in HA is substituted. In Ac-HA-Na acylation mainly occurred either at position 4 or 6 of *N*-acetyl-D-glucosamine, while in Ac-HA-H in position 6. The absorption data suggest a more significant aggregation of acyl chains in Ac-HA-Na, which could have resulted from the vicinity of acyl chains within Ac-HA-Na secondary structure and easier formation of 'micelle-like' conformation as compared to Ac-HA-H. True micelles are not of course expected to form. Such conformation, however, seems to be concentration dependent.

3.5. Thermal analysis

Recent study has shown that methods of thermal analysis are useful in the determination of hyaluronan conformation by

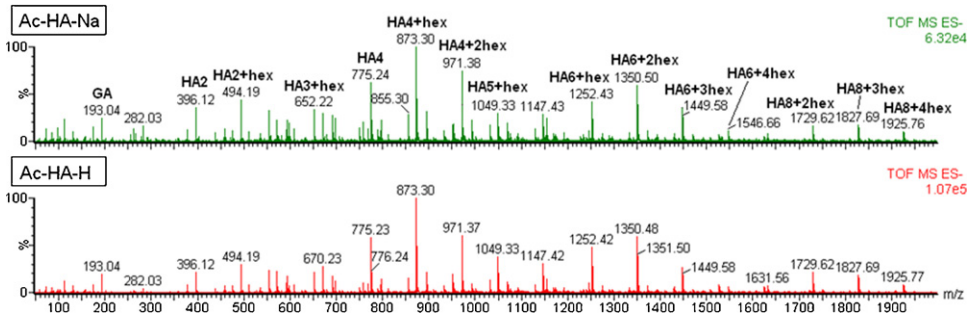

Fig. 4. ESI-MS spectra of Ac-HA-H and Ac-HA-Na after enzymatic degradation. HA2–HA8 stands for dimer–octamer of HA, GA for glucuronic acid and hex for hexyl chain.

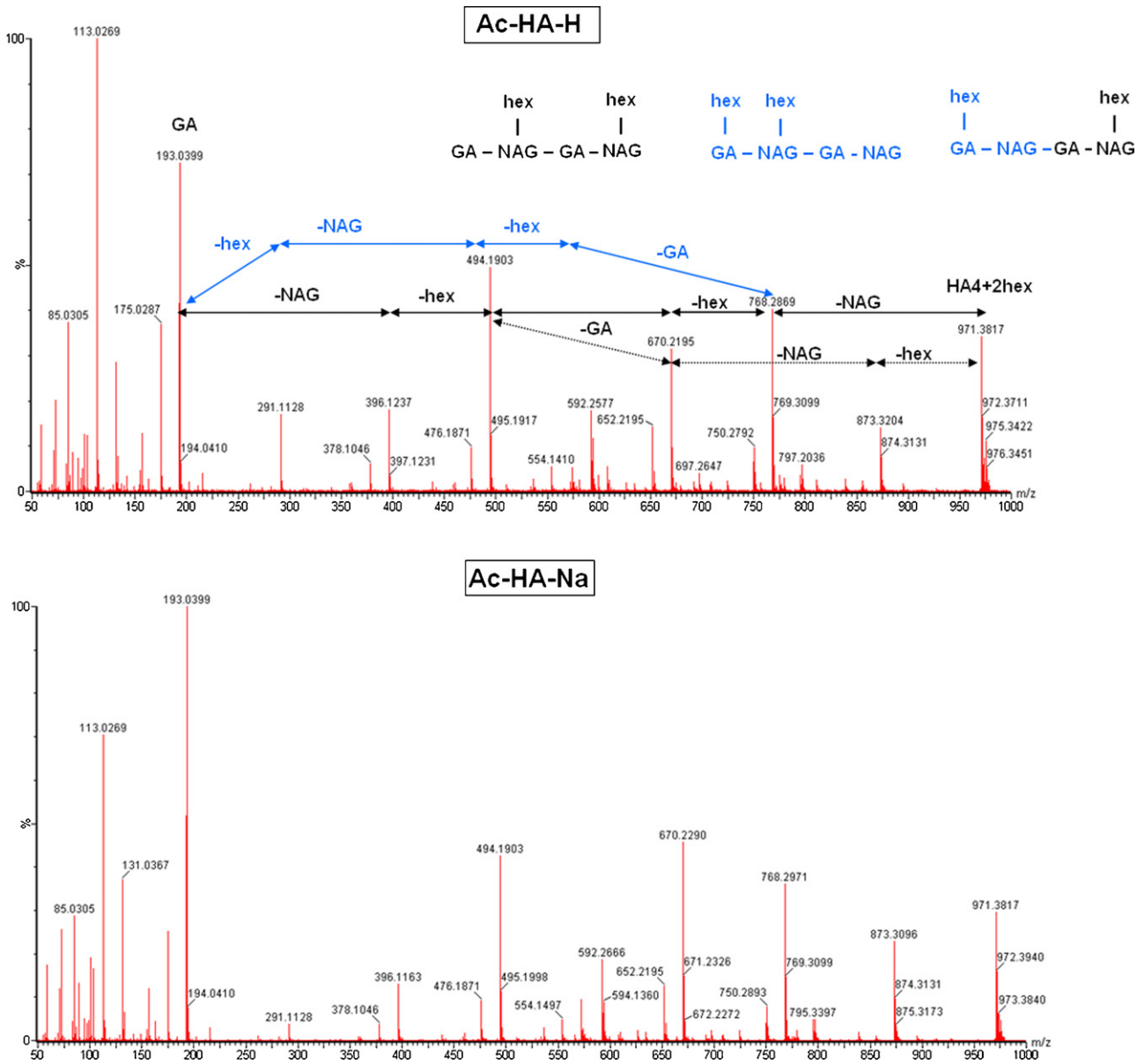

Fig. 5. MS/MS fragmentation (sampling cone set at 40 V) of $m/z = 971$ of Ac-HA-H and Ac-HA-Na with designed possible fragmentation pathways corresponding to the three indicated structures. NAG stands for *N*-acetyl-D-glucosamine, GA for glucuronic acid and hex for hexyl chain.

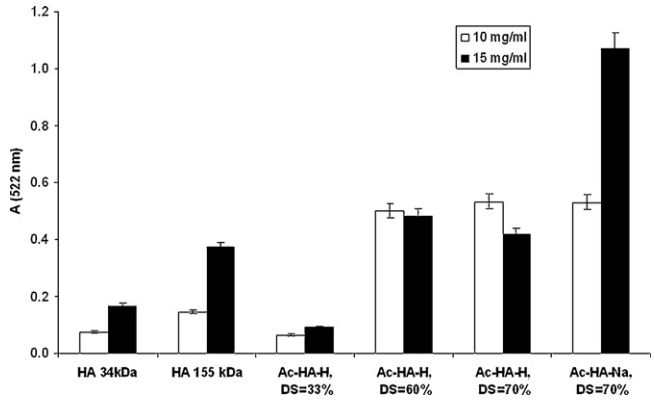

Fig. 6. Oil Red O absorption by HA and acylated HA with different degree of substitution (DS).

comparing hyaluronan hydration (Průšová et al., 2010). In this study we have repeated similar hydration experiments, namely water evaporation and melting. There were no obvious differences between hydration numbers of HA derivatives obtained from water evaporation experiments (data not shown). A clear difference was evidenced when comparing hydration data from classical melting experiments. It implies differences in the physical structure of dry derivatives and original hyaluronan. In principle, hydration numbers obtained from evaporation experiments reflect the state of structure in which a minimum of water molecules are present and strong interactions among hyaluronan segments take part (Průšová et al., 2010). Such number indicates solely the starting concentration but not the mechanisms of drying process itself. The derivatization causes small changes in flexibility and spatial arrangement of modified segments causing anomalies in physical structure of derivatives after drying. This was reflected mainly as differences in water vaporization enthalpies in individual samples (results no shown). In contrast, melting experiments provide hydration numbers indicating the state of (still preserved) physical

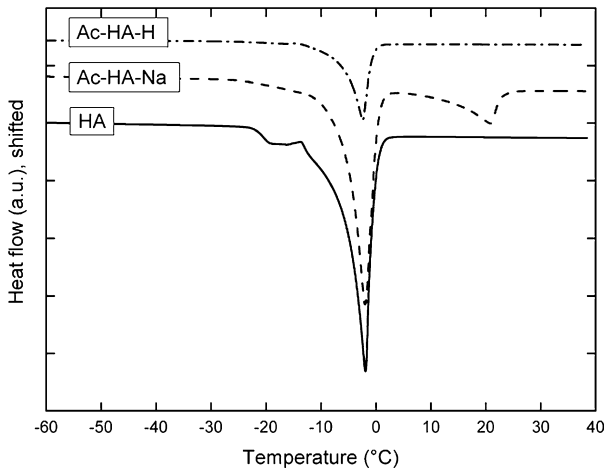

Fig. 7. Comparison of ice melting in native and acylated HA.

structure of dry hyaluronan covered by the monomolecular water layer. Therefore, using this approach the difference in pore size distribution and different surface wettability can be much better visualized. The DSC melting curves of ice present in acylated samples are shown in Fig. 7. As it can be seen, the melting behavior of Ac-HA-Na significantly differed from that of HA and Ac-HA-H. The main difference was in the detection of the second melting peak in Ac-HA-Na in the temperature range from 0 to 25 °C (Fig. 7). This peak was observable regardless the amount of water content in sample and its presence was confirmed on crystallization curve (data not shown). The detection of two distinguishable peaks on DSC curves (Fig. 7) indicates, that there exist two possible way of water binding in Ac-HA-Na sample reflected by two different crystallization/melting mechanisms. The first type of water binding resembles the hydration of ordinary structure of HA. Second type of water binding detected only in Ac-HA-Na derivates cannot be associated with hydration of ordinary HA structure and shows different hydration behavior, which is most probably associated with the presence of confined water. Confined water can be found in granular and porous materials and around and within macromolecules and gels (Chaplin, 2010). Physical properties and state of that water may vary widely depending on the molecular characteristics of the cavity surface and the confinement dimensions, as well as temperature and pressure. The properties of the confined water are difficult to predict and may be very different from those of bulk water which is particularly true when the confinement is on the nano-scale level (Chaplin, 2010). For example surface interactions and the confinement diameter may cause that the ice is formed at 400 K in very narrow pores (0.6–1.0 nm diameter) in porous glass (Venzel, Egorov, Zhizhenkov, & Kleiner, 1985). In accordance with literature, we hypothesize, that Ac-HA-Na sample contains cavity with both hydrophilic and hydrophobic surface. The cavity size and wettability influences the physical properties of encapsulated water which in turn causes anomaly high melting temperature of formed ice.

4. Conclusion

In summary, HA acylation in DMSO and DMSO/H_2O yields structurally different products which were elucidated by means of NMR, MS, DSC and UV/vis. Acylation reaction carried out in DMSO (Ac-HA-H) was more selective as compared to that performed in DMSO/H_2O (Ac-HA-Na). NMR analyses indicated that Ac-HA-H was preferentially substituted in position 6 of *N*-acetyl-D-glucosamine, while either position 6 or 4 of *N*-acetyl-D-glucosamine unit were acylated in Ac-HA-Na. Mass analyses detected that in average there is a maximum of 1 acyl chain per HA dimer unit for both types of acylated products. However, due to the different positions of functionalization in HA structure, DSC and UV/vis analyses revealed different conformational and hydration behavior of the two derivates. For concentrated samples, the formation of hydrophobic domains was inevitably detected in the solution of Ac-HA-Na. These results are useful for developing biomedical application of this biomaterial as drug carrier.

Acknowledgement

AP and JK thank the Ministry of Education, Youth and Sport of the Czech Republic project no. 0021630501.

References

Abatangelo, G., Barbucci, R., Brun, P. & Lamponi, S. (1997). Biocompatibility and enzymatic degradation studies on sulphated hyaluronic acid derivates. *Biomaterials*, *18*, 1411–1415.

Akiyoshi, K. & Sunamoto, J. (1996). Supramolecular assembly of hydrophobized polysaccharides. *Supramolecular Science*, *3*, 157–163.

Chaplin, M. F. (2010). Structuring and behaviour of water in nanochannels and confined spaces. In L. J. Dunne, & G. Manos (Eds.), *Adsorption and phase behaviour in nanochannels and nanotubes* (pp. 241–256). Netherlands: Springer.

Collis, L., Hall, C., Lange, L., Ziebell, M., Prestwich, R. & Turley, E. A. (1998). Rapid hyaluronan uptake is associated with enhanced mobility: Implications for an intracellular mode of action. *FEBS Letters*, *440*, 444–449.

Deleu, M. & Paquot, M. (2004). From renewable vegetables to microorganisms: New trends in surfactants. *Comptes Rendus Chimie*, *7*, 641–646.

Entwistle, J., Hall, C. L. & Turley, E. A. (1996). HA receptors: Regulators of signaling to the cytoskeleton. *Journal of Cellular Biochemistry*, *61*, 569–577.

Hill, K. & LeHen-Ferrenbach, C. (2008). Sugar-based surfactants for consumer products and technical applications. In C. C. Ruiz (Ed.), *Sugar based surfactants. Fundamentals and applications* (pp. 1–20). New York: CRC Press.

Kawaguchi, Z., Matsukawa, K. & Ishigami, Y. (1993). Conformational changes of hyaluronates with partial palmitoylation and the adsorption structures on the surface of oil droplets. *Carbohydrate Polymers*, *20*, 183–187.

Kong, M., Chen, X. & Park, H. (2011). Design and investigation of nanoemulsified carrier based on amphiphile-modified hyaluronic acid. *Carbohydrate Polymers*, *83*, 462–469.

Laurent, T. C. (1998). *The chemistry, biology and medical applications of hyaluronan and its derivates*. London: Portland Press.

Oh, E. J., Park, K., Kim, K. S., Kim, J., Yang, J.-A., Kong, J.-H., et al. (2010). Target specific and long-acting delivery of protein, peptide, and nucleotide therapeutics using hyaluronic acid derivates. *Journal of Controlled Release*, *141*, 2–12.

Oudshoorn, M. H. M., Rissmann, R., Bouwstra, J. A. & Hennink, W. E. (2007). Synthesis of methacrylated hyaluronic acid with tailored degree of substitution. *Polymer*, *48*, 1915–1920.

Podzimek, S., Hermannová, M., Bílerová, H., Bezáková, Z. & Velebný, V. (2010). Solution properties of hyaluronic acid and comparison of SEC-MALS–VIS data with off-line capillary viscometry. *Journal of Applied Polymer Science*, *116*, 3013–3020.

Prestwitch, G. D., Marecak, D. M., Marecek, J. F., Vercruysse, K. P. & Ziebell, M. R. (1998). Controlled chemical modification of hyaluronic acid: Synthesis, applications, and biodegradation of hydrazide derivates. *Journal of Controlled Release*, *53*, 93–103.

Prestwitch, G. D. & Vercruysse, K. P. (1998). Profiles therapeutic applications of hyaluronic acid and hyaluronan derivates. *Pharmaceutical Science & Technology Today*, *1*, 42–43.

Průšová, A., Šmejkalová, D., Chytil, M., Velebný, V. & Kučerík, J. (2010). An alternative approach to study hydration of hyaluronan. *Carbohydrate Polymers*, *82*, 498–503.

Scott, J. E. (1998). Chemical morphology of hyaluronan. In T. C. Laurent (Ed.), *The chemistry, biology and medical applications of hyaluronan and its derivates* (pp. 7–15). London: Portland Press.

Scott, J. E., Cummings, C., Brass, A. & Chen, Y. (1991). Secondary and tertiary structures of hyaluronan in aqueous solution, investigated by rotary shadowing-electron microscopy and computer simulation. Hyaluronan is a very efficient network-forming polymer. *Biochemical Journal*, *274*, 699–705.

Scott, J. E., Cummings, C., Greiling, H., Stuhlsatz, H. W., Gregory, J. D. & Damle, S. P. (1990). Examination of corneal proteoglycans and glycosaminoglycans by rotary shadowing and electron microscopy. *International Journal of Biological Macromolecules*, *12*, 180–184.

Šoltés, L., Mendichi, R., Kogan, G., Schiller, J., Stankovská, M. & Arnhold, J. (2006). Degradative action of reactive oxygen species on hyaluronan. *Biomacromolecules*, *7*, 659–668.

Taglienti, A., Valentini, M., Sequi, P. & Crescenzi, V. (2005). Characterization of methylprednisolone esters of hyaluronan in aqueous solution: Conformation and aggregation behavior. *Biomacromolecules*, *6*(3), 1648–1653.

Venzel, B. I., Egorov, E. A., Zhizhenkov, V. V. & Kleiner, V. D. (1985). Determination of the melting point of ice in porous glass in relation to the size of the pores. *Journal of Engineering Physics and Thermophysics*, *48*, 346–350.

Appendix 4

Kučerík, J., Bursáková, P., Průšová, A., Grebíková, L., Schaumann, G. E. (2012) Hydration of humic and fulvic acids studied by DSC. Journal of thermal analysis and calorimetry 110: 451–459.

J Therm Anal Calorim (2012) 110:451–459
DOI 10.1007/s10973-011-2178-1

Hydration of humic and fulvic acids studied by DSC

Jiří Kučerík · Petra Bursáková · Alena Průšová · Lucie Grebíková · Gabriele Ellen Schaumann

CEEC-TAC1 Conference Special Issue
© Akadémiai Kiadó, Budapest, Hungary 2012

Abstract Qualitative and quantitative aspects of hydration of four humic acids (HA) and three fulvic acids (FA) originating from different sources were investigated. DSC experiments at subambient temperatures were carried out in order to monitor differences in ice behavior originating from freezable water surrounding humic molecules. It was found that kinetic effects play a significant role in hydration processes of both HA and FA. In fact, the hydration took part over 21 days which was detected as a progressive decrease in ice melting enthalpy. Simultaneously, the peak shapes and positions changed indicating structural changes in the physical structure of the humic substances. In case of FA, the dependency of melting enthalpy on water concentration showed a linear trend resembling a complete hydration previously observed for water-soluble hydrophilic polymers. In contrast, the melting enthalpy of some HA increased in a step-like way with increasing water content, suggesting preservation of original hydrophobic scaffold during the hydration. The differences between the rather young FA and the rather old HA lead to the conclusion that water can play a significant role in processes of humification. We assume that separation of hydrophobic and hydrophilic domains and thus increase in nanoscale heterogeneity represents an important physical contribution to the overall humification process. It was also demonstrated that the higher content of oxygen in humic molecules is not the only indicator of higher water holding capacity. Instead the porosity of humic matrix seems to contribute as additional parameter into these processes.

Keywords Humic and fulvic acids · Hydration · Water · Differential scanning calorimetry · Humification

J. Kučerík (✉) · G. E. Schaumann
Department of Environmental and Soil Chemistry, Institute of Environmental Sciences, University of Koblenz-Landau, Fortstrasse 7, 76829 Landau, Germany
e-mail: kucerik@uni-landau.de

J. Kučerík · P. Bursáková · A. Průšová
Faculty of Chemistry, Brno University of Technology, Purkynova 118, 612 00 Brno, Czech Republic

L. Grebíková
Department of Inorganic, Analytical and Applied Chemistry, University of Geneva, 30, Quai Ernest-Ansermet, 1211 Geneva 4, Switzerland

Introduction

Humic substances (HS) represent a complex mixture of various molecules formed in nature as a by-product of biomass and dead animal bodies' decomposition. Chemically, HS can be visualized as a mixture of both substituted aromatic and aliphatic molecules forming various physical structures stabilized by intermolecular interactions [1]. The primary structure reflects the conditions of formation, such as parental material, climate conditions, and character of present microorganisms. In soils, their role is, among others, closely linked with soil stability, sorption processes, water holding capacity, and cell biology of soil living organisms [2, 3]. The most important fractions of natural organic matter (NOM) are fulvic acids (FA) and humic acids (HA); FA are fractions of NOM soluble at all pH values, while HA are soluble only in alkaline solutions [2].

Hydration is the crucial factor playing role in biological function of molecules in both living and natural systems. Water represents an important medium for nutrient transport, cell membrane processes, induces biologically active conformation of biomolecules, etc. It is also the case of NOM. Due to the presence of solid particles, molecular

assemblies or single molecules, water properties in terms of vapor pressure, enthalpy, entropy, viscosity, and density will differ from nanosite to nanosite in the OM matrix [3]. In general, water can be subdivided into free water which physical structure is not influenced by the presence of additional molecules. Another type is bound water, whose properties are more or less modified by the respective interaction partners [4]. Consequently, supplementary types of water can also be considered, resulting in distinguishing of four water categories: (i) free water: water non-associated with solid particles and including void water not affected by capillary force, (ii) interstitial water: water trapped inside crevices and interstitial spaces of flocs and organisms, (iii) surface (or vicinal) water: water held on to the surface of solid particles by adsorption and adhesion, (iv) bound (or hydration) water [5–7]. Using differential scanning calorimetry (DSC), three types of water belonging to above groups can be distinguished [7]: free water (W_f) whose melting/crystallization temperature and enthalpy are not significantly different from those of bulk water [water type (i)]; water species exhibiting large differences in phase transition enthalpies and temperatures known as freezing-bound water [W_{fb}; water type (ii)]; and non-freezing water (W_{nf}) which is strongly associated with the molecule and shows neither crystallization exotherms nor melting endotherms on DSC curves [water types (iii) and (iv)] [8, 9].

Recent studies have shown that hydration of NOM results in physicochemical changes of soil organic matter (SOM) [10–12]. It may strongly affect its sorptive properties, such as sorption kinetics and binding of hydrophobic organic compounds [13–16], swelling [10], increased flexibility [17], alterations in conformation or changes in ionization status of polar functional groups [12]. These hydration-driven changes can have an impact on nutrient or pollutant retention and transport of solutions (e.g., hydrophobic pollutants) through the organic matter of soils and sediments [13–15].

Furthermore, the hydration kinetics of SOM is influential factor for transport and sorption processes in soil. Nevertheless, knowledge about wetting and swelling processes, which both control the overall hydration kinetics, is limited [10]. Many studies have shown that the sorption of organic substances in SOM depends among the others on the water content, number of drying and wetting cycles, hydration time, and the type of water binding [10]. The quality of studied organic material and its pore size distribution plays a significant role in hydration kinetics as well [12]. After the absorption of water, size of inner pores of organic matter will increase due to swelling while size of external ones decreases. Hydration process of soils can be divided into two steps. The first step includes the wetting of mineral and organic soil components. After wetting, water is distributed within the pore volume. Possibly, swelling of SOM and clay minerals as well as hydration of salts may follow [10]. This dynamic process is based on the assumption that the structure and properties of organic matter is similar to that of hydrogels since there is still a certain parallelism with their properties [12]. This is rather questioned by the observation that in a peat and SOM matrix water becomes a short-term plasticizer and long-term anti-plasticizer [18]. Furthermore, the structure of HS does not seem to be that reversible considering their supramolecular assembly, differences in polarity or mechanical properties (elasticity) of individual components.

In this work, we studied the character of hydration water in water/humic substance systems. The goal was to determine both quantitative and qualitative aspects of hydration of HS in solid and liquid phase via its freezing–melting behavior and to explore the differences in properties of water in contact with humic matter using DSC. The working hypothesis of this study is that the hydration level is a crucial factor influencing both state of water in humic matrix as well as character of physical structure of respective HS. We assume that the degree of humification, i.e., history of HS development, should have a strong influence on hydration processes of these materials. Last but not least, the similarity of hydration mechanisms with more homogeneous hydrogels or biopolymers is questioned as well.

Materials and methods

Materials

The following standard samples were purchased from the International Humic Substances Society (IHSS) and were measured as received: Suwannee river II HA 2S101H (SRHA), Suwannee river II FA 2S101F (SRFA), Elliot soil HA 1S102H (ESHA), Elliot soil II FA 2S102F (ESFA), Pahokee peat HA 1S103H (PPHA), Pahokee peat II FA 2S103F (PPFA), Leonardite HA 1S104H (LHA). Elemental analysis of investigated samples (Table 1) was obtained from official IHSS web site (http://www.ihss.gatech.edu/elements.html), where also other structural details can be found.

DSC to study the freezing–melting behavior of hydrated HS

Approximately 2 mg of each sample was placed in an aluminum DSC Tzero pan and excess of water was added. Surplus water was allowed to evaporate slowly at room temperature until the desired water content was obtained.

Table 1 Elemental composition in % (w/w) of dry, ash-free IHSS samples (http://www.ihss.gatech.edu/elements.html)

IHSS samples	C	H	O	C/O	C/H
LHA	63.8	3.70	31.3	2.04	17.3
SRHA	52.6	4.28	42.0	1.25	12.3
SRFA	52.3	4.36	43.0	1.22	12.0
ESHA	58.1	3.68	34.1	1.71	15.8
ESFA	50.1	4.28	42.6	1.18	11.7
PPHA	56.4	3.82	37.3	1.51	14.8
PPFA	51.3	3.53	43.3	1.18	14.5

Subsequently, the pans were hermetically sealed. DSC was performed using the TA Instruments Q200 equipped by a rapid cooling system (RCS) in order to study the melting process of ice formed by freezable water. An empty hermetically sealed pan was used as reference. The measurements were conducted ranging from 40 to −90 °C at 3 °C/min, and then from −90 to 30 °C at 5 °C/min under the flow of nitrogen (50 mL/min). The temperature scale and heat of transition were calibrated using distilled water and indium as standards, respectively. Each measurement ran through three immediately subsequent identical cycles to test reproducibility of ice melting and to investigate potential changes in the hydrated HS structure due to the freezing–melting cycles. In this way, it was also verified that sample pans were well hermetically sealed so no water was evaporating and that formation of ice, due to its volume expansion, does not cause the HS supramolecular destruction. Selected samples were prepared in triplicates and no significant difference in the DSC record and respective melting enthalpy was observed.

Determination of water content by thermogravimetric analysis

TGA Q5000IR (TA Instruments, New Castle, USA) was used to determine the moisture content of purchased IHSS standard samples and to obtain the precise concentration of water (W_c) in the samples. Experiments were carried out in open Pt pans. The temperature range of the experiments was from 25 to 180 °C at 3 °C/min under the flow of nitrogen.

The W_c nomenclature used in this study is based on the ratio between mass of water with respect to the dry mass and is defined as grams of water per gram of dry sample.

Results and discussion

Hydration state after 1 day of HS-water contact time

In this part, hydration of IHSS samples in the W_c range between 0.1 and 2.0 (g/g) were investigated. The DSC records were obtained 24 h after the first contact between water and HS. Representative examples of heating curves of FA and HA originating from Suwannee river of different W_c are given in Figs. 1 and 2, respectively. The records are plotted in the temperature range from −40 to 10 °C since at lower temperatures no thermal events were detected.

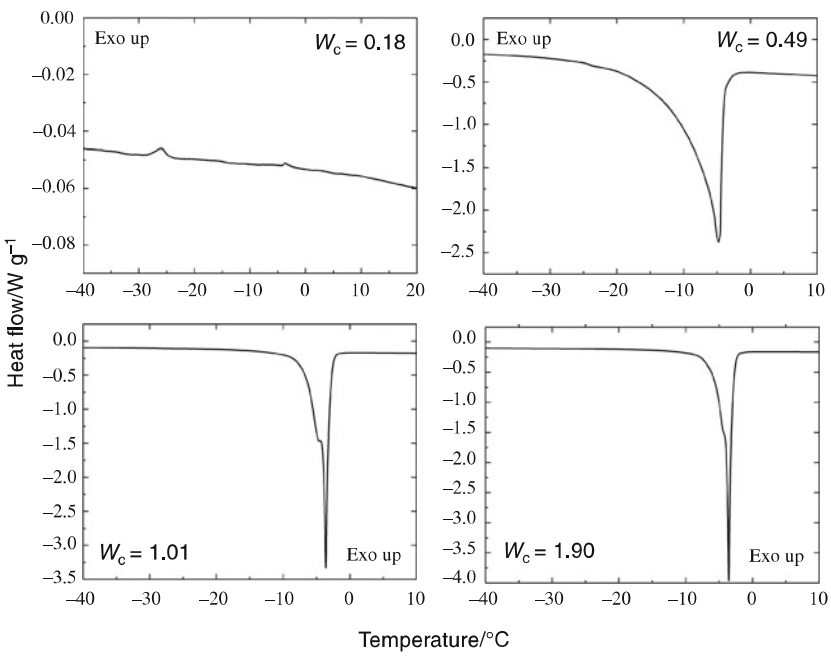

Fig. 1 DSC heating curves of ice melting in hydrated SRHA measured after 1 day of hydration

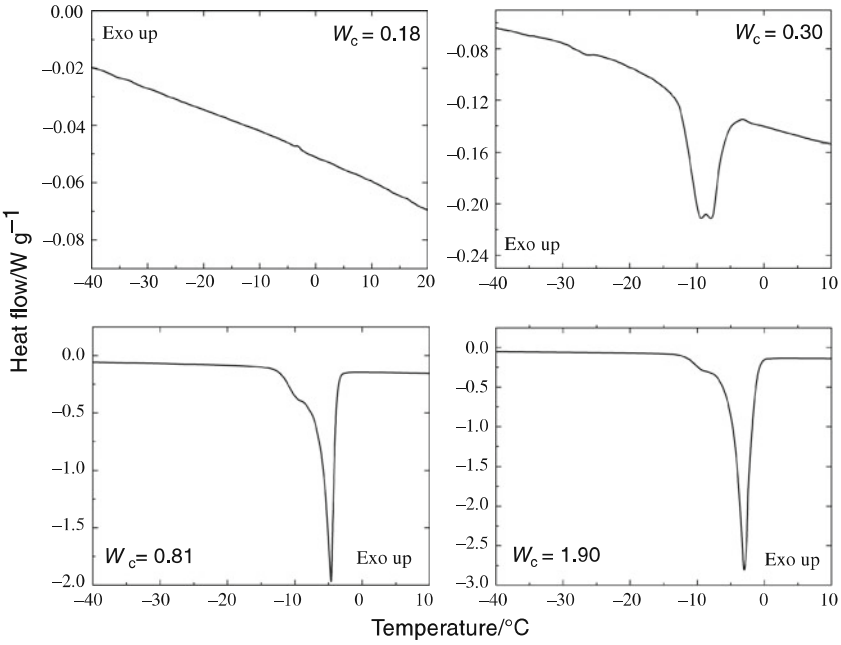

Fig. 2 DSC heating curves of ice melting in hydrated SRFA measured after 1 day of hydration

Figure 1 shows the melting behavior of hydrated SRHA acid after a water contact time of 1 day. For $W_c = 0.18$, no endothermal phase transitions were detected, only several small exothermal peaks associated with system restructuralization. This is in accordance with the assumption that at very low water content, all water molecules are present in the form of non-freezing water, i.e., all of them are restricted by the intimate contact with the humic molecules surface and thus they cannot participate in ice formation [12]. Increasing the water content to $W_c = 0.49$ resulted in an endothermal event around −5 °C which indicates the melting of ice originating from the presence of freezable water. A further increase in water content to $W_c = 1.01$ and $W_c = 1.90$ increased the peak area (see the changes in *Y*-axes range) and peak temperature were slightly shifted to higher values. Simultaneously, a small shoulder appeared in both thermograms indicating overlapping processes which can reflect melting of different types of freezing-bound water. With this respect, it is noteworthy that the peak width decreased with increasing water concentration which implies either decrease in heterogeneity of ice structures with increasing water content or occurrence of additional processes during the ice melting (e.g., transition from cubic to hexagonal ice, see e.g., Ref. [19].).

The hydrated SRFA samples (Fig. 2) show a comparable qualitative melting behavior as SRHA. Like for SRHA, the peak temperature decreased with increasing water content and the melting peaks split similarly to those for SRHA, although the shape of the double peak differs from that of SRHA. However, unlike SRHA, SRFA reveals also a small endothermic peak around −25 °C at concentration $W_c = 0.30$, and the main melting peak occurred around −10 °C.

As freezing-bound water represents a kind of water/ice whose structure is affected by the interaction with humic molecules, mainly by polar groups and by the distribution of pores in the physical structure [12], the differences between the melting enthalpy of ice in SRHA and SRFA show that SRFA has a stronger impact on the ice structure than SRHA.

The other IHSS samples of HA and FA investigated in this study showed similar behavior and therefore their thermograms have not been plotted.

In none of the investigated samples, thermograms obtained from three subsequent freezing–melting cycles differed from each other. This suggests that the freezing–melting process of the water did not affect the physical structure of hydrated FA and HA. This is in contrast to polysaccharide Konjac mannan where peak number was reduced in the second and third heating cycle [9].

Hydration state after 21 days

Figure 3 reports the change of the DSC melting curves of SRFA at $W_c = 0.51$ during the hydration period up to 21 days. The record from the first day displays a peak with maximum around −5 °C. In fact, the position of the peak did not significantly change during the period of hydration. In contrast, the melting enthalpy decreased confirming the incorporation of larger amount of water in hydration, i.e., progressively larger amount of total water content is present as non-freezing water. Further, as can be seen mainly at 4th and 10th day, there appeared an exothermal peak preceding the ice melting which can be attributed to the cold crystallization resulting from the crystallization of

glassy water [20, 21] which is typical (among others) for water/biopolymer system [22]. These observations confirm that during hydration not only new surfaces are wetted but also the change in the physical structure of HS takes part. This causes the existence of "restricted" water which is reflected by appearance of cold crystallization on DSC exotherm. The peak broadening suggests an increase in heterogeneity in the sample, potentially caused by an increase in the distribution of inner places and surfaces in humic matrix, such as cavities and holes in which water molecules experience a variety of interactions and physical states.

Similar records were obtained for the SRHA sample, but the melting enthalpy decrease was more intensive in case of SRFA. Assuming that the extent of this decrease indicates a more intensive interaction between HS and water, this observation can be explained by the higher polarity of SRFA than SRHA (see oxygen content and C/O in Table 1) resulting in a higher hydrophilicity and in faster wetting and swelling of SRFA than SRHA.

Unlike the more homogeneous hydrophilic biopolymers, where the hydration processes are usually completed within hours to days (even in case of insoluble ones), the kinetics of hydration in HS evidently plays a more important role as well as the hydration mechanism appears to be different which is in line with the recent results implying that hydration of e.g., peat can be as long as several months [10, 12].

As reported in our recent work, hydrophobic hydration plays a crucial role in chemistry of HA; FA are more polar and their influence on mobility of water molecules is generally larger [23]. The motion of water confined in polar cavities or bound on the polar surface is more restricted and therefore the formation of ice is associated with formation of less perfect crystals or even amorphous ice than in case of bulk water or water on hydrophobic surface [24]. This explanation agrees with the observation of cold crystallization for the SRFA. When the HS/water system is cooled rapidly, part of water might remain in a supercooled state due to above-mentioned restrictions in the form of so-called glassy water [20, 21]. On heating, the molecular motion of glassy water is enhanced and water changes to crystal ice [9]. That phenomenon was only minor in records of the first day and last day (Fig. 3), which points to the importance of kinetic factor while considering hydration processes of HS, i.e., wetting and swelling. It also indicates that the structure has been stabilized during the preceding hydration period.

Hydration kinetics

In order to evaluate the time development of hydration more quantitatively and draw qualitative conclusions on hydration kinetics, the endothermic peaks were integrated to obtain the melting enthalpies. Figure 4 representatively shows the melting enthalpies for four selected W_c of Leonardite HA (LHA), Suwanee river HA and FA (SRHA and SRFA, respectively) as a function of time.

In general, the melting enthalpy decreases with increasing hydration time, although the decrease functions differ qualitatively between the three samples and between the four water contents. During the first 7 days, melting enthalpy decreased fast in all samples. After that time period, the decrease became more moderate. This seems to

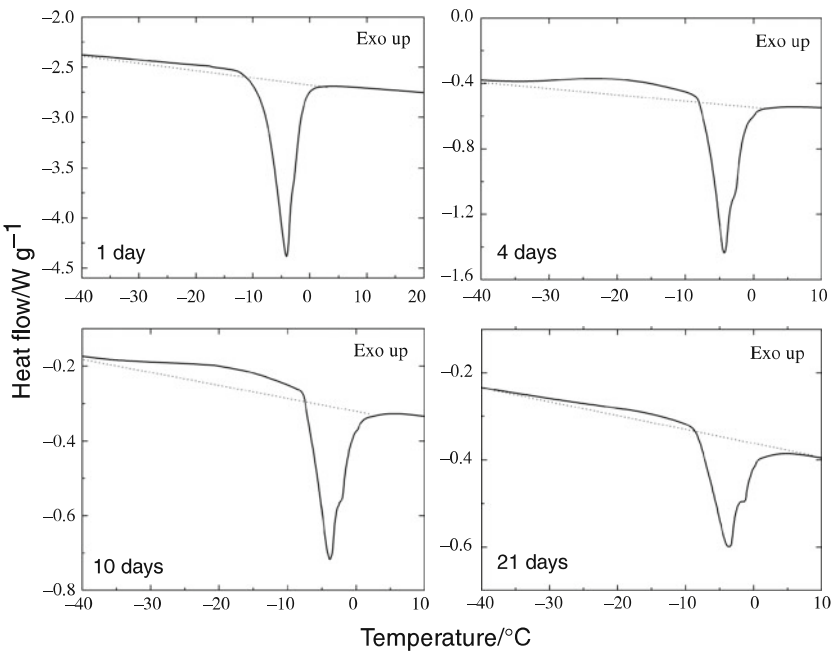

Fig. 3 DSC heating curves of ice melting in hydrated SRHA at a water content of $W_c = 0.51$ at four time points between 1 and 21 days

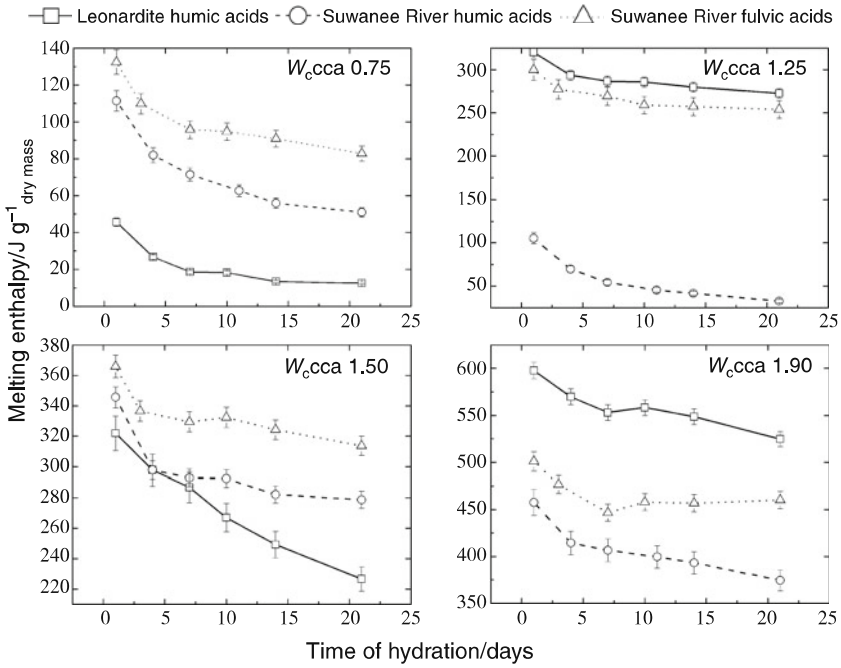

Fig. 4 Development of melting enthalpy of ice in hydrated LHA, SRHA, and SRFA samples as function of hydration time for four different water contents

be in line with the recent statement that the wetting of SOM proceeds in two steps [10]. The first step includes wetting of the surfaces and after that the water is distributed to the pore volume. In contrast, Jaeger et al. [12] described hydration of peat as a three step process including breaking of hydrogen bonds, water diffusion, and reorientation of molecular chains during hydration. These differences are most probably due to significantly larger heterogeneity of the whole peat sample in contrast to the purified HS used in our study.

Figure 5 shows the melting enthalpy as a function of the water content for 1 and 21 days of hydration of LHA. As expected, the melting enthalpy increases with increasing water content. However, unlike the hydration of biopolymers (compare for example with Ref. [22]), this dependence does not show a linear trend. Instead, the melting enthalpy increases in two stages. It increases from $W_c = 0.8$ to $W_c = 1.2$, remains constant (1 day), respectively, even decreases significantly (21 days) at $W_c = 1.4$ and then continues the increase.

This can be explained as follows: due to LHA porous structure, water is present in different states influencing the ice melting enthalpy. The step-like dependency indicates the mechanisms of hydration: water penetrates the cavity and increases its volume by swelling while the water still remains largely freezable, and the melting enthalpy increases with increasing water content up to $W_c = 1.2$. As soon as the water content exceeds the capacity of the cavity, weak interactions stabilizing the domain are broken and water can penetrate further and wet another set of surfaces, which are most probably more hydrophobic as they are wetted only at higher water content. This explains the stagnation or respective decrease in melting enthalpy around $W_c = 1.4$. We assume that the spatial separation between hydrophilic and hydrophobic hotspots of the HA is at least partially induced by the hydration process itself; as a result of the hydrophobic effect, hydrophobic molecules are thermodynamically separated and "packed" away forming porous scaffold. As reported recently, HA are present as aggregates even in diluted solution [23]. In aqueous environment, supramolecular structures consisting of hydrophobic and amphiphilic molecules are stabilized significantly by hydrophobic interactions, such as van der Waals, π–π and CH–π dispersive forces [1]. The same interactions can be expected to stabilize the scaffold in the solid state or at water concentrations used in this study.

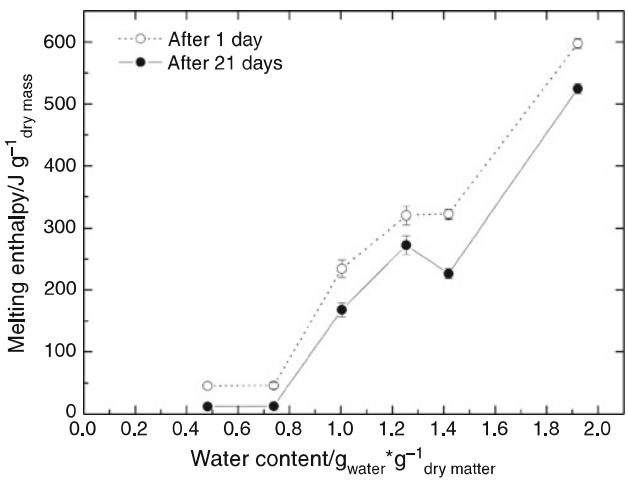

Fig. 5 Dependence of the melting enthalpy of ice on water content in hydrated LHA

In this way, water changes the structure of LHA, the scaffold stabilizing the structure is preserved and potentially strengthened during hydration as indicated by the stronger expression of the stepwise curve after 21 days of hydration.

Figure 6 summarizes results for the rest of HS investigated in this study. It shows that the melting enthalpy of SRFA increased linearly with water content, while SRHA showed a two-stage behavior like demonstrated for LHA, with the intermediate decrease of melting enthalpy also occurring around $W_c = 1.40$.

Like SRFA, other IHSS humic and fulvic samples showed a nearly linear dependency between melting enthalpy and water content, similar as for hydrophilic polymers [8, 22] with no indication of the "scaffolding" suggested by our results for the HAs. Extrapolation of the melting enthalpy–water content relations to zero melting enthalpy in Fig. 5 indicates the content of non-freezing water [8, 22]. The content of non-freezing water did not differ between the HAs and their related FAs. Rather, contents of non-freezable water were tendentially higher for the HAs. We assume that the more complicated inner structure of HA with higher porosity allows the water molecules to hydrate higher surface than in FA.

Discussion and future perspectives

Thermal analysis in natural organic matter characterization has been already recognized; however, in most cases, it included thermal-degradation approaches [25, 26]. Only rare studies employ non-destructive methodology (see e.g., Ref. [18]). In this study, DSC proved itself to be a powerful technique in characterization hydration of organic matter via freezing–melting processes. Our results show that hydration changes the physical structure of HS. The two-stage hydration characteristics deduced from the non-linear dependency between melting enthalpy and water content suggests that hydration, due to hydrophobic effect,

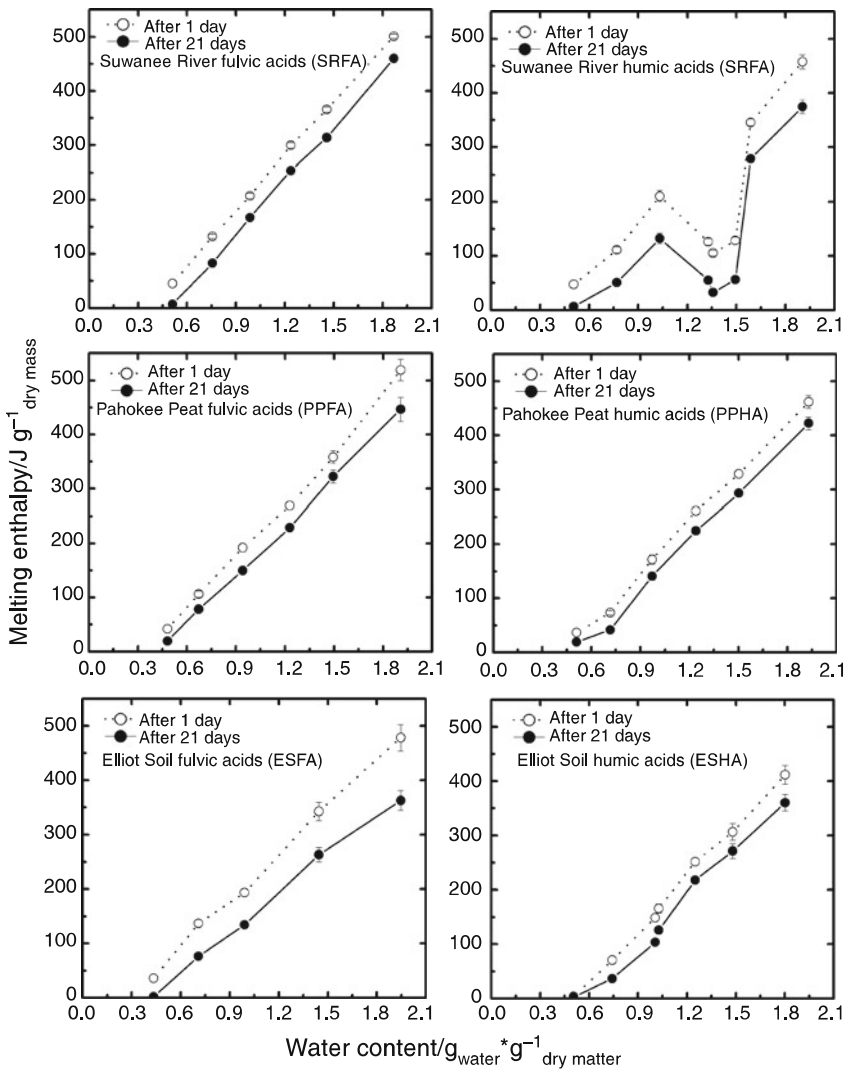

Fig. 6 Dependence of the melting enthalpy of ice in hydrated Suwanee river, Elliot soil, and Pahokee peat FA, and HA after 1 and 21 days of hydration

separates hydrophobic and hydrophilic microregions in the HAs. DSC results indicate that at specific concentrations and in some cases hydrophobic domains [23] are interconnected by non-specific weak interactions; as a result, "hydrophobic scaffold" is formed resembling a quasi-porous structure with rigid hydrophobic moieties surrounded by flexible, swollen hydrophilic moieties, which penetrate the pore system. This separation effect is furthermore supported by latest results of molecular modeling, which showed that hydrophobic supramolecular structures are more stable in hydrophilic environments and hydrophilic structures, vice versa, are more stable in hydrophobic environment [27]. Like the results of our study, these finding suggest that upon aging and hydration–dehydration processes, hydrophobic as well as hydrophilic microregions in the HA matrix will concentrate more and more, forming successively more distinct hotspots and resulting in an increase in nanospatial heterogeneity in the HA matrix.

In accordance with recent supramolecular concept suggested by Piccolo et al. [28] (see Ref. therein), it can be agreed that humification in soil can be considered as a two-step process: (i) biodegradation of dead-cells components, (ii) hydration–dehydration driven aggregation of the degradation products. In light of the previous discussion, formation of new covalent bonds during the humification process producing humus is not the only alternative. Instead, humification or at least part of it can be considered as the progressive self-association of the mainly hydrophobic molecules resistant to biodegradation supported by repeating wetting and drying. In this way, the hydrophobic scaffold is formed allowing to some molecules to be separated from water and therefore to be excluded from microbiological degradation.

Conclusions

In this study, both the qualitative and quantitative aspects of hydration of HS were investigated and the differences in properties of water surrounding humic matter were explored. The DSC measurements of HS/water confirmed that the kinetics plays a significant role in hydration processes of HS. Unlike most hydrophilic biopolymers, the dependency of melting enthalpy change of freezable water (ice) on W_c was not constant after 24 h from preparing the sample because of its incomplete hydration. Therefore, the phase transition behavior was monitored over the period of 21 days. During this period, the melting enthalpy change of melting decreased for all samples. The results confirmed earlier observations that the hydration of HS is not a straightforward process. Mainly until approximately day 7, the rapid decrease in change of melting enthalpy occurred. After that time period, the diminution became more moderate. A crucial factor in distinguishing between HA and FA seems to be the different solubility of particular molecules. In FA, most of molecules are hydrophilic; therefore, their hydration resembles the hydrophilic biopolymers. In contrast, HA consist of a mixture of molecules of various polarity and therefore different wettability. The more complicated inner structure of HA with higher porosity allows the water molecules to hydrate higher surface than in FA. It seems that the younger (or less humified) the HS are, the easier and faster the change of their physical structure is.

References

1. Sutton R, Sposito G. Molecular structure in soil humic substances? The new view. Environ Sci Technol. 2005;39:9009–15.
2. Stevenson FJ. Humus chemistry: genesis, composition, reactions. 2nd ed. New York: Wiley; 1994.
3. Schaumann GE, Hurrass J, Műller M, Rotard W. Swelling of organic matter in soil and peat samples: Insights from proton relaxation, water absorption and PAH extraction. In: Ghabbour EA, Davies G, editors. Humic substances: nature's most versatile materials. New York: Taylor and Francis; 2004. p. 101–17.
4. Vaxelaire J, Cézac P. Moisture distribution in activated sludges: a review. Water Res. 2004;38:2215–30.
5. Vesilind PA. The role of water in sludge dewatering. Water Environ Res. 1994;66:4–11.
6. Tsang KR, Vesilind PA. Moisture distribution in sludges. Water Sci Technol. 1990;22:135–42.
7. Vesilind PA, Hsu CC. Limits of sludge dewaterability. Water Sci Technol. 1997;36:87–91.
8. Liu J, Cowman MK. Thermal analysis of semi-dilute hyaluronan solutions. J Therm Anal Cal. 2000;59:547–57.
9. Prawitwong P, Takigami S, Phillips GO. Phase transition behavior of sorbed water in Konjac mannan. Food Hydrocoll. 2007;21:1368–73.
10. Hurrass J, Schaumann GE. Hydration kinetics of wettable and water-repellent soils. Soil Sci Soc Am J. 2007;71:280–8.
11. Schaumann GE. Matrix relaxation and change of water state during hydration of peat. Colloid Surf A. 2005;265:163–70.
12. Jaeger F, Shchegolikhina A, Van As H, Schaumann GE. Proton NMR relaxometry as a useful tool to evaluate swelling processes of peat soils. Open Magn Reson J. 2010;3:27–45.
13. Graber ER, Borisover MD. Hydration-facilitated sorption of specifically interacting organic compounds by model soil organic matter. Environ Sci Technol. 1998;32:258–63.
14. Borisover M, Reddy M, Graber ER. Solvation effect on organic compound interactions in soil organic matter. Environ Sci Technol. 2001;35:2518–24.
15. Borisover M, Graber ER. Relationship between strength of organic sorbate interactions in NOM and hydration effect on sorption. Environ Sci Technol. 2002;36:4570–7.
16. Graber ER, Tsechansky L, Borisover M. Hydration-assisted sorption of a probe organic compound at different peat hydration levels: the link solvation model. Environ Sci Technol. 2007;41:547–54.
17. Schaumann GE, Bertmer M. Do water molecules bridge soil organic matter molecule segments? Eur J Soil Sci. 2008;59:423–9.

18. Schaumann GE, Leboeuf EJ. Glass transitions in peat: their relevance and the impact of water. Environ Sci Technol. 2005;39:800–6.
19. Yoshida H, Hakateyama T, Hakateyama H. Characterization of water in polysaccharide hydrogels by DSC. J Therm Anal. 1993;40:483–9.
20. Takigami S, Takigami M, Phillips GO. Hydration characteristics of the cross-linked hyaluronan derivative hylan. Carbohydr Polym. 1993;22:153–60.
21. Hakateyama H, Hakateyama T. Interaction between water and hydrophilic polymers. Thermochim Acta. 1998;308:3–22.
22. Průšová A, Šmejkalová D, Chytil M, Velebný V, Kučerík J. An alternative DSC approach to study hydration of hyaluronan. Carbohydr Polym. 2010;82:498–503.
23. Kučerík J, Čechlovská H, Bursáková P, Pekař M. The thermodynamic stability and molecular feature of lignite humic acids aggregates studied by high resolution ultrasonic spectroscopy. J Therm Anal Cal. 2009;96:637–43.
24. Uchida T, Nagayama M, Shibayama T, Gohara K. Morphological investigation of disaccharide molecules for growth inhibition of ice crystals. J Cryst Growth. 2007;299:125–35.
25. Fernandez JM, Plante AF, Leifeld J, Rasmussen C. Methodological considerations for using thermal analysis in the characterization of soil organic matter. J Therm Anal Cal. 2011;104:289–98.
26. Siewert C, Demyan MS, Kučerík J. Interrelation between soil respiration and its thermal stability. J Therm Anal Cal. 2010. doi:10.1007/s10973-011-2099-z.
27. Aquino A, Tunega D, Pasalic H, Schaumann GE. Molecular dynamics simulations of water molecule-bridges in polar domains of humic acids. Environ Sci Technol. 2011. doi:10.1021/es201831g.
28. Piccolo A. The supramolecular structure of humic substances. Soil Sci. 2001;166:810–32.

Appendix 5

Průšová, A., Conte, P., Kučerík, J., Alonzo, G. (2010) Dynamics of hyaluronan aqueous solutions as assessed by fast field cycling NMR relaxometry. Analytical and Bioanalytical Chemistry 397: 3023–3028.

Anal Bioanal Chem (2010) 397:3023–3028
DOI 10.1007/s00216-010-3855-9

ORIGINAL PAPER

Dynamics of hyaluronan aqueous solutions as assessed by fast field cycling NMR relaxometry

Alena Průšová · Pellegrino Conte · Jiří Kučerík · Giuseppe Alonzo

Received: 9 April 2010 / Revised: 15 May 2010 / Accepted: 17 May 2010 / Published online: 14 June 2010
© Springer-Verlag 2010

Abstract Fast field cycling (FFC) NMR relaxometry has been used to study the conformational properties of aqueous solutions of hyaluronan (HYA) at three concentrations in the range 10 to 25 mg mL^{-1}. Results revealed that, irrespective of the solution concentration, three different hydration layers surround hyaluronan. The inner layer consists of water molecules strongly retained in the proximity of the HYA surface. Because of their strong interactions with HYA, water molecules in this inner hydration layer are subject to very slow dynamics and have the largest correlation times. The other two hydration layers are made of water molecules which are located progressively further from the HYA surface. As a result, decreasing correlation times caused by faster molecular motion were measured. The NMRD profiles obtained by FFC-NMR relaxometry also showed peaks attributable to ^{1}H–^{14}N quadrupole interactions. Changes in intensity and position of the quadrupolar peaks in the NMRD profiles suggested that with increasing concentration the amido group is progressively involved in the formation of weak and transient intramolecular water bridging adjacent hyaluronan chains. In this work, FFC-NMR was used for the first time to obtain deeper insight into HYA–water interactions and proved itself a powerful and promising tool in hyaluronan chemistry.

A. Průšová · J. Kučerík
Faculty of Chemistry, Brno University of Technology,
Purkyňova 118,
612 00 Brno, Czech Republic

P. Conte (✉) · G. Alonzo
Dipartimento di Ingegneria e Tecnologie Agro-Forestali,
Università degli Studi di Palermo,
v.le delle Scienze 13, edificio 4,
90128 Palermo, Italy
e-mail: pellegrino.conte@unipa.it

Keywords FFC-NMR · Relaxometry · Correlation time · Quadrupole interactions · Hydration layer

Introduction

Hyaluronan (HYA) is a linear, unbranched, high-molecular-weight glycosaminoglycan polymer whose repeating unit is a dimer formed from D-glucuronic acid and *N*-acetyl-D-glucosamine [1]. The two monosaccharides are held together by a β-(1→3) glycosidic bond. The disaccharides are, then, bound to each other by β-(1→4) glycosidic linkages.

HYA is an important biopolymer ubiquitous in vertebrates' tissues and in some bacteria but absent from fungi, plants, and insects [2–5]. It is a crucial biopolymer involved in embryonic development, extracellular matrix homeostasis, wound healing, and tissue regeneration [6]. Its solutions are very important in medical applications, for example ophthalmology, pharmacology, drug delivery, viscoprotection, orthopedy, rheumatology, dermatology, and plastic surgery [4, 5, 7]. HYA is also used in cosmetics and cryo-biology [4].

In the last few years, many papers have appeared in literature dealing with the chemical and physical properties of hyaluronan solutions [7–15]. In all this work the structure and conformational behaviour of hyaluronan and hyaluronan derivatives have been studied by application of traditional analytical techniques, for example NMR [7–16], force spectroscopy [17], rheology [8, 15], infrared spectroscopy [8–20], thermal analysis [21], and computational chemistry [23] or by classical wet chemical methods [12, 14, 24]. To the best of our knowledge, no paper describing application of fast field cycling (FFC) NMR relaxometry in hyaluronan research has ever appeared in the scientific literature.

FFC-NMR relaxometry probes the molecular dynamics of complex systems, for example plant tissues [25], food

[26–30], seeds [31], archaeological materials [32], nanoporous media [33], and environmental matrices [25, 34] by measurement of longitudinal (T_1) relaxation times [35–38]. When analyzing liquid systems the technique seems to be very sensitive to solvent molecules (e.g. water); because of interactions with solutes the solvent molecules become slower so their relaxation times decrease. For this reason, information about the structure and dynamics of solvents in closest proximity to solutes can be obtained [25]. Further advantages of FFC-NMR relaxometry are its sample non-destructivity, speed, and the possibility of isolating typical relaxation features associated with molecular processes characterized by very long correlation times (e.g. molecular surface dynamics and collective effects) [37].

The basic FFC-NMR or NMR dispersion (NMRD) experiment consists in application of a Zeeman magnetic field (B_0) which cycles through three different values known as the polarization (B_{POL}), relaxation (B_{RLX}), and acquisition (B_{ACQ}) fields [37, 38]. B_{POL} is applied for a fixed period of time (T_{POL}) in order to achieve magnetization saturation and sensitivity enhancement [37]. Then, the magnetic field is switched to a new one, B_{RLX}, applied for a period (τ) during which magnetization intensity changes to reach a new equilibrium condition. Finally, acquisition of the free induction decay (FID) is achieved by application of the magnetic field B_{ACQ} concomitantly with a 90° pulse on the investigated nucleus.

The T_1 relaxation times (and, as a consequence, the longitudinal relaxation rates $R_1=1/T_1$) of the observed nuclei are measured at each fixed B_{RLX} intensity by progressive variation of the τ values. The longitudinal relaxation rates plotted versus the applied magnetic field strengths represent the NMRD profiles (or dispersion curves) which can provide information about the physical/chemical properties of complex materials [35–38]. For example, ^{1}H NMRD analyses of hens' eggs revealed that quality loss during storage can be associated with the acidity increase arising from carbon dioxide diffusion through the eggshell [39]. Further, a two-stage gelation process (first formation of strongly linked dimers, then weak inter-dimer aggregation) was discovered for $CaCl_2$ low methoxy pectin water solutions [40].

The objective of the work discussed in this paper was to apply fast field cycling NMR relaxometry in order to evaluate the conformational properties of hyaluronan solutions as affected by different HYA concentrations. Results confirmed literature data concerning the organization of water molecules surrounding hyaluronan. In addition, it was revealed that with increasing concentration (from 10 to 25 mg mL^{-1} in this study) the N atoms of amido groups are progressively employed in weak and transient water bridges with adjacent HYA chains causing non-ideal behaviour of HYA solutions.

Materials and methods

Samples

A bacterial 1.36 MDa hyaluronan (HYA; the molecular weight was measured by size-exclusion chromatography) was kindly provided by CPN Company (Dolní Dobrouč, Czech Republic). HYA solutions were obtained by dissolution of hyaluronan powder in Milli-Q water in order to obtain concentrations 10, 15, and 25 mg mL^{-1}. The solutions were prepared by stirring HYA–water mixtures at room temperature for 24 hours as recommended by Takahashi et al. [41]. The pH of the HYA water solutions was neutral, thereby enabling pH buffer effects to be neglected in further considerations.

FFC-NMR experiments

^{1}H NMRD profiles (i.e. relaxation rates R_1 or $1/T_1$ vs. proton Larmor frequencies) were acquired on a Stelar Spinmaster-FFC-2000 Fast-Field-Cycling Relaxometer (Stelar s.r.l., Mede, PV–Italy) at a constant temperature of 293 K. Field-switching time was 3 ms and spectrometer dead time was 15 μs. The proton spins were polarized at a polarization field (B_{POL}) corresponding to a proton Larmor frequency (ω_L) of 29 MHz for a period of polarization (T_{POL}) included in the range 6–10 s. A recycle delay of 10 s was always applied. The longitudinal magnetization evolution was recorded at values of a relaxation magnetic field (B_{RLX}) corresponding to ω_L in the range 0.010–20 MHz. The NMR signal was acquired with 1 scan for 16 linearly spaced time sets, each of them was adjusted at every relaxation field to optimize the sampling of the decay/recovery curves. Within experimental error, all the decay/recovery curves of longitudinal magnetization were exponential. Free induction decays (FID) were recorded after a single ^{1}H 90° pulse applied at an acquisition field (B_{ACQ}) corresponding to the proton Larmor frequency of 16.2 MHz. A time domain of 100 μs sampled with 512 points was also applied. The decay/recovery curves at each B_{RLX} value (i.e. ^{1}H signal intensity-vs-τ) were fitted by using a 1st-order exponential decay/recovery function after export of the experimental data to OriginPro 7.5 SR6 (Version 7.5885, OriginLab, Northampton, MA, USA).

FFC-NMR data elaboration

The NMRD profiles were fitted in OriginPro 7.5 SR6 with a Lorentzian function of the type [37, 42]:

$$R_1 = \sum_1^n \frac{A_i \tau_{C,i}}{1 + \left(\omega_L \tau_{C,i}\right)^2} \quad (1)$$

In eq. (1), R_1 is the longitudinal relaxation rate, ω_L is the proton Larmor frequency, A_i is a constant containing the proton quantum-spin number, the proton magnetogyric ratio, the Planck constant, and the electron-nuclear hyperfine coupling constant describing interactions between resonant protons and unpaired electrons. $\tau_{C,i}$ is the correlation time of the *i*th relaxing component measuring the time needed for molecular re-orientation. It is a typical property of the spectral density which, in turn, describes random molecular motion [37]. The number, *n*, of Lorentzians that were included in eq. (1) without unreasonably increasing the number of terms were determined by means of the Merit function analysis [35]. In this work, $n=3$ was used for mathematical fitting of the NMRD profiles. In addition, all fitting was done by excluding from the mathematical fitting iterations all the maxima corresponding to distortions of Lorentzian curves because of ^1H–^{14}N quadrupolar interactions.

Results and discussion

Differences among longitudinal relaxation rates of hyaluronan solutions

High-field (HF) NMR results (data not reported) revealed that the sole detectable component of the aqueous HYA solutions was water. Because of the lower spectral sensitivity of FFC-NMR relaxometry compared with traditional HF NMR, it is conceivable that the NMRD profiles of the three different hyaluronan (HYA) solutions (Fig. 1) describe only the dynamics of the water molecules surrounding such a glycosaminoglycan polymer.

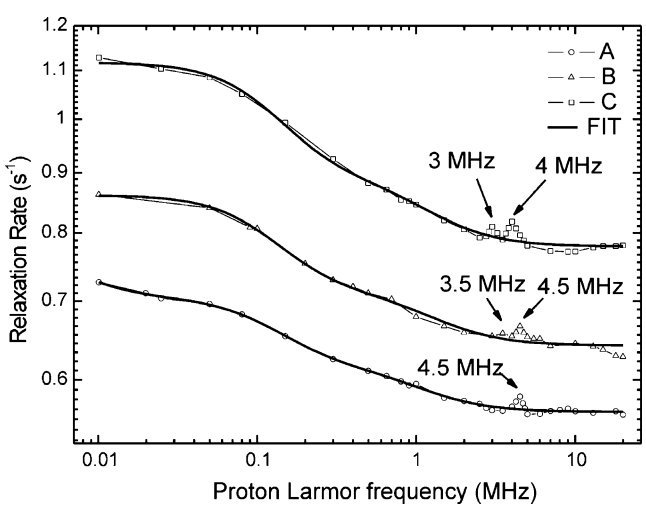

Fig. 1 ^1H NMRD profile of hyaluronan aqueous solutions. **A**. HYA concentration 10 mg mL^{-1}; **B**. HYA concentration 15 mg mL^{-1}; **C**. HYA concentration 25 mg mL^{-1}. The arrows indicate nitrogen nuclear quadrupole resonance. Both x and y scales are logarithmic. The line is the best fit of the experimental data

Figure 1 shows that the relaxation rates describing the dispersion curves of the HYA solutions varied in the order R_1 (25 mg mL^{-1})>R_1 (15 mg mL^{-1})>R_1 (10 mg mL^{-1}).

The longitudinal or spin–lattice relaxation rate ($R_1=1/T_1$) represents the lifetime of the first-order process that returns the magnetization to the Boltzman equilibrium [43]. The magnitude R_1 depends on the nature of the nuclei, the physical state of the system (solid or liquid), its viscosity, and temperature [43]. Spin–lattice relaxation occurs when the lattice creates magnetic fields fluctuating at frequencies resembling those of the observed protons. Fluctuating fields are created by molecular motion, which strongly affects dipolar interactions [43]. In particular, the faster the motion, the lower the dipolar interaction strengths, thereby favouring lower R_1 values [43]. Conversely, slower molecular dynamics are associated with faster spin–lattice relaxation rates, because of stronger intra and inter-proton dipolar interactions [43].

Hyaluronan contains polar sites, for example hydroxyl, carboxyl, and amido groups (Fig. 2). For this reason, it can form intra and inter-molecular H-bonds with water molecules which are the main cause of the enhanced solution stiffness as HYA concentration is increased [1]. Increasing HYA rigidity because of stiffness enhancement results in more efficient energy exchange between excited nuclear spins and their environment. Because of the direct relationship between molecular motion and relaxation rates [43], it is conceivable that the relaxation rates of HYA solutions change in the order R_1 (25 mg mL^{-1})>R_1 (15 mg mL^{-1})>R_1 (10 mg mL^{-1}) over the entire range of magnetic field frequencies investigated in this study.

Molecular dynamics of hyaluronan at different concentrations

NMRD profiles are usually used to retrieve correlation times (τ_c) which measure the time needed for molecular re-orientation in solution [44]. As a general rule, the larger the molecular size, the slower the correlation time (longer τ_c values for slow motion) [43]. In addition, τ_c values are also increased when molecules are involved in weak interactions, for example hydrogen bonding and van der Waals interactions [43].

In this study, three different τ_c values were obtained after application of eq.(1) (Table 1). Table 1 shows that the correlation times varied in the order $\tau_{c1}>\tau_{c2}>\tau_{c3}$ for all HYA concentrations, thereby revealing that three different mechanisms of water dynamics can describe the behaviour of water molecules surrounding hyaluronan.

A molecular model which can be used to explain the three different τ_c values reported in Table 1 can be based on the findings of Fouissac et al. [45] and Cowmann et al. [8] also supported by results of Almond [46, 47], Haxaire et al.

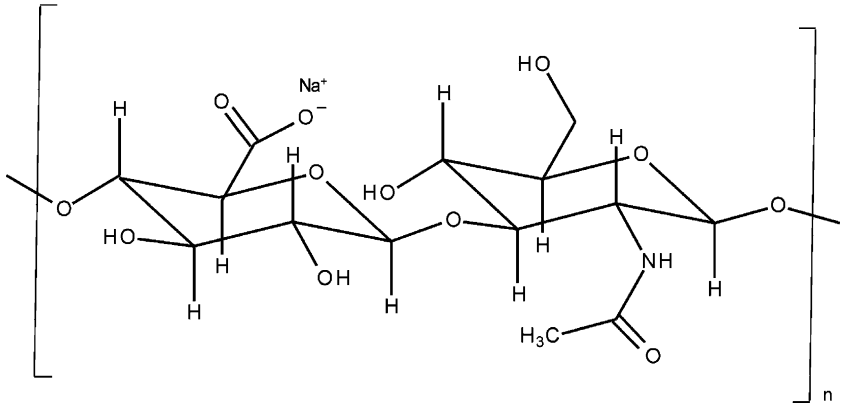

Fig. 2 Structure of the dimer repeating unit in hyaluronan

[18, 19], Maréchal et al. [20], and Matteini et al. [15]. Namely, HYA solutions below the overlapping concentration contain random coil worm-like chains, whereas as the amount of HYA becomes larger than the overlapping concentration, the chains form three-dimensional superstructures stabilized by intermolecular water bridges and intramolecular H-bonds [18–20, 43, 46]. In particular, water molecules surrounding the HYA are involved in diffusion dynamics between at least three different hydration layers. The first hydration layer is made by bound water (BW) which is strongly fixed to the hyaluronan surface by electrostatic interactions [18–20], thereby providing the longest correlation time τ_{c1} (Table 1). The second hydration layer contains water molecules, also recognized as partly-bound (PBW), which are not directly interacting with the HYA chains. Being more mobile than BW, the PBW molecules may supply the correlation time indicated as τ_{c2} in Table 1. Finally, water molecules, whose dynamics resemble that of bulk water or free water (FW) [21, 22, 41, 48] are characterized by the shortest τ_{c3} value (Table 1).

More recently, the BW-PBW-FW model has been modified to account for hyaluronan at very high concentrations [15]. In fact, it has been revealed that when the HYA concentration ranges between 10 and 100 mg mL^{-1}, as in this study, the bound water, the partly bound water, and the free water molecules must be considered, more correctly, as network water (NW), intermediate water (IW), and multimer water (MW) systems, respectively [15]. According to this new view, water molecules belonging to the NW organization are regarded as being connected tetrahedrally as in ice, thereby generating instantaneous H-bonded low-density pathways that extend to a supramolecular level [15]. Because of the rigidity of the NW ice-like water molecules, correlation times describing the re-orientation rate of molecules in solution are expected to be the longest as reported in Table 1 (τ_{c1}). The intermediate water molecules are connected to each other by distorted H-bonds and have an average amount of connections lower than that of the water molecules participating in the NW systems [15]. The faster molecular motion of the IW molecules whose dynamics are described by τ_{c2} (Table 1) ensure that $\tau_{c2}<\tau_{c1}$. The third type of water molecule (MW) corresponds to poorly connected molecules which occur as dimers or trimers [15]. The highest degree of freedom of such molecules causes the shortest τ_{c3} values in Table 1.

Table 1 shows that no changes of τ_{c1} and τ_{c2} values can be observed when HYA concentration is increased from 10 to 25 mg mL^{-1}. Conversely, τ_{c3} values change in the order τ_{c3} (10 mg mL^{-1})<τ_{c3} (15 mg mL^{-1})<τ_{c3} (25 mg mL^{-1}) (Table 1). This reveals that the mobility of water molecules in the distant hydration layer is progressively reduced as the concentration of hyaluronan is increased. In fact, as the hydration volume is increased, long-distance connectivity of water molecules are favoured over small sized water aggregates, and reduction of τ_{c3} values can be observed (Table 1) [15]. This behaviour may also be explained by considering the effect of the increasing ionic strength as HYA concentration increases from 10 mg mL^{-1} to 25 mg mL^{-1}. Ionic strength enhancement enables long-range interactions among electrically charged species such as organic biopolymer and water, thereby favouring the mobility reduction of water molecules encompassed within the third HYA hydration layer.

Table 1 Correlation times determined by fitting experimental data to eq. (1) for HYA solutions at three different concentrations

Concentration (mg mL^{-1})	τ_{c1} (s)	τ_{c2} (s)	τ_{c3} (s)
10	$(1.3\pm0.1)\times10^{-6}$	$(1.6\pm0.1)\times10^{-7}$	$(9.8\pm0.1)\times10^{-10}$
15	$(1.1\pm0.2)\times10^{-6}$	$(1.6\pm0.1)\times10^{-7}$	$(5.9\pm0.2)\times10^{-9}$
25	$(1.2\pm0.1)\times10^{-6}$	$(1.5\pm0.1)\times10^{-7}$	$(4.7\pm0.1)\times10^{-8}$

Hyaluronan backbone fluctuations

Kimmich and Anoardo [37] reported that the internal dynamics of organic molecules can be divided into side-group motion (for example rotation of methyl groups and flips of phenyl rings) and backbone fluctuations. Whereas the former are detected at high magnetic field frequencies (e.g. proton Larmor frequencies of the order of hundreds of megahertz), the latter become important at low frequency. Backbone fluctuations in nitrogen-containing organic systems (i.e. proteins, liquid crystals, and drugs) are normally detected as peaks in the NMRD profiles originating from relaxation sinks formed by quadrupole nuclei in N–H groups [37]. Namely, when the proton Larmor frequency resembles the resonance frequency of the quadrupolar ^{14}N, the excited protons in water molecules exchange energy with nitrogen nuclei in the lattice at a relaxation rate faster than that between ^{1}H–^{1}H nuclei. This exchange occurs preferentially when, in dry or hydrated systems, molecular motion is restricted, and, therefore, the motional averaging is incomplete at the scale of the fast field cycling experiment [37].

Figure 1 reveals that the NMRD profiles of hyaluronan solutions contain maxima centred at different proton Larmor frequencies according to the HYA concentration under investigation. In particular, two peaks appear at 3 and 4 MHz at the concentration of 25 mg mL^{-1} (Fig. 1A), they are shifted to 3.5 and 4.5 MHz at the concentration of 15 mg mL^{-1} (Fig. 1B), and only one peak at 4.5 MHz appears in the NMRD profile of the 10 mg mL^{-1} HYA solution (Fig. 1C).

It is recognised that the structure of hyaluronan goes from intra-molecular hydrogen-bonded organization to the inter-molecular hydrogen-bonded structure in which water molecules can bridge the carboxyl and amido groups of adjacent saccharide units of HYA chains [17]. In particular, at the low HYA concentrations it can be expected that the amido groups are involved mainly in intra-molecular water bridges whereas when the concentration of hyaluronan is larger, increasing numbers of inter-molecular water bridges between the quadrupole ^{14}N and other polar group of neighbouring HYA molecules can be hypothesized [49]. In fact, when the concentration is lowest (i.e. 10 and 15 mg mL^{-1}), the macromolecular backbone motional freedom is the largest, thereby providing the smallest quadrupole NMRD peaks centred at the largest frequencies of the magnetic field (Fig. 1) [37]. Conversely, when the largest concentration of 25 mg mL^{-1} is achieved the backbone motions are restricted by the intermolecular H-bonds with water bridges. For this reason, the number of quadrupole peaks is highest and they are positioned at the lowest magnetic field frequencies (Fig. 1) [37]. Finally, notwithstanding its macroscopic gel properties, hyaluronan is regarded as a non-gel forming polysaccharide [49]. The non-ideal behaviour and unusual rheological properties of highly concentrated HYA solutions can be explained by formation of intermolecular H-bonds between amidic nitrogen and water molecules as the concentration is raised.

Conclusions

In this paper we report, for the first time, application of fast field cycling NMR relaxometry to characterization of the molecular dynamics of hyaluronan solutions. In accordance with previous results obtained by use of a variety of techniques [14, 15, 17, 21, 22, 41, 48], FFC-NMR data confirmed that three different hydration layers surround hyaluronan irrespective of HYA concentration. The first hydration layer was recognised to consist of strongly restrained water molecules with the slowest motion. These molecules interact with a second hydration layer which in turn is surrounded by a third layer. Molecular mobility seemed to increase going from the intermediate water hydration layer to the multimer layer. In addition, FFC NMR relaxometry supplied information about macromolecular backbone fluctuations of hyaluronan, which are directly related to the conformational arrangement of such molecules in solution. In fact, it was suggested that at low concentrations of HYA in water, the amido group is involved mainly in intra-molecular water bridges whereas at high concentrations inter-molecular water bridges become much more important. These interactions can justify the non-ideal behaviour and the unusual rheological properties of the highly concentrated aqueous solutions of hyaluronan, which is reported to be a non-gel forming polysaccharide.

Acknowledgments This work was partially funded by Ce.R.T.A.s.c.r.l. (Centri Regionali per le Tecnologie Alimentari; http://www.certa.it/default.asp) and by the Ministry of Education, Youth and Sport of the Czech Republic, project no. 0021630501. A.P. acknowledges an Erasmus project which enabled her to work at the Università degli Studi di Palermo. The authors kindly acknowledge Dr. Vladimír Velebný (CPN company, Dolní Dobrouč, Czech Republic) for providing the hyaluronan sample.

References

1. Garg HG, Hales CA (2004) Chemistry and biology of hyaluronan. Elsevier Ltd, Oxford
2. De Angelis PL (2002) Glycobiology 12:9R–16R
3. McDonald JA, Camenisch TD (2003) Glycoconjugate J 19:331–339
4. Kogan G, Šoltéz L, Stern R, Gemener P (2007) Biotechnol Lett 29:17–25
5. Rinaudo M (2008) Polym Int 57:397–430
6. Leach JB, Schmidt CE (2004) In: Encyclopedia of Biomaterials and Biomedical Engineering, 1st edn. Marcel Dekker, pp 779–789

7. Taglienti A, Sequi P, Valentini M (2009) Carbohydr Res 344:245–249
8. Cowman MK, Matsuoka S (2005) Carbohydr Res 340:791–809
9. Blundell CD, Reed MAC, Almond A (2006) Carbohydr Res 341:2803–2815
10. Almond A (2007) Cell Mol Life Sci 64:1591–1596
11. Giannotti MI, Rinaudo M, Vancso GJ (2007) Biomacromolecules 8:2648–2652
12. Deschrevel B, Tranchepain F, Vincent J-C (2008) Matrix Biol 27:475–485
13. Hargittai I, Hargittai M (2008) J Struct Chem 19:697–717
14. Tømmeraas K, Melander C (2008) Biomacromolecules 9:1535–1540
15. Matteini P, Dei L, Carretti E, Volpi N, Goti A, Pini R (2009) Biomacromolecules 10:1516–1522
16. Blundell CD, Reed MAC, Almond A (2006) Carbohydr Res 341:2803–2815
17. Giannotti MI, Rinaudo M, Vancso GJ (2007) Biomacromolecules 8:2648–2652
18. Haxaire K, Maréchal Y, Milas M, Rinaudo M (2003) Biopolymers 72:10–20
19. Haxaire K, Maréchal Y, Milas M, Rinaudo M (2003) Biopolymers 72:149–161
20. Maréchal Y, Milas M, Rinaudo M (2003) Biopolymers 72:162–173
21. Hatakeyama T, Hatakeyama H (1998) Thermochim Acta 308:3–22
22. Lui J, Cowman MK (2000) J Therm Anal Calorim 59:547–557
23. Pogány P, Kovács A (2009) Carbohydr Res 344:1745–1752
24. Rinaudo M (2006) Macromol Symp 245–246:549–557
25. Conte P, Bubici S, Palazzolo E, Alonzo G (2009) Spectrosc Lett 42:235–239
26. Bertram HC, Wiking L, Nielsen JH, Andersen HJ (2005) Int Dairy J 15:1056–1063
27. Davenel A, Schuck P, Mariette F, Brulé G (2002) Lait 82:465–473
28. Gianferri R, Maioli M, Delfini M, Brusio E (2007) Int Dairy J 17:167–176
29. Hernández-Sánchez N, Hills BP, Barreiro P, Marigheto N (2007) Postharvest Biol Technol 44:260–270
30. Tang HR, Zhao BL, Belton PS, Sutcliffe LH, Ng A (2000) Magn Reson Chem 38:765–770
31. Prestes RA, Colnago LA, Forato LA, Vizzotto L, Novotny EH, Carrilho E (2007) Anal Chim Acta 596:325–329
32. Casieri C, Bubici S, Viola I, De Luca F (2004) Solid State Nucl Magn Reson 26:65–73
33. Kausik R, Fatkullin N, Hüsing N, Kimmich R (2007) Magn Reson Imaging 25:489–497
34. Melton JR, Kantzas A, Langford CH (2007) Anal Chim Acta 605:46–52
35. Halle B, Johannesson H, Venu K (1998) J Magn Reson 135:1–13
36. Wang YL, Belton PS (2000) Chem Phys Lett 325:33–38
37. Kimmich R, Anoardo E (2004) Prog Nucl Magn Reson Spectrosc 44:257–320
38. Ferrante G, Sykora S (2005) Adv Inorg Chem 57:405–470
39. Laghi L, Cremonini MA, Placucci G, Sykora S, Wright K, Hills B (2005) Magn Reson Imaging 23:01–510
40. Dobies M, Kuśmia S, Jurga S (2005) Acta Phys Pol A 108:33–46
41. Takahashi M, Hatakeyama T, Hatakeyama H (2000) Carbohydr Polym 41:91–95
42. Lauffer RB (1987) Chem Rev 87:901–927
43. Bakhmutov VI (2005) Pratical NMR relaxation for chemists. John Wiley & Sons Ltd, Chichester
44. Bertini I, Luchinat C (1986) In: Gray ABP, Deries HB (eds) NMR of paramagnetic molecules in biological systems. The Benjamin/Cummings Publishing Company Inc, California
45. Fouissac E, Milas M, Rinaudo M (1993) Macromol 26:6945–6951
46. Almond A, Sheehan JK, Brass A (1997) Glycobiology 7:597–604
47. Almond A (2007) Cell Mol Life Sci 64:1591–1596
48. Wolfe J, Bryant G, Koster KL (2002) CryLetters 23:157–166
49. Hardingham T (2004) In: Garg HG, Hales CA (eds) Chemistry and biology of hyaluronan. Elsevier Ltd, Oxford

Appendix 6

Průšová, A., Vergeldt, F.J., Kučerík, J. (2013) Influence of water content and drying on the physical structure of native hyaluronan. Carbohydrate Polymers 95: 515–521.

Carbohydrate Polymers 95 (2013) 515–521

Contents lists available at SciVerse ScienceDirect

Carbohydrate Polymers

journal homepage: www.elsevier.com/locate/carbpol

Influence of water content and drying on the physical structure of native hyaluronan

Alena Průšová[a,b], Frank J. Vergeldt[a], Jiří Kučerík[b,*]

[a] Laboratory of Biophysics, Department of Agrotechnology & Food Sciences, Wageningen University, Dreijenlaan 3, 6703 HA, Wageningen, The Netherlands
[b] Institute of Environmental Sciences, University of Koblenz-Landau, Fortstrasse 7, 768 29 Landau, Germany

ARTICLE INFO

Article history:
Received 16 January 2013
Received in revised form 18 February 2013
Accepted 6 March 2013
Available online 16 March 2013

Keywords:
Hyaluronan
Hydration kinetics
Plasticization
Glass transition
DSC
TD-NMR

ABSTRACT

Hydration properties of semi-diluted hyaluronan were studied by means of time domain nuclear magnetic resonance. Based on the transverse proton relaxation times T_2, the plasticization of hyaluronan which was precipitated by isopropylalcohol and dried in the oven have been determined at water content 0.4 g of water per g of hyaluronan. Above this water content, the relaxation times increased and levelled off around 0.8 g of water per g of hyaluronan which agrees well with values determined earlier by differential scanning calorimetry and dielectric relaxometry. The freeze dried and oven dried samples showed differences in their physical structure such as glass transition, plasticization concentration and sample topography which influenced their kinetics and mechanisms of hydration. Results confirmed earlier hypothesis that some native biopolymer structures can be easily modified by manipulation of preparation conditions, e.g. drying, giving fractions with specific physicochemical properties without necessity of their chemical modification.

© 2013 Elsevier Ltd. All rights reserved.

1. Introduction

Hydrated polysaccharides are nowadays the subject of intense research efforts motivated both by fundamental research and by their industrial applications, e.g. in cosmetics and pharmaceuticals. Hyaluronan (HYA) has received growing attention compared with other polysaccharides because of its biological activity, water-retention capacity and hydration properties (Garg & Hales, 2004). HYA is an anionic, unbranched, non-sulphated glycosaminoglycan composed of repeating disaccharides units (β-1-3 D-N-acetylglucosamine, β-1-4 D-glucuronic acid).

HYA is a main component of the extracellular matrix in connective, epithelial, and neural tissues (Garg & Hales, 2004) as well as the synovial fluid which lubricates and maintains the cartilage (Sutherland, 1998). HYA is a water-soluble polysaccharide that produces a viscoelastic fluid, but does not form a gel (Almond, DeAngelis, & Blundell, 2006). It is assumed that when dissolved in water, the antiparallel HYA chains overlap in a meshwork stabilized by specific H-bonds (i.e. up to five H-bonds per tetrasaccharide unit of HYA) and hydrophobic interactions. Such a highly cooperative structure is formally equivalent to the β-sheet formed by proteins (Scott & Heatley, 1999). Scott and Heatley conclude that the characteristic behaviour of HYA solutions is the molecular-mass-dependent transition between tertiary structures of β-sheet and 2-fold helices by which important biological properties are controlled (Scott & Heatley, 2002). HYA's polarity and the formation of such a meshwork is a potential reason for the higher osmotic pressure in solution which is the cause of HYA's high water retention capacity (Davies, Gormally, Wynjones, Wedlock, & Phillips, 1983).

HYA hydration is frequently studied by means of differential scanning calorimetry (DSC). The classical DSC approach, which includes cooling and thawing of water present in a biopolymer, has been used by many research groups (Hatakeyama & Hatakeyama, 2004; Liu & Cowman, 2000; Takahashi, Hatakeyama, & Hatakeyama, 2000). This approach allows the categorization of water into different fractions according to its behaviour during cooling. The water fraction, which is in intimate contact with HYA and does not freeze, is called "non-freezing water". Next water fraction which exhibits melting/crystallization, shows considerable supercooling, and significantly smaller enthalpy than the bulk water is referred to as "freezing-bound water". The third fraction is bulk water. The sum of the freezing-bound and non-freezing water fractions is the "bound water content". The concept of bound water in (bio)polymers has been questioned by some authors. Their alternative explanation is that such water is only restricted by the junction zones in gel-like structures (Belton, 1997), or as a consequence of further growth of ice crystals after transformation of the (bio)polymer from a rubbery state into a glassy one (Bouwstra, Salomonsdevries, & Vanmiltenburg, 1995). However, other authors have reported contrasting results which demonstrate that surface water shows a coherent hydrogen bond pattern with

* Corresponding author. Tel.: +49 (0)6341 280 31 582; fax: +49 (0)6341 280 31 576.
E-mail addresses: kucerik@uni-landau.de, kucerik@email.cz (J. Kučerík).

0144-8617/$ – see front matter © 2013 Elsevier Ltd. All rights reserved.
http://dx.doi.org/10.1016/j.carbpol.2013.03.031

a large, net dipole field (Yokomizo, Nakasako, Yamazaki, Shindo, & Higo, 2005). Such hydrogen bonds between water and biopolymers (proteins in this case) are stronger and have longer lifetimes compared with hydrogen bonds in bulk water (Chakraborty, Sinha, & Bandyopadhyay, 2007). That water is unavailable for colligative effects. Recently, an alternative approach based on water evaporation has been introduced. It was shown that in the course of water evaporation from a HYA solution a linear dependency of evaporation enthalpy normalized by dry mass was abruptly interrupted at $W_C = 0.34\ g_{H20}/g_{HYA}$. This revealed that at this particular water content the evaporation from HYA is compensated by another processes associated probably with heat release (Prusova, Smejkalova, Chytil, Velebny, & Kucerik, 2010). This value was confirmed when enthalpy of evaporation was determined at every conversion degree during water evaporation (Kucerik et al., 2011). In the comparative study by (Mlcoch & Kucerik, 2013) it was showed that in the concentration interval 0.1–2 $g_{water}/g_{polysaccharide}$ this abrupt process can be observed only in HYA. However, the hydration numbers determined by thermoanalytical techniques reflect the state of water under non-equilibrium conditions and in a particular temperature range.

Therefore the results obtained from DSC experiments should be verified using an independent technique such as for example nuclear magnetic resonance (NMR). Such a technique does not require extrapolation from observations made at temperatures far from the point of interest as is often done in the case of DSC. Besides, it is well known that the nuclear spin relaxation times, the spin-lattice relaxation time (T_1) and the spin–spin relaxation time (T_2) of hydrogen nuclei within water molecules are determined by the physicochemical environment of the water (Shapiro, 2011). Consequently, the measurement of proton nuclear spin relaxation times provides information on polymer–water interactions and water dynamics in such a system. In fact, water mobility slows because the water is involved in H-bonds and other weak interactions. Water mobility is also slower when it is restricted in pores or cavities formed by molecules for example water soluble HYA. Therefore proportionally shorter relaxation times are expected to be measured (Topgaard & Soderman, 2002).

Past efforts to develop techniques to reprocess polysaccharides have addressed mainly the hydrophobic/hydrophilic properties and gave little attention to how much the native structure was compromised or physically changed. Understanding how polysaccharides interact with themselves, each other, and with water in semi-diluted systems is of great importance as it determines its final structure and physical properties. As shown recently by Kucerik et al. (2011), HYA potentially has alternate physical structures due to the presence of two types of glycosidic bonds and variability of reactive groups. It has been suggested that manipulation of drying conditions could bring about differences in physical structure of HYA, thus extending the potential applications of native, chemically non-modified, HYA.

The first aim of this study is to test whether the results obtained by several DSC approaches under non-isothermal conditions reported recently (Prusova et al., 2010) are comparable with results obtained using time domain NMR (TD-NMR). It is shown that both approaches give comparable data and shed light on the processes taking part in HYA structure at low water content. It is shown that the above-mentioned compensating process is the plasticization point above which the HYA segments have higher molecular motion, i.e. the physical structure is more susceptible to any modification during drying. Therefore, the second aim of this study is to test whether using of various drying methods have an influence on the resulting physical structure (mechanical properties, pore sizes, and hydration kinetics) of native HYA. This was tested by means of DSC, TD-NMR, and Environmental scanning electron microscopy techniques.

2. Experimental

The sodium salt form of bacterial HYA with a molecular weight of 800 kDa (measured by size-exclusion chromatography, results not reported) was kindly provided by Contipro Pharma, Ltd. (Dolní Dobrouč, Czech Republic). This sample was prepared by precipitating the solution through the addition of isopropylalcohol and then oven-dried. This sample is referred to as precipitated hyaluronan (P-HYA) or as "original" HYA.

2.1. Sample preparation

Hyaluronan powder was put into standard 20 mm NMR tubes (two parallel samples were measured) which were then placed in a moisturizing container with 100% relative humidity at a constant temperature of 19 °C. Samples were regularly homogenized and measured every 48 h using TD-NMR. The increasing water content (W_C), i.e. mass of water per gram of hyaluronan, was determined by regularly weighing the HYA sample. In order to achieve a W_C of 1 or higher, liquid water was added and the sample was homogenized for a period of 72 h.

To study the effect of drying on the physical structure of HYA, the hyaluronan-water solution was prepared with a concentration of 2.5% (w/w) and stirred for 24 h at room temperature. Two different drying methods were used: static drying of the solution in an oven at 25 °C, and freeze-drying. Therefore, three different hyaluronan samples were obtained: (i) static dried in the oven (O-HYA), ii) freeze dried (F-HYA) and (iii) original HYA sample (P-HYA). The prepared samples were stored in the desiccator at 19 °C and studied using DSC and TD-NMR techniques.

2.2. Time domain NMR

Time domain nuclear magnetic resonance (TD-NMR) measurements were performed using a MiniSpec (Bruker, Germany) instrument, operating at the proton Larmor frequency of 7.5 MHz for protons. T_2 relaxation decays, as a function of the W_C of the sample, were obtained by applying the Carr–Purcell–Meiboom–Gill (CPMG) pulse sequence. Echo time was kept constant at 0.1 ms, and the number of echoes and repetitions was changed depending on the W_C. The repetition time between scans was five times T_1 to avoid the T_1 weighting. To calculate T_2 values, the transverse relaxation curves from CPMG decays were fitted with Eq. (1) using RI-WinFit software (Version 2.4, Resonance Instrument Ltd., Oxfordshire, United Kingdom) with either bi-exponential or tri-exponential functions (in dependency on statistical parameters such as χ^2, standard error and R^2):

$$F(t) = \Sigma A_i \exp\left(\frac{-t}{T_{2,i}}\right), \quad (1)$$

where A is amplitude, t is time and T_2 is spin–spin relaxation time. The experiments were carried out at 25 °C.

2.3. Environmental scanning electron microscopy (ESEM)

ESEM microscopy was carried out on a Quanta 250 instrument (FEI, Brno, Czech Republic) in a low vacuum mode. A large field detector (LFD) was used with voltage 2–10 kV and spot size 3–4. Depending on the sample structure, a pressure between 50 and 70 Pa was used. The dwell time for picture acquisition was 30 μs. All samples were stored and equilibrated in the desiccator over the NaOH pellets for 3 days prior to imaging.

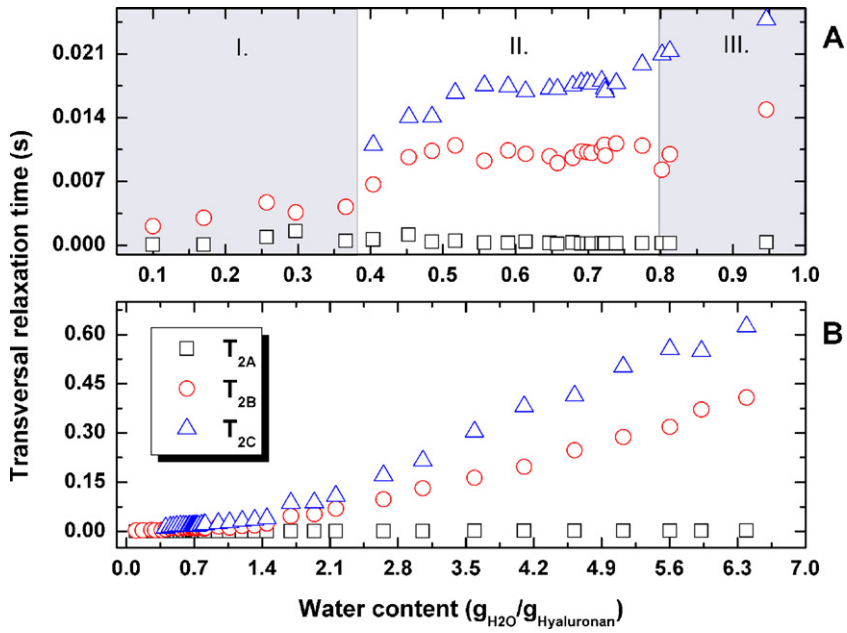

Fig. 1. T_2 relaxation times versus respective water fraction.

2.4. Thermal analysis

Differential scanning calorimetry (DSC) measurements were performed in order to analyze the difference in physical state of HYA samples obtained using various drying modes. The TA Instruments DSC Q1000, equipped with cooling accessory RCS90, was used and data were assessed by TA Universal Analysis 2000 software. The temperature and enthalpy calibration of the device were carried out using In and Sn as standards. Samples of approximately 5 mg (weighed to an accuracy of ± 0.01 mg) were placed in an aluminium open pan (Tzero® technology, DSC Q1000 TA Instruments). The following thermal protocol was used: started at 30.0 °C; equilibrated at −55 °C and then isotherm for 1 min. The next step was heating from −55.0 °C to 160 °C at four different heating rates: 30, 20, 10 and 5 °C min^{-1}. The flow rate of the dynamic nitrogen atmosphere was 50 mL min^{-1}.

It is necessary to point out that prior to data acquisition, samples were placed into the open DSC pan, cooled to −50 °C and then heated up to 150 °C before being cooled down again to −50 °C in order to set the same thermal history of the sample and evaporate the moisture from the HYA structure. This approach allowed the dependence of transitions on the heating rate to be tested.

The equilibrium moisture content of all three HYA samples and limits for DSC experiments, the temperature at which hyaluronan decomposition starts, were studied using evolved gas analysis, i.e. thermogravimetry (TG) coupled with mass spectrometry (MS) (NETZSCH STA 449 F3 Jupiter, Selb, Germany). Samples were placed into the alumina crucible and heated from room temperature to 800 °C at a rate of 5 °C min^{-1}. The reaction atmosphere was synthetic air, flow rate 50 mL min^{-1}.

3. Results and discussion

3.1. Hydration numbers determined with TD-NMR

Fig. 1 shows the transverse relaxation times determined by fitting Equation 1 to the transverse relaxation decay curves (not shown). As can be seen in Fig. 1A, for the low water content system (region I in Fig. 1A), two proton transverse relaxation times were determined: a slower one, T_{2B}, with an initial value of 2 ms, and a faster one, T_{2A}, with an initial value of 0.7 ms. Increasing the water content of the sample caused a moderate increase in T_{2A} and a more pronounced increase of T_{2B}. Upon reaching a W_C of around 0.4 g_{H20}/g_{HYA} (start of region II in Fig. 1A), a new proton pool with transverse relaxation time T_{2C} appeared. Both T_{2B} and T_{2C} irregularly but significantly grew with increasing water content. In contrast, the fastest component T_{2A} changed gradually to only 2.1 ms for the maximum water fraction investigated in this study i.e. W_C = 6.5 g_{H20}/g_{HYA} (Fig. 1B). Neither the standard deviation of the fitting nor the repeat measurements are shown in Fig. 1 as in all cases, the standard deviation is smaller than the symbol size and values of repetitive measurement are close to those reported in Fig. 1.

Multi-exponential behaviour of transverse relaxation decay curves, as observed in this study, is typical behaviour for viscoelastic systems like hydrated polysaccharides (Mariette, 2009). There are a number of mechanisms used as relaxation pathways in water–polysaccharide systems (McBrierty, Martin, & Karasz, 1999). Nevertheless proton exchange between polysaccharide hydroxyl protons and water molecules is thought to be the main relaxation mechanism in water–polysaccharide system (Okada, Matsukawa, & Watanabe, 2002) (Nestor, Kenne, & Sandstrom, 2010).

As can be seen in Fig. 1A, over the investigated water content range T_{2A} values are rather low. According to the Fuoss–Kirkwood distribution (Bakhmutov, 2004), such fast transverse relaxation can be attributed to transversal relaxation of large molecules, thus T_{2A} reflects relaxation of non-exchangeable HYA macromolecule protons. The slight increase in T_{2A} values over the range of W_C values is caused by gradual hydration of the hyaluronan structure which brings about an increase in hyaluronan macromolecule mobility.

As can be seen in Fig. 1A, a W_C of 0.4 g_{H20}/g_{HYA} is a border concentration above which a new proton pool T_{2C} is introduced. In general, water molecules are in mutual diffusive exchange. However, in the case of enormously rigid systems, when the water diffusion is sufficiently slow compared to the NMR time scale, relaxation is in the slow exchange regime and multi-component relaxation is observed. Consequently different water proton pools can be discriminated (Shapiro, 2011), i.e. T_{2B} and T_{2C} were observed. Above this border water content (0.4 g_{H20}/g_{HYA}) an abrupt increase in T_{2B} and T_{2C} values appears. This indicates changes in HYA structure

upon hydration. In a similar way, Froix & Nelson (1975) analyzed the state of water in cellulose and concluded that an abrupt increase of T_2 dependency on water content corresponds to the plasticization point above which both the cellulose chains and bound water acquire added modes of freedom (Froix & Nelson, 1975). This is in accordance with the behaviour of HYA in this study. In fact below this threshold the structure is "glass-like" and the gradual hydration brings about only a moderate increase in T_{2B} relaxation time. Conversely, above the plasticization concentration a significant increase in T_{2B} and T_{2C} can be observed (Fig. 1A) and the structure becomes "rubber-like". In other words, water molecules plasticize the structure and thus support molecular mobility, i.e. the structure is less rigid above this water content. As a result, water can much more easily penetrate the HYA structure. The value of this threshold ($W_C = 0.4\ g_{H20}/g_{HYA}$) agrees well with DSC results reported by Prusova et al. (2010) and Kucerik et al. (2011). In both cases it was concluded that during drying, when the water content corresponds to a value of around 0.34 g_{H20}/g_{HYA}, a competitive parallel process in HYA structure occurs. It was inferred that the formation of new intra/intermolecular interactions takes place which is associated with energy release. Thus, the results obtained in this study with TD-NMR indicate that this process is associated with a glass transition, which is known to be accompanied by the abrupt change in heat capacity (Wunderlich, 2005). In fact, the transition from a glassy into rubbery state increases the heat capacity of the system due to the higher mobility of chains and the free volume generated by segmental motion. Therefore, the compensation process detected by DSC during drying reported in (Prusova et al., 2010) is partially or fully caused by a decrease in heat capacity of the system.

The appearance of two components T_{2B} and T_{2C} reveals the existence of two types of water proton pools in HYA above the plasticization point. Since their transversal relaxation times are significantly lower than that of free water (around 2 s), it can be assumed that both proton fractions are affected by the presence of HYA macromolecules. The values of the relaxation times increased up to 0.5 and remained constant up to 0.8 g_{H20}/g_{HYA}. Above 0.8 g_{H20}/g_{HYA} (region III in Fig. 1A) a gradual increase in T_{2B} and T_{2C} values can again be seen. In fact, in the region from 0.5 to 0.8 g_{H20}/g_{HYA}, T_{2B} and T_{2C} values are rather short and close to T_{2A} values. It can therefore be concluded that this constant region can be seen as a saturation of the structure by water. With respect to recent results obtained using DSC (Prusova et al., 2010), we can assume that a water content of 0.5–0.8 g_{H20}/g_{HYA} is associated with the formation of non-freezing water fraction and some structural changes connected with wetting and swelling of HYA structure. Under experimental conditions, the driving force in water adsorption is the condensation of water vapor on curved surfaces and pores in accordance with the Kelvin and Young–Laplace equations. Moreover, adsorption onto polar groups of the HYA chain takes place and as a result, water bridges arise to stabilize the hydrated HYA structure leading the system to the lower energy (Almond et al., 2006; Nestor et al., 2010). DSC measurements on non-freezing water (Prusova et al., 2010) and dielectric relaxation (Hunger, Bernecker, Bakker, Bonn, & Richter, 2012) show the hydration number around 0.8 g_{H20}/g_{HYA}. It can therefore be assumed that both types of water, i.e. water proton pools with transversal relaxation times T_{2B} or T_{2C} below this W_C, represent the non-freezing water fraction.

The amplitudes of fitting (A), given by Eq. (1), are proportional to the relative fractions of protons involved in relaxation with T_2 longer than the echo time (the time between 90° and 180° radio frequency pulses) in CPMG pulse sequence. For $W_C = 0.75\ g_{H20}/g_{HYA}$, a ratio of amplitudes A_{2C}:A_{2B} is 5.8, which means that only 0.11 g of water per gram of HYA (ca. three water molecules per HYA disaccharide unit) have the faster relaxation time (T_{2B}) and thus these water molecules are more restricted in their motion. 0.64 grams of water per gram of HYA (fourteen water molecules per HYA disaccharide unit) is represented by T_{2C}. In light of the above discussion, a shorter T_{2B} relaxation time might notionally represent water integrated into HYA hydrophilic pores and therefore in intimate contact with polar groups. Due to free volume generation above the plasticization point, T_{2C} might represent water structurally restricted between hyaluronan chain double helices. This hypothesis is supported by the change in ratio between amplitudes upon increasing W_C: for $W_C = 2\ g_{H20}/g_{HYA}$ a ratio of amplitudes A_{2C}:A_{2B} is 0.6. This indicates that the progressive swelling, increase in pore size, and the collapse of present cavities causes a decrease in the proportional content of structurally restricted water. This was demonstrated by Kucerik et al. (2011) where for $W_C = 2\ g_{H20}/g_{HYA}$ the enthalpy of melting of ice formed in such cavities already resembled the melting enthalpy of pure water. This means the restriction of water is lower and hexagonal ice can be formed. It can be assumed that for sufficiently high values of W_C, components T_{2B} and T_{2C} will merge. It can be inferred from Fig. 1 that the dynamics of HYA hydration and/or drying are linked to complicated structural changes.

3.2. Morphology of the sample obtained under different drying conditions

3.2.1. Microscopy

Samples of HYA were prepared in three different ways as reported in the experimental section. First, the morphology of the surface was studied with electron microscopy under low vacuum conditions. Fig. 2A shows P-HYA. This sample shows a compact structure with heterogeneous surface features composed of both smaller and larger grains. It is also full of cavities and holes. This partially supports the statements from previous paragraph. Fig. 2B shows the hydrated surface of P-HYA (0.9 g_{H20}/g_{HYA}). The individual grains are swollen and mostly interconnected. On the other hand, F-HYA (Fig. 2C) shows a looser, crusty structure with a larger surface area. The surface is less heterogeneous than that of P-HYA. In Fig. 2D, we see O-HYA which shows a compact fragile structure with an even surface with no visible cavities or holes as in the case of P-HYA.

3.2.2. Phase transitions in the dried samples

The prepared HYA samples were tested by thermal analysis in order to observe differences in their physical structure. Prior to the DSC experiments, thermogravimetry coupled with mass spectrometry was used to determine the range of temperatures applicable for DSC and to determine the moisture content of the sample. Fig. 3 shows the mass loss and the ion current signals for CO_2 and H_2O as a function of temperature for the P-HYA sample. It can be seen that the temperature region up to 210 °C is associated only with the evaporation of moisture. Such a conclusion is based on the fact that up to 210 °C, there is only an ion current signal from H_2O and none from CO_2. Above 210 °C, a steep decrease in mass loss and the appearance of the first peaks in both the CO_2 and H_2O ion current signals indicates the beginning of HYA decomposition. Therefore DSC experiments can be performed up to a temperature of 200 °C.

The representative DSC record for different heating rates is depicted in Fig. 4. In the DSC record of all HYA samples, an exothermic peak occurs in the range −37 °C to −13 °C (marked as "I"). The peak temperature is heating rate dependent which indicates that this is a kinetic process. The exothermic peak "I" is followed by another two much smaller exothermic peaks. Thus, it is impossible to correctly determine the maxima of these two peaks. It is worth mentioning that the character of these peaks is independent of moisture content (tested in separate experiments – results not shown).

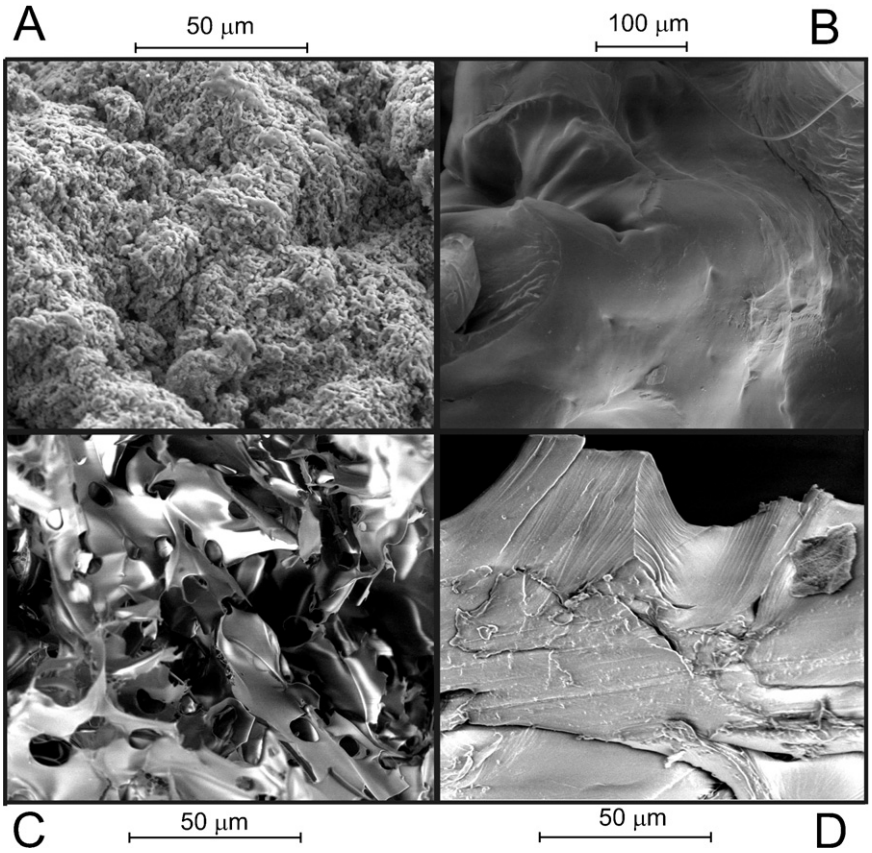

Fig. 2. ESEM image of different hyaluronan samples. (a) P-HYA, (b) F-HYA, (c) hydrated HYA ($W_C = 0.9\ g_{H20}/g_{HYA}$), (d) O-HYA.

Another thermal event appears in the 50–110 °C temperature range (marked as "II"). It is again dependent on the heating rate which implies that it is a kinetic process. In contrast to the exothermic peak "I" observed at low temperature, this thermal event "II" is dependent on the water content of the HYA sample, i.e. drying shifts this thermal event to higher temperature region.

The literature does not report much about the phase transitions in dry HYA. The dynamical mechanical analysis of the HYA film reported by Dave, Tamagno, Marsano, and Focher (1995) shows that the process occurring at room temperature is associated with the large-scale motion of the molecular chain segments, namely the glass transition. Observations of the kinetic character of process "II" in the present work are in line with this conclusion. Furthermore, the initial storage modulus E' of the HYA films decreased slightly as the temperature is raised from −100 °C up to −22 °C, and then showed simple discontinuity around 25 °C. Finally, it was shown an increase as the temperature was raised above 25 °C. This was considered a strain-induced crystallization with an increase in the

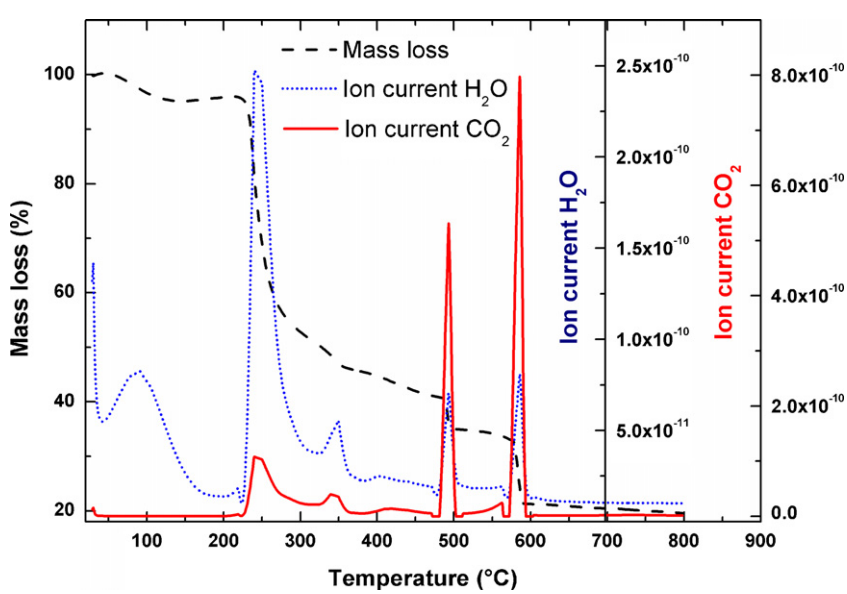

Fig. 3. TG and MS record of HYA, mass loss, CO_2 and H_2O ion current signals as a function of temperature.

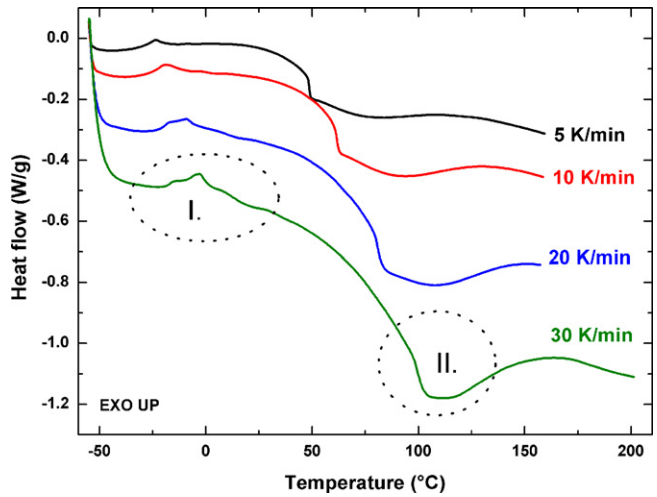

Fig. 4. The DSC record for the F-HYA sample (all runs were repeated twice).

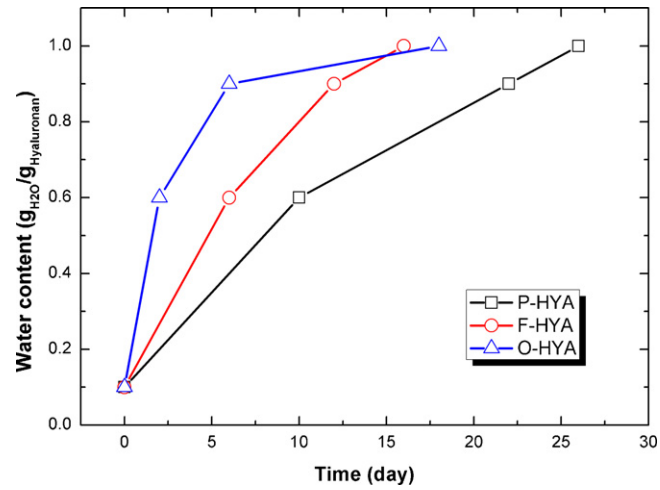

Fig. 5. Hydration progress for different HYA samples.

number of intermolecular and/or intramolecular hydrogen bonds before high-temperature relaxation phenomena occurred (Dave et al., 1995). Results shown in Fig. 4 support the hypothesis put forward by Dave et al. (1995) concerning the crystallization processes interrupted by glass transition. However, we can reject the hypothesis about its strain-induced origin since the process was observed using DSC in this work.

Table 1 summarizes the characteristic temperatures of both processes measured with DSC. The peak temperature in the crystallization process ("I") and the midpoint of the glass transition ("II") are both evaluated in the traditional way (Wunderlich, 2005). It can be seen that using different methods to dry the HYA has only a small effect on crystallization "I" but a pronounced effect on the amorphous transition "II". The temperature of the glass transition is highest for F-HYA and lowest for P-HYA. This means that from a mechanistic point of view, freeze-drying provides the most rigid structure at room temperature. The data in Table 1 shows the dependency of the glass transition temperature on the heating rate which allows extrapolation of glass transition temperature to quasi-isothermal conditions (the zero heating rate). The temperatures for quasi-isothermal conditions were for F-HYA = 34.7 °C, O-HYA = 28.7 °C, and P-HYA = 25.5 °C. This result indicates that at room temperature all samples are in the glassy state (below the glass transition temperature).

The temperature of the glass transition reflects the qualitative aspect of the amorphous phase while the change in the heat capacity associated with the glass transition provides more quantitative information. Put simply, the larger the change, the larger the part of the sample that is amorphous. Comparing changes in the heat capacities showed that the F-HYA sample exhibits the highest change in heat capacity (1.05 J g^{-1} K^{-1}) and O-HYA the lowest (0.1 J g^{-1} K^{-1}). The P-HYA sample showed a change in heat capacity of 0.7 J g^{-1} K^{-1}. We conclude that the O-HYA sample shows the lowest amorphous content. The recrystallization enthalpy calculation of exothermal peaks in area "I" gave for F-HAY = 3.21 J g^{-1}, P-HYA = 1.27 J g^{-1}, and O-HYA = 1.68 J g^{-1}. Those values reflect the energy necessary for reorganization of crystalline-like structures in individual HYA samples.

3.2.3. Hydration characteristics of HYA samples prepared under different drying conditions

In order to characterize the differences in the hydration characteristics of HYA samples, TD-NMR was used. All samples (P-HYA, O-HYA and F-HYA) were exposed to 100% relative humidity and analyzed as described in the experimental section. The plasticization point was determined in the same manner as in the Section 3.1, i.e. by the appearance of a new water proton pool. The results for the P-HYA sample were consistent with the previous results (Section 3.1); the plasticization point was determined as slightly below 0.4 g_{H20}/g_{HYA}. For the F-HYA sample, the plasticization point was between 0.55–0.65 g_{H20}/g_{HYA} and for the O-HYA sample 0.8–0.9 g_{H20}/g_{HYA}. The plasticization order determined by TD-NMR is different from that determined by DSC, where the sample with the lowest plasticization temperature was P-HYA followed by O-HYA and finally the F-HYA sample (see Table 1). In fact, the plasticization points determined with TD-NMR and DSC differ in their physicochemical meaning. In TD-NMR, the plasticization point is a water content, and so is a measure of rigidity with water molecules acting as plasticizers. In the case of DSC experiments, the heat and associated temperature is the cause of higher molecular mobility and the glass transition. Those differences are clear indicators of the specificity of the HYA samples. It is worth mentioning that both techniques observe the same phenomenon i.e. glass transition, but under different conditions.

The TD-NMR data show the difference between the hydration mechanisms of the samples. As can be seen in Fig. 5, HYA samples have different kinetics of hydration, with O-HYA having the fastest. That can be explained by the lowest T_{2B} value (among three different HYA samples) up to W_C = 0.9 g_{H20}/g_{HYA}. Simultaneously, the associated amplitude, reflecting the proton fraction, is highest up

Table 1
The peak maxima and glass transition temperatures for different HYA samples.

HYA	Process "I" exothermic peak (°C)				Process "II" glass transition (°C)			
	Heating rate (°C/min)				Heating rate (°C/min)			
	30	20	10	5	30	20	10	5
P-HYA	−2.6	−8.8	−19.1	−24.4	81.5	65.3	45.9	36.2
O-HYA	−2.8	−8.6	−18.1	−23.9	87.7	72.7	52.8	41.5
F-HYA	−2.7	−9.2	−19.1	−23.7	99.2	82.7	61.6	48.6

to $W_C = 0.9\ g_{H20}/g_{HYA}$ and then is approximately equal to amplitude associated with T_{2C} relaxation time (data not shown). This means that below $0.9\ g_{H20}/g_{HYA}$, O-HYA has the largest fraction of structurally integrated water protons. In other words, O-HYA has the largest number of small pores. These cannot be seen from the scanning electron microscope pictures under applied conditions and resolution (Fig. 2), but explain the fast kinetics of hydration (see Fig. 5).

In our recent work, analysis of the P-HYA sample at different W_C values using DSC gave a plasticization point of $0.34\ g_{H20}/g_{HYA}$ (Prusova et al., 2010; Kucerik et al., 2011) which is in agreement with results obtained by TD-NMR in this work. In contrast, samples prepared under different drying conditions gave rather different results in terms of physicochemical properties and behaviour such as glass transition and response to the moisturizing conditions. This further emphasises our earlier statement that hydration, especially in the case of hyaluronan, is a "dynamic" value and reflects the sample's history (preparation, conditioning, drying...), the technique used for its determination, and slightly also the conditions under which the experiment is carried out.

4. Conclusion

In this study, HYA samples were prepared under three different drying conditions yielding the original, freeze-dried, and oven-dried HYA sample. It was demonstrated that DSC and TD-NMR are complementary techniques in terms of HYA hydration. The non-freezing water fraction in semi-diluted HYA can be determined using both techniques. Further, by using TD-NMR it is possible to determine the hydration kinetics of HYA and also to determine the water content of an HYA sample that corresponds to the glass-to-rubbery-state transition which is a measure of the rigidity of a system. The oven-dried sample has the fastest whereas the precipitated HYA sample has the slowest hydration kinetics. Based on the glass transition temperature, it was observed that the sample prepared by freeze-drying was the most rigid one and the oven-dried sample had the lowest amorphous fraction. Hence it was demonstrated that the supramolecular structure of native HYA is modified by drying conditions. This represents a promising strategy for further application of this polysaccharide in its native state, for example in the pharmaceutical industry in drug delivery systems with delayed wetting, swelling, and consequent release of transported drugs.

Acknowledgements

The authors wish to thank Prof. Dr. Gabriele E. Schaumann and Dr. Jette Schwarz from Universität Koblenz-Landau in Landau, Germany and Assoc. Prof. Dr. Henk Van As from Wageningen University, The Netherlands for their support and help, to Assoc. Prof. Dr. Vladimír Velebný from CPN Company, Dolní Dobrouč, Czech Republic for providing of hyaluronan and Andrew Cuthbert (MPhys) from Wageningen University, The Netherlands for correction of English style and grammar.

References

Almond, A., DeAngelis, P. L., & Blundell, C. D. (2006). Hyaluronan: the local solution conformation determined by NMR and computer modeling is close to a contracted left-handed 4-fold helix. *Journal of Molecular Biology*, *358*(5), 1256–1269.

Bakhmutov, V. I. (2004). *Practical NMR relaxation for chemists*. Chichester, West Sussex, England: Wiley.

Belton, P. S. (1997). NMR and the mobility of water in polysaccharide gels. *International Journal of Biological Macromolecules*, *21*(1/2), 81–88.

Bouwstra, J. A., Salomonsdevries, M. A., & Vanmiltenburg, J. C. (1995). The thermal behaviour of water in hydrogels. *Thermochimica Acta*, *248*, 319–327.

Chakraborty, S., Sinha, S. K., & Bandyopadhyay, S. (2007). Low-frequency vibrational spectrum of water in the hydration layer of a protein: A molecular dynamics simulation study. *Journal of Physical Chemistry B*, *111*(48), 13626–13631.

Dave, Y., Tamagno, M., Marsano, E., & Focher, B. (1995). Hyaluronan acide (hydroxypropyl) cellulose blends – A solution and solid-state study. *Abstracts of Papers of the American Chemical Society*, *209*, 149–150.

Davies, A., Gormally, J., Wynjones, E., Wedlock, D. J., & Phillips, G. O. (1983). A study of factors influencing hydration of sodium hyaluronate from compressibility and high-precision densitometric measurements. *Biochemical Journal*, *213*(2), 363–369.

Froix, M. F., & Nelson, R. (1975). Interaction of water with cellulose from nuclear magnetic resonance relaxation times. *Macromolecules*, *8*(6), 726–730.

Garg, H. G., & Hales, C. A. (2004). *Chemistry and Biology of Hyaluronan*. Amsterdam, Nederland: Elsevier.

Hatakeyama, T., Hatakeyama, H. (2004). Thermal Properties of Green Polymers and Biocomposites.

Hunger, J., Bernecker, A., Bakker, H. J., Bonn, M., & Richter, R. P. (2012). Hydration dynamics of hyaluronan and dextran. *Biophysical Journal*, *103*(1), L10–L12.

Kucerik, J., Prusova, A., Rotaru, A., Flimel, K., Janecek, J., & Conte, P. (2011). DSC study on hyaluronan drying and hydration. *Thermochimica Acta*, *523*(1/2), 245–249.

Liu, J., & Cowman, M. K. (2000). Thermal analysis of semi-dilute hyaluronan solutions. *Journal of Thermal Analysis and Calorimetry*, *59*(1/2), 547–557.

Mariette, F. (2009). Investigations of food colloids by NMR and MRI. *Current Opinion in Colloid & Interface Science*, *14*(3), 203–211.

McBrierty, V. J., Martin, S. J., & Karasz, F. E. (1999). Understanding hydrated polymers: The perspective of NMR. *Journal of Molecular Liquids*, *80*(2/3), 179–205.

Mlcoch, T., & Kucerik, J. (2013). Hydration and drying of various polysaccharides studied using DSC. *Journal of Thermal Analysis and Calorimetry*, http://dx.doi.org/10.1007/s10973-013-2946-1

Nestor, G., Kenne, L., & Sandstrom, C. (2010). Experimental evidence of chemical exchange over the beta(1 → 3) glycosidic linkage and hydrogen bonding involving hydroxy protons in hyaluronan oligosaccharides by NMR spectroscopy. *Organic & Biomolecular Chemistry*, *8*(12), 2795–2802.

Okada, R., Matsukawa, S., & Watanabe, T. (2002). Hydration structure and dynamics in pullulan aqueous solution based on H-1 NMR relaxation time. *Journal of Molecular Structure*, *602*, 473–483.

Prusova, A., Smejkalova, D., Chytil, M., Velebny, V., & Kucerik, J. (2010). An alternative DSC approach to study hydration of hyaluronan. *Carbohydrate Polymers*, *82*(2), 498–503.

Scott, J. E., & Heatley, F. (1999). Hyaluronan forms specific stable tertiary structures in aqueous solution: A C-13 NMR study. *Proceedings of the National Academy of Sciences of the United States of America*, *96*(9), 4850–4855.

Scott, J. E., & Heatley, F. (2002). Biological properties of hyaluronan in aqueous solution are controlled and sequestered by reversible tertiary structures, defined by NMR spectroscopy. *Biomacromolecules*, *3*(3), 547–553.

Shapiro, Y. E. (2011). Structure and dynamics of hydrogels and organogels: An NMR spectroscopy approach. *Progress in Polymer Science*, *36*(9), 1184–1253.

Sutherland, I. W. (1998). Novel and established applications of microbial polysaccharides. *Trends in Biotechnology*, *16*(1), 41–46.

Takahashi, M., Hatakeyama, T., & Hatakeyama, H. (2000). Phenomenological theory describing the behaviour of non-freezing water in structure formation process of polysaccharide aqueous solutions. *Carbohydrate Polymers*, *41*(1), 91–95.

Topgaard, D., & Soderman, O. (2002). Changes of cellulose fiber wall structure during drying investigated using NMR self-diffusion and relaxation experiments. *Cellulose*, *9*(2), 139–147.

Wunderlich, B. (2005). *Thermal analysis of Polymeric Materials*. Berlin: Springer-Verlag.

Yokomizo, T., Nakasako, M., Yamazaki, T., Shindo, H., & Higo, J. (2005). Hydrogen-bond patterns in the hydration structure of a protein. *Chemical Physics Letters*, *401*(4–6), 332–336.

PUBLICATIONS

Peer-reviewed:

- Průšová, A., Šmejkalová, D., Chytil, M., Velebný, M., Kučerík, J. (2010). An alternative DSC approach to study hydration of hyaluronan. Carbohydrate Polymers 82: 498-503.
- Průšová, A., Conte, P., Kučerík, J., Alonzo, G. (2010) Dynamics of hyaluronan aqueous solutions as assessed by fast field cycling NMR relaxometry. Analytical and Bioanalytical Chemistry 397: 3023-3028.
- Kučerík, J., Průšová, A., Rotaru, A., Flimel, K., Janeček, J., Conte, P. (2011). DSC study on hyaluronan hydration and dehydration. Thermochimica acta 523: 245-249.
- Šmejkalová, D., Hermannová, M., Šulánková, R., Průšová, A., Kučerík, J., Velebný, M. (2012) Structural and conformation differences of acylated hyaluronan modified in protic and aprotic solvent system. Carbohydrate Polymers 87: 1460-1466.
- Kučerík, J., Bursáková, P., Průšová, A., Grebíková, L., Schaumann, G.E. (2012) Hydration of humic and fulvic acids studied by DSC. Journal of thermal analysis and calorimetry 110: 451-459.
- Špérová, M., Kučerík, J., Nasadil, P., Průšová, A. (2012) A hint on the correlation between cellulose fibres polymerization degree and their thermal and thermo- oxidative degradation. Journal of Thermal Analysis and Calorimetry 110: 71-76.
- Průšová, A., Vergeldt, F.J., Kučerík, J. (2013) Influence of water content and drying on the physical structure of native hyaluronan. Carbohydrate Polymers 95: 515-521.

Oral presentations:

- Alena Průšová, Petra Bursáková, Jiří Kučerík. “Hydration of hyaluronan”.4th Meeting on Chemistry & Life 2008, Brno, Czech Republic.
- Alena Průšová, Pellegrino Conte, Jiří Kučerík, Claudio De Pasquale, Giuseppe Alonzo. “Dynamics of water solutions of natural polysaccharides by fast field cycling NMR relaxometry” European Geosciences Union General Assembly 2010 Vienna, Austria.
- Alena Průšová, Jiří Kučerík, Gabriele E. Schaumann. “A comparative DSC and ^{1}H NMR relaxometry study on hyaluronan hydration” 1st Central and Eastern European Conference on Thermal Analysis and Calorimetry 2011, Craiova, Romania.

Poster presentations:

- Alena Průšová, Claudio De Pasquale, Vittorio Loddo, Leonardo Palmisano. "TiO_2-H_2O interactions by fast field cycling (FFC) NMR relaxometry" European Geosciences Union General Assembly 2010 Vienna, Austria.
- Alena Průšová, Pellegrino Conte, Jiří Kučerík, Giuseppe Alonzo. "Dynamics of hyaluronan aqueous solutions as affected by molecular size and ionic strength" 7th conference of field cycling NMR relaxometry 2011, Torino, Italy

CURRICULUM VITAE

Contact

Name:	Alena Průšová
Address:	Haldereng 29, Bennekom 6721XR, The Netherlands
Email:	alena.prusova@gmail.com
Telephone:	0031 657 766 595

Personal data

Date of birth:	09.06.1984
Place of birth:	Ceske Budejovice, Czech Republic
Nationality:	Czech

Education

Date:	2012 –2013
Qualification:	Ph.D. study
University:	University of Koblenz-Landau, Germany

Date:	2008 –2011
Qualification:	Ph.D. study
University:	Brno University of Technology, Czech Republic

Date: 2003 –2008

Qualification: Physical and Consumer Chemistry, Dipl. Ing

University: Brno University of Technology, Czech Republic

Date: 1999 –2003

Qualification: GCSE in Food Chemistry

Secondary technical school in České Budějovice, Czech Republic